Universität Bremen

marum
Center for Marine
Environmental Sciences

The influence of climate variability on the mass balance of Canadian Arctic land-terminating glaciers, in simulations of the last millennium

Dissertation

by

Anouk Vlug

MARUM - Center for Marine Environmental Sciences
and Faculty of Geosciences

University of Bremen

April 2021

First reviewer:	Prof. Dr. Michael Schulz MARUM - Center for Marine Environmental Sciences Department of Geosciences University of Bremen
Second reviewer:	Prof. Dr. Gerard Roe Department of Earth and Space Sciences University of Washington
Doctoral Colloquium:	10 December 2021

Daily supervisor:	Dr. Matthias Prange MARUM - Center for Marine Environmental Sciences Faculty of Geosciences University of Bremen
Primary supervisor:	Prof. Dr. Michael Schulz MARUM - Center for Marine Environmental Sciences Faculty of Geosciences University of Bremen
Supervisor:	Prof. Dr. Ben Marzeion Institute of Geography MARUM - Center for Marine Environmental Sciences University of Bremen
External supervisor:	Dr. Fabien Maussion Department of Atmospheric and Cryospheric Sciences University of Innsbruck

To my little sisters
Pippa, Rover, Liv & Jip
Never forget that you can follow your dreams

Summary

Glacier mass loss has been one of the main contributors to sea-level rise in the 20^{th} century and it is expected to remain a large contributor in the 21^{st} century. Because of the large glacier volume in the Canadian Arctic Archipelago and its recent increase in glacier mass loss, it is important to understand the sensitivity of these glaciers to regionally changing climatic conditions. Due to the relatively high density in climate data over the last 1000 years, it is a useful period to quantify the relative importance of natural and anthropogenic forcing to the climate. In this context we placed the recent glacier mass loss in the perspective of the last millennium, by simulating the land-terminating glaciers with the Open Global Glacier Model over the last millennium. In these simulations the model was forced with 2-m air temperature and the precipitation of the fully forced ensemble members of the Community Earth System Model Last Millennium Ensemble.
The sensitivity study leading up to this shows that neglecting or under-representing temperature variability may result in a significant overestimation of glacier volume. This effect is caused by the non-linear response of the glacier surface mass-balance to air temperature, where both the changed mean and variability of the equilibrium line altitude play a role. The significance of this effect has implications for any glacier modelling study driven by climate model output, and calls for a careful treatment of the downscaling of gridded data to the glacier scale.

The fully forced transient simulations have been validated with present-day observations and the RACMO2.3 simulation. Our simulations show that glacier mass loss over the period 2006-2016 CE might not be unprecedented in the last millennium. However under the RCP8.5 scenario it will reach a mass loss rate in the next decade that was unprecedented during the last millennium. The orbital and volcanic forcing contributed most to the build up of glacier volume throughout the last millennium. The single forced simulations show that without the increase in greenhouse gas emissions since 1850 CE, the glacier volume in the region would still be growing. Because the anthropogenic ozone and aerosols largely counter balances the negative influence of the greenhouse gas emissions, the net contribution of the anthropogenic climate forcings over the last millennium might still be positive; however, there are large uncertainties in this regard.

Zusammenfassung

Der Massenverlust von Gletschern stellt einen Hauptbeitrag zum Meeresspiegelanstieg im 20. Jahrhundert dar und wird voraussichtlich auch im 21. Jahrhundert einen großen Beitrag liefern. Wegen des großen Gletschervolumens im kanadisch-arktischen Archipel und des kürzlichen Anstieges des dortigen Gletschermassenverlustes ist es wichtig, die Sensitivität dieser Gletscher bezüglich sich regional verändernder klimatischer Bedingungen zu verstehen. Aufgrund der relativen Häufigkeit an Klimadaten aus den letzten 1000 Jahren ist dies ein nützlicher Zeitraum, um die relative Wichtigkeit von natürlichem und anthropogenem Antrieb für das Klima zu quantifizieren. In diesem Kontext haben wir den kürzlichen Gletschermassenverlust zu dem des letzten Jahrtausends in Beziehung gesetzt, indem wir die Gletscher mit Landterminierung während des letzten Jahrtausends mit dem Open Global Glacier Model simuliert haben. In diesen Simulationen wurde das Modell mit Zwei-Meter-Temperaturen und Niederschlägen des Community Earth System Model Last Millenium Ensembles angetrieben.
Die hierzu führende Sensitivitätsstudie zeigt, dass das Vernachlässigen oder Unterschätzen der Temperaturvariabilität in einer signifikanten Überschätzung des Gletschervolumens resultieren kann. Dieser Effekt wird durch die nicht-lineare Reaktion der Gletscheroberflächenmassenbilanz auf die Lufttemperatur verursacht, wobei sowohl der veränderte Mittelwert als auch die Variabilität der Höhe der Gleichgewichtslinie eine Rolle spielen. Die Signifikanz dieses Effekts hat Auswirkungen für jede Gletschermodellstudie, die mit Ergebnissen aus Klimamodellen betrieben wird und verlangt eine vorsichtige Behandlung bei der Herunterskalierung von Gitterdaten auf die Größenordnung von Gletschern.

Die transienten Simulationen wurden mit Beobachtungen aus der Gegenwart und der RACMO2.3-Simulation validiert. Unsere Simulationen zeigen, dass der Massenverlust von Gletschern während des Zeitraums 2006-2016 CE möglicherweise auch schon im letzten Jahrtausend vorkam. Allerdings wird er unter Annahme des RCP8.5-Szenarios in der nächsten Dekade eine Verlustrate erreichen, die im letzten Jahrtausend ohne Beispiel ist. Der orbitale und vulkanische Antrieb haben im letzten Jahrtausend am meisten zum Aufbau des Gletschervolumens beigetragen. Die individuell angetriebenen Simulationen zeigen, dass das Gletschervolumen in der Region ohne den Anstieg der Treibhausgas-Emissionen seit 1850 CE immer noch ansteigen würde. Da anthropogenes Ozon und Aerosole dem negativen Einfluss der Treibhausgas-Emissionen großteils entgegenwirken,

könnte der Nettobeitrag der anthropogenen Klimaantriebe in der Vergangenheit dennoch positiv sein; es herrschen diesbezüglich allerdings große Unsicherheiten.

Own Contribution

This thesis has been written by me (Anouk Vlug) and contains contributions by others that have been made in the context of preparing manuscripts and supervision. These contributions include giving feedback on the text and having numerous discussions. Both their and my own contributions will be specified in this chapter, with the main goal to clarify my own contribution to this thesis. My PhD was officially supervised by Matthias Prange (daily supervisor), Ben Marzeion and Michael Schulz (primary supervisor); also being referred to as my supervision team. Fabien Maussion was my external supervisor.

The sensitivity study that is being presented in the first half of chapter 3 was originally written as a manuscript, with Matthias Prange, Fabien Maussion, Ben Marzeion, Eliza Dawson and Michael Schulz as co-authors. The idea for the sensitivity study was conceived by the supervision team, and jointly with me further developed. Eliza Dawson contributed to the preliminary study of this sensitivity study during her 10-week DAAD RISE internship with me. I coded functions to pre-process the CESM-LME climate data and run OGGM with that data that ended up in the OGGM code base (Maussion et al., 2019a,b, `https://github.com/OGGM/oggm/commits?author=anoukvlug`). I created the set-up and ran the experiments, while receiving support and significant contributions by Fabien Maussion. The model set-up I developed in the early stage of my PhD has been successfully used in a study by Goosse et al. (2018). I wrote the chapter and all co-authors contributed with discussions and edits of the manuscript. This part of the chapter also contains implemented suggestions from three anonymous reviewers.

The second part of chapter 3 was initially written as a separate manuscript, with Matthias Prange, Fabien Maussion, Ben Marzeion, Brice Noël and Michael Schulz as co-authors. The idea for this study has been largely developed by me and has been further developed with contributions from all supervisors. I did the set-up and ran all experiments. Brice Noël prepared the RACMO2.3 data for comparison with the OGGM simulations. I wrote a first version of the manuscript and all co-authors contributed with discussions and edits.

The idea for chapter 4 was conceived by the supervision team and further developed and executed by me. I wrote the first version of the chapter, which will serve as draft

for a manuscript. All remaining chapters were written by me. Though they contain contributions by the others that have been made in the context of preparation of the manuscripts (e.g. parts of introductions of the manuscripts have been used for the introduction chapter). I prepared all the figures, except for figure 1.1 and 1.2, that are being presented in this thesis. The layout of this document is largely based on a latex template has been kindly provided by Charlotte Janßen. The credits for the translation of the Summary, the "Zusammenfassung", go to Valentin Ludwig.

Contents

1 Introduction

1.1 Glacier mass loss - Linking climate change and sea-level rise

Internationally serious efforts are being made to mitigate global warming, ranging from top down efforts like the Paris Agreement that was negotiated by the Conference of the Parties (COP) to bottom up initiatives that call for action like Fridays for Future. One of the reasons for pursuing this challenge is the influence a warming climate has on the sea level. The sea level rises both due to thermal expansion of ocean water and as a result of the decrease of water that is stored on land in the form of ice (Oppenheimer et al., 2019). However, a rising sea level is not a new phenomenon. The sea level has fluctuated through time and has been significantly higher in the past during warmer periods. The last time this occurred was 125,000 years ago, during the previous interglacial in a period called the Eemian, when the global mean sea level was 5.5 to 9 m higher than today (Dutton and Lambeck, 2012). There is however a big difference between us and the Homo sapiens in the Eemian, that where hunters and gatherers. The first agricultural revolution (Neolithic revolution), that led in the end to larger settlements, had for instance not taken place yet. This revolution started in the early Holocene (Svizzero, 2017), when the estimated population size was about 5 million (Deevey, 1960) and the sea level was about 35 m lower than at present (Lambeck et al., 2014). In the meantime things changed, and it has been estimated that 230 million people are living within the first meter above the current high tide line and 1 billion people within the first ten meters (Kulp and Strauss, 2019). Therefore sea-level rise would, from a human perspective, have severe consequences now. Ironically, people do now, in contrast to during the Eemian, have a significant influence on the climate. The global mean temperature has risen by approximately 1 °C with respect to pre-industrial levels due to anthropogenic causes (Allen et al., in press), while previously it were the only changes in natural forces (e.g. volcanism and the Milankovitch cycles[1]) and feedbacks within the climate system that drove climate change.

[1]The Milankovitch cycles refers to the cyclical changing position of the Earth with respect to the sun, as a result of eccentricity (shape of the orbit), obliquity (tilt of the Earth axis) and precession (the direction of the tilt), that have a periodicity of respectively roughly 100.000, 41.000 and 23.000 years.

It is virtually certain that the global mean sea level (GMSL) is rising and there is a very high confidence that shrinking glaciers[2] are the dominant source for this (Oppenheimer et al., 2019). Land ice has a huge potential for increasing the sea level further, as the Antarctic Ice Sheet contains 58 m (Fretwell et al., 2013) and the Greenland Ice Sheet contains 7 m GMSL rise equivalent of ice (Morlighem et al., 2017). The glaciers and ice caps (GIC) together would cause a GMSL rise of 0.32 ± 0.08 m when all completely melted (Farinotti et al., 2019), which is lower than the previously estimated 0.41 m (Vaughan et al., 2013). Though the GIC contain a relatively small portion of all land ice, due to their smaller size they respond more rapidly to a changing climate. The GIC have been one of the of the main contributors to GMSL rise over the last century and it is expected that the GIC remain a large contributor during the 21^{st} century (Slangen et al., 2017).

The formation of glaciers is a slow process. Glacier ice can form due to accumulation and the densification of snow. Fresh snow can be as light as 50 kg/m^3. After the snow survives for a year without melting away it becomes firn. Though this transition is based on the age, it includes changes in its properties. The process of densification starts with relocation of the snow grains. Later the density will further increase due to vitrification, the fusion of ice crystals. Firn becomes ice once its density passes the threshold of 830 kg/m^3, the air filled pores are then no longer interconnected. The duration of this process is very much depended upon the local conditions. Under warm and wet conditions this process might take a few years, while it might take a couple of hundred years under cold and dry conditions. In addition, pressure has a positive influence on the densification speed. Based on the mass balance[3] a glacier can be divided into two zones. In the accumulation zone there is more mass gain throughout a year than mass loss and this is the other way around in the ablation zone. Ice ends up in the ablation zone of a glacier through the flow of ice (Fig. 1.1). The flow of glacial ice is driven by gravity and restricted by lateral and basal drag. The height where the accumulation is equal to the ablation over a year is the equilibrium line altitude (ELA, see Fig. 1.2 for an overview of the different mass balance components that a glacier can have). The ELA

[2] A commonly used definition for a glacier is: *"a perennial mass of ice, and possibly firn and snow, originating on the land surface by the recrystallization of snow or other forms of solid precipitation and showing evidence of past or present flow"* - Cogley et al., 2011. However, there is some ambiguity related to this term. Glaciers can be further subdivided into categories, including one carrying the same name: glaciers, ice caps, and ice sheets. In this subcategory glaciers are defined by these ice masses that are confined by the topography, while the latter two are not (e.g. Benn and Evans, 2010). An ice cap is dome shaped and has a radial flow. Once an ice body is larger than the commonly used threshold of 50 000 km^2, than it is referred to as an ice sheet (Cogley et al., 2011). When the term glacier is being used in this thesis, it is a reference to all these three types of ice masses, unless specified otherwise. In practise, it means that the glaciers often referred to in this thesis consist of both glaciers and ice caps, as there is currently no ice sheet in the Canadian Arctic.

[3] The glacier mass balance is the change in glacier mass, or a part of that, over a stated span of time (Cogley et al., 2011). It is the sum of the ablation and the accumulation.

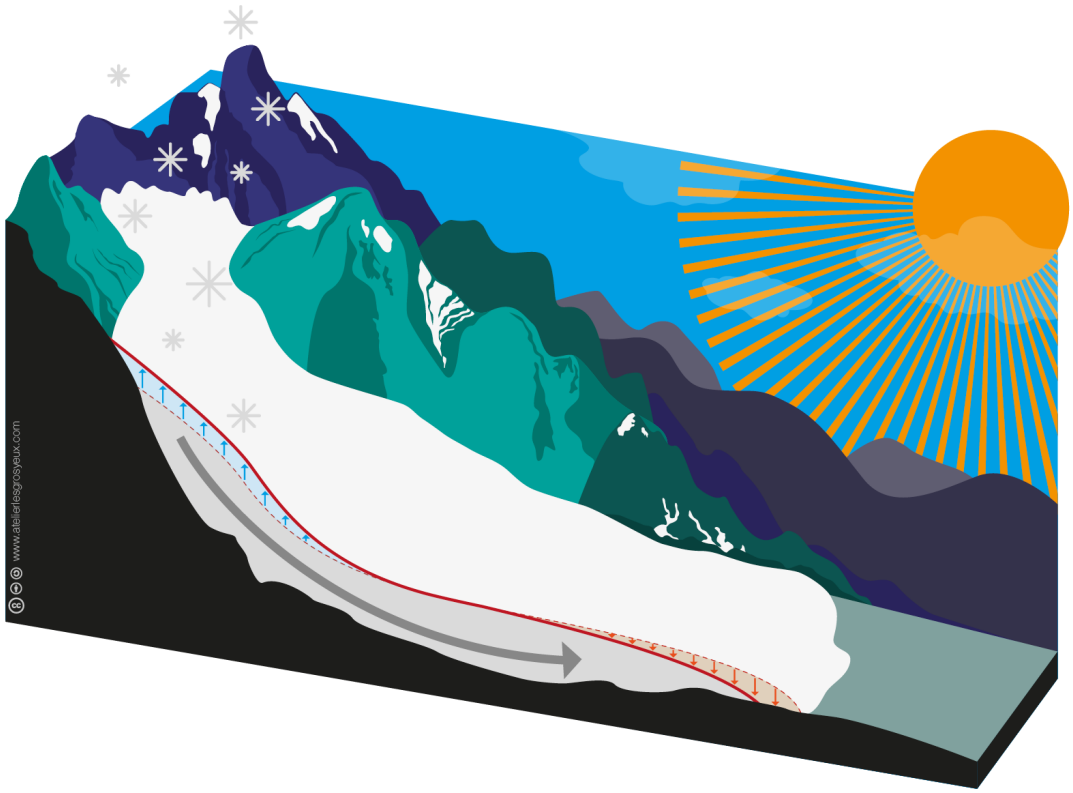

Figure 1.1: Schematic glacier. In blue the net gain is indicated in the accumulation zone and in red the net loss is indicated in the ablation zone. The border between these two zones is the ELA. The grey arrow indicates the flow of the glacier ice. (Figure credit: Anne Maussion, Atelier les Gros yeux)

is not necessarily located on the glacier. In a year with a very positive/negative mass balance, the ELA can be respectively lower/higher than the lowest/highest point of the glacier. It is then at the altitude where the specific mass balance would theoretically be zero. Due to the densification of snow and firn over time, a change in surface elevation of a glacier can not directly be transferred to mass change. As a results it is very labour intensive to get local mass balance measurements. Uncertainty is being added when these point measurements are being extrapolated over an entire glacier.

1.2 Canadian Arctic glacier mass balance

Approximately 23% of the glacier ice volume, not taking into account the ice sheets, is located in the Canadian Arctic Archipelago (CAA, Farinotti et al., 2019). Due to a combination of positive feedback mechanisms, referred to as Arctic Amplification, the

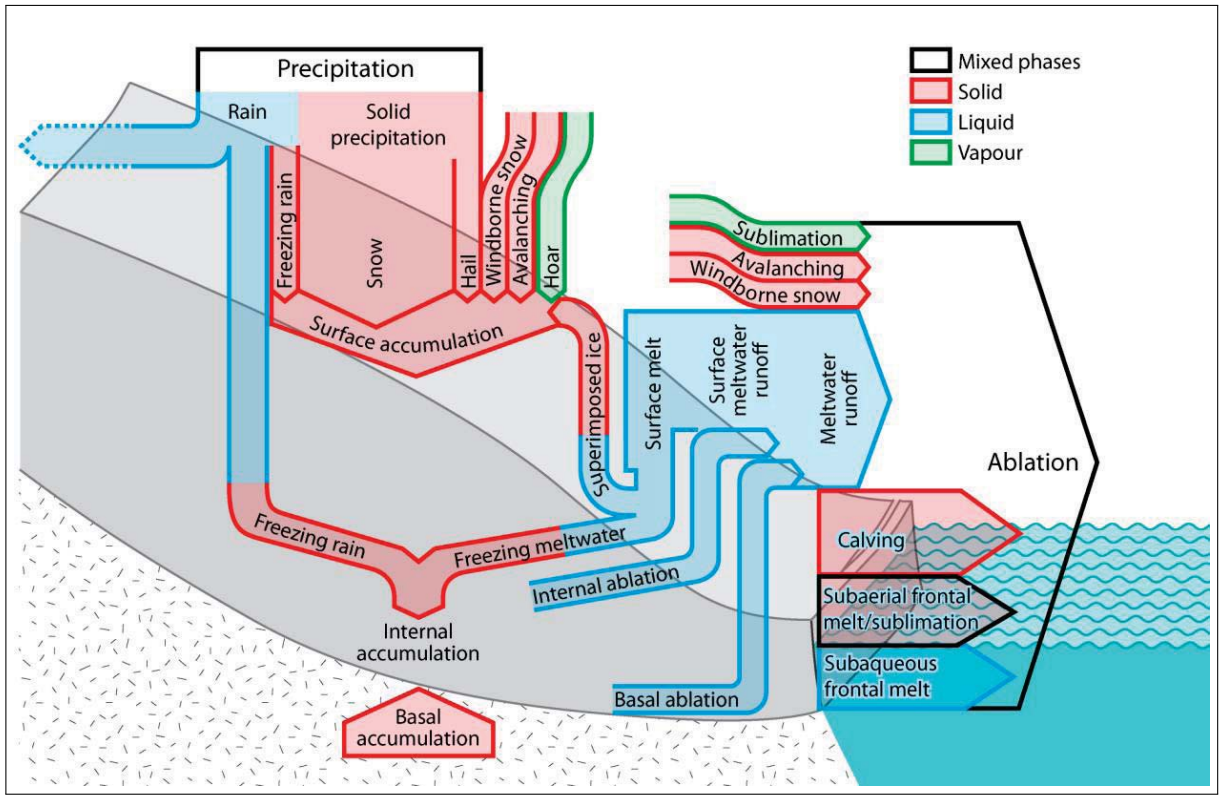

Figure 1.2: Glacier mass balance components. (Figure credit: Cogley et al., 2011.)

surface air temperature in the Arctic has changed on average with a factor 3 to 4 more than the Northern Hemisphere mean, on a range of time scales over the last 3 million years (Miller et al., 2010). There is a high confidence that over the last two decades the surface air temperature has increased more than double the global average in the Arctic (Meredith et al., 2019). During this period the mean near-surface summer temperature increased by 1.1 °C in the CAA (Noël et al., 2018). This resulted in a doubling of the Southern CAA glacial surface mass loss and an even higher increase in the Northern CAA compared to the pre-1996 surface mass loss (Noël et al., 2018). For the period 2003-2009 CE there are different mass-balance estimates for the CAA: −60 Gt/yr (Gardner et al., 2013), −40 Gt/yr (Marzeion et al., 2015) and −47 Gt/yr (Box et al., 2018). Harig and Simons (2016) reported based on data from the Gravity Recovery and Climate Experiment (GRACE) a mass loss acceleration for the region of 11 ± 3 Gt/yr^2. Due to the sharp increase in mass loss the CAA was probably the largest cryospheric contributor to sea-level rise between 2007 and 2009 CE, with an ice loss of 92 ± 12 Gt/yr, without taking into account the ice sheets (Gardner et al., 2011). This is not just the case over this relatively short time window. There are more recent studies that show that the CAA has also lately over a slightly longer period, e.g. 2006-2016 CE, been the region with the largest non ice sheet ice loss as well (Zemp et al., 2019; Wouters et al., 2019; Ciracì

et al., 2020). Understanding the sensitivity of the Canadian Arctic glaciers to regionally changing climate conditions is therefore important for sea-level rise projections, even more so because Arctic Amplification means that the temperature rise in the Arctic is expected to continue to be double that of the global mean (Overland et al., 2019). In addition glacial mass loss in the CAA has an influence on the local hydrology, which can effect the ecology and the fresh water supply to local communities (Sharp et al., 2014).

Several of the ice caps in the Canadian Arctic are remnants of the Innuitian and Laurentide Ice Sheets (Koerner and Fisher, 2002; England et al., 2006), of which some are now smaller than at any time in the last 44 ka (Miller et al., 2013). Other glaciers and ice caps disappeared during the early-to-mid Holocene, before reforming with the cooling climate during the late Holocene (Koerner and Fisher, 2002). The cooling trend in the Arctic corresponds with a period of decreasing Northern Hemisphere summer insolation driven by orbital forcing (Kaufman et al., 2009). Over the last millennium there have however been different episodes of glacier advances and retreats (Solomina et al., 2016). During this period not solar forcing, but volcanic eruptions and changes in GHG concentration have been probably the most important influence on the climate (Schurer et al., 2014). Though volcanic aerosols stay only briefly in the atmosphere, it has been suggested that volcanic eruptions, coincident with a period of minimum insolation driven by orbit forcing, triggered sea-ice/ocean feedbacks that caused the onset of the Little Ice Age (LIA) in the CAA (Miller et al., 2012). On the other hand Slawinska and Robock (2018) made a similar argument, but instead of the orbitally driven insolation minimum they suggest the solar minimum as an enabling forcing. In contrast, it has been argued that glacier build-up in the neighbouring Arctic Atlantic region could have occurred through a combination of stochastic atmospheric cooling and feedbacks without the need for changes in forcing (van der Bilt et al., 2019). Also, changes in land use and land cover had a cooling effect in the CAA over the last millennium (Peng et al., 2020) and could therefore have contributed to glacier advances.

The trend of glacier growth in the CAA has recently been reversed: ice cores suggest that Devon and Aggasiz ice caps have been losing mass at a faster rate in the period 1983-2008 CE than at any time in the last 4000 years (Fisher et al., 2012). The ELA increase from the LIA up to 1960 in the Northern CAA is spatially very variable, ranging from 0 to >600 m (Wolken et al., 2008). There are 11962 glaciers in the CAA (RGI Consortium, 2017), that each have their own characteristics and therefore do not all necessarily respond in the same way to a changing climate. According to a study by Marzeion et al. (2014), an anthropogenic signal can be detected with high confidence in the recent regional glacier mass balance. However the glaciers were out of balance with the climate since 1850 CE. Therefore it would be beneficial to know what led to the mass build-up during the LIA for placing the recent mass loss into perspective and

distinguishing between the different sources of mass loss (Marzeion et al., 2014).

1.3 Goals and Outline

Here the following questions are being raised:

- Is the recent glacier mass loss of land-terminating glaciers in the CAA unprecedented for the last millennium?
- What is the long-term contribution of individual forcings to the recent glacier mass loss?
- How will the glacier volume evolve over the 21^{st} century under a high emission scenario?

Of all the 11962 glaciers in the region (RGI Consortium, 2017), only six have mass-balance measurement time series in the World Glacier Monitoring Service (WGMS, 2017) database with over 10 years of observations: Devon ice cap NW (1960-2016, 56 obs), Baby Glacier (1959-2005, 34 obs), White Glacier (1959-2016, 54 obs), Ward Hunt Ice Rise (1958-1985, 23 obs), Melville South Ice Cap (1962-2016, 54 obs), and Meighen Ice Cap (1959-2016, 57 obs). These time series cover at most about half a century and are not all continuous (Fig 1.3). Little is known about the climate in the northern part of the CAA up to 1946, as from before that year there are only some scattered records of meteorological data from early expeditions (Bradley and England, 1978a). There are however climate reconstructions that go further back in time, like the temperature reconstruction of the Arctic for the last 2000 years by McKay and Kaufman (2014), though its resolution is much coarser than that of the instrumental data. Due to this scarcity of glacier mass balance and climate data, both in time and space, model studies are needed to get a better insight into natural climate variability and glacier evolution.

Here we used the Open Global Glacier Model (OGGM, Maussion et al., 2019a) to simulate the glaciers in the Canadian Arctic over the last millennium. This model allows glaciers to advance, which is an essential feature when simulating glacier evolution over the last millennium. The simulations were started from present day glaciers, because their geometry a millennium ago is poorly known. The initial glacier states are thus not based on the correct geometry for the glaciers at the time. Therefore we assessed, with a sensitivity experiment, the influence that the initial glacier geometry has in the simulations on the glacier evolution and the mass balance. The simulations were forced with the Community Earth System Model Last Millennium Ensemble (CESM-LME, Otto-Bliesner et al., 2016), an ensemble that was designed to study climate variability over the last millennium as a result of both internal variability within the climate system and

changes in individual external forcings.

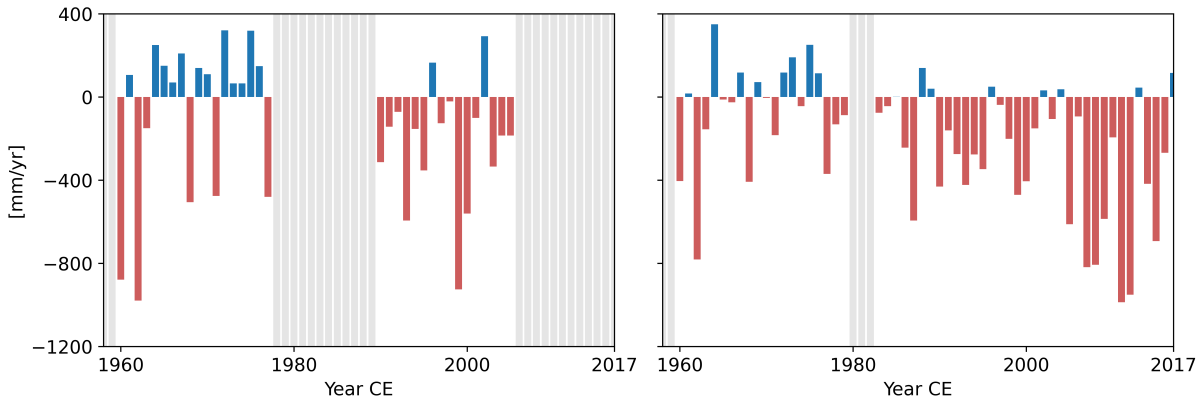

Figure 1.3: The surface mass balance record of Baby Glacier (left) and White Glacier (right) (WGMS, 2020). The grey bars indicate a data gaps.

There are different methods to separate the internal climate variability from the forced response. Taking the ensemble mean of climate simulations reduces and, depending on the ensemble size, might even averages out the internal variability, leaving the response to the external climate forcing (Frankcombe et al., 2015). In case of a single model ensemble mean this gives a good estimate of the true forced signal (Frankcombe et al., 2018). Goosse et al. (2005) showed for last millennium simulations that taking a such mean mostly reduces the inter-annual temperature variability. There is however an asymmetry in the glacier mass balance between warm and cold years (Malone et al., 2019). So even if the mean climate is constant, a change in its variability could have an effect on the mass balance. In the CAA it has been observed that one year with a very negative mass balance can remove the mass that was gained over many years with a positive mass balance (Koerner, 2005). This leads to the question:

- How important is the amplitude of internal variability within the forcing climate for the simulation of glaciers over the last millennium?

While addressing this question with sensitivity experiments, there is a specific focus on the effect of using the ensemble mean as forcing compared to forcing the model with the different ensemble members.

Tidewater glaciers have very specific modelling challenges, not only in their dynamics but also for the ice thickness inversion (e.g. Recinos et al., 2019). Currently 35.7% of the 145999 km^2 by glacier covered area in the CAA are tidewater glaciers (RGI Consortium, 2017). Still about 92% of the glacier mass loss in the region comes from melt water

Figure 1.4: Glacier and ice caps in the CAA according to the RGI v6 (2017). The land-terminating glacier and ice caps (dark blue) are the focus of this study, while the tidewater glacier (light blue) are being excluded. Note there are are many small glaciers in the region, that are not visible due to the size of the map.

run-off and only 8% is due to calving (Gardner et al., 2011). However, it is suggested that throughout the 20^{th} century the mass loss in the Northern CAA, where 258 of the 326 tidewater glaciers are located (RGI Consortium, 2017), primarily occurred through calving (Lenaerts et al., 2013). Over the period 1991-2005 CE 52% of the glacier mass loss on Queen Elizabeth Island was a result of calving. However this share decreased to 10% with increasing mass losses over the following decade (Millan et al., 2017). Even though Cook et al. (2019) show that atmospheric forcing appears to be the primary driver of their changes since the 1950s (unlike in other regions, which are primarily driven by ocean temperatures), it cannot be assumed that that was the case throughout the last millennium. Therefore it has been decided to focus in this study on land-terminating glaciers and ice caps in the region only (Fig. 1.4).

Outline

Addressing the response of CAA land-terminating glaciers to a warming climate requires longer time series with higher spatial resolution than that of the available in situ surface mass balance (SMB) the measurements, which began only around 1959 CE and are available for only a small number of glaciers (WGMS, 2017). Therefore a modelling study was conducted to answer the research questions. The simulations were preformed with OGGM (Maussion et al., 2019a) forced with the CESM-LME (Otto-Bliesner et al., 2016). Chapter 2 gives a general overview of the method that is being used. Chapter 3 presents the sensitivity study, that led to the model set-up that is being used in the second part of chapter 3 and in chapter 4. The focus of this sensitivity study is on the influence of climate variability on glacier evolution and addresses specifically the effect of using ensemble mean climate forcing compared to that of individual ensemble members on the glacier evolution. In the second part of chapter 3 we present and evaluate simulations of the glacier volume evolution of land-terminating glaciers over the last millennium, including those for the initial glacier sensitivity test. The transient last millennium simulations extend to the year 2100 CE under the Representative Concentration Pathway (RCP) 8.5 scenario. These simulations are used to answer the first and third research questions. In addition these transient simulations have been used as a base for studying the influence of individual forcings and to address with that the second research question (Chapter 4). In the final chapter, the conclusions are summarized and an outlook is given.

2 Methods

2.1 Glacier modelling

OGGM is a relatively new and open source model that is in constant development (Maussion et al., 2019a). In this study we use the OGGM v1.0.3 and v1.1 (Maussion et al., 2018, 2019b) to simulate the glacier volume evolution in the CAA (Fig. 1.4). OGGM uses a glacier centric approach (i.e., every single glacier is modelled independently from the others), using ice masks based on the Randolph Glacier Inventory (RGI Consortium, 2015, 2017) and topography derived from the DEM3 data for the CAA (`http://viewfinderpanoramas.org/dem3.html`). The ice thickness is being computed, by using an ice thickness inversion method that is based on Farinotti et al. (2009). OGGM is a flowline model that uses the isothermal shallow ice approximation for its dynamics and defines the flowlines, which consist of a main flowline with possibly tributary branches, by following the method of Kienholz et al. (2014). For the mass balance a variation of the temperature index model by Marzeion et al. (2012) is used. An overview of the workflow in OGGM can be found in figure 2.1.

2.1.1 Mass balance model

The monthly mass balance m_i at altitude z is calculated as follows:

$$m_i(z) = p_f P_i^{solid}(z) - \mu^* max(T_i(z) - T_{melt}, 0) - \beta^*.$$

Where monthly solid precipitation P_i^{solid} is multiplied by the precipitation correction factor p_f (set to 2.5 globally). As there is no precipitation lapse rate in the model, p_f can be seen as a global correction factor for orographic precipitation, avalanches, and wind-blown snow. The precipitation is treated as liquid above 2 °C, solid below 0 °C and the fraction of solid precipitation is being linearly interpolated between these two boundary values. The temperature lapse rate is set by default to 6.5 °C/km. For the monthly mean temperature T_i exceeding the melting point (T_{melt}; −1 °C by default), the temperature excess [°C] is multiplied by the temperature sensitivity parameter μ^* [mm

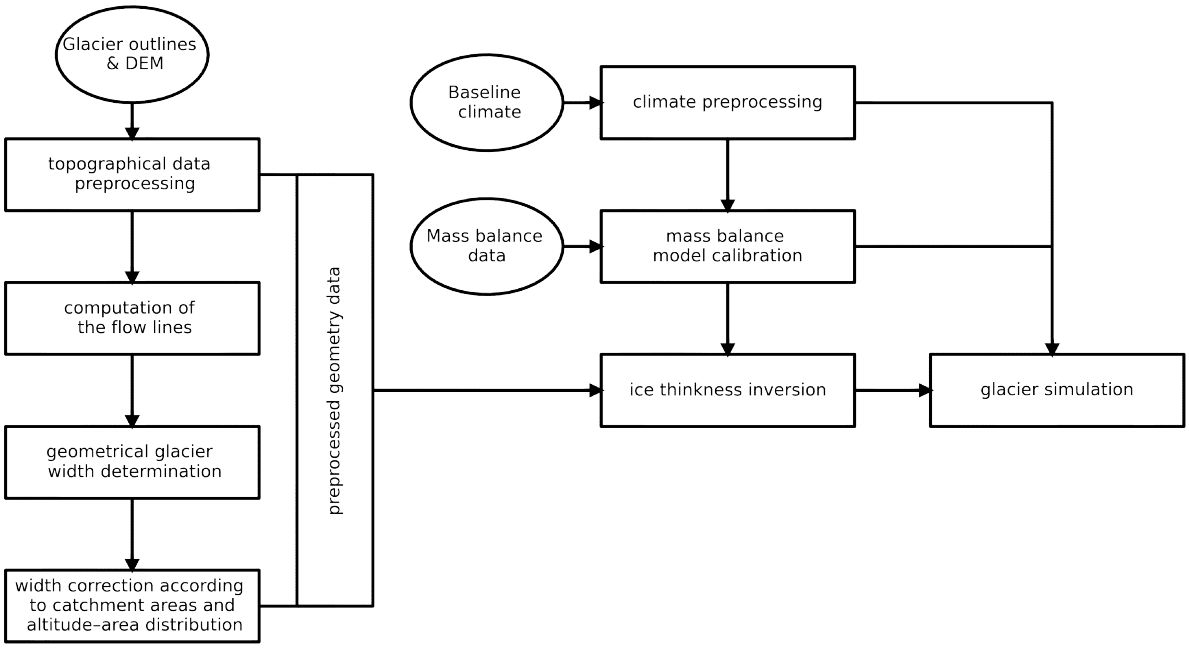

Figure 2.1: A simplified schematic of the workflow in OGGM. The left side of the flow chart presents the steps for preprocessing the surface geometry of the glacier and its surroundings, including generating flowlines both for the glacier itself and down stream of the glacier tongue. The geometrical glacier width determination is the calculation of glacier width perpendicular for each grid point along the flowline. Because this does not conserve the total area of the glacier and the distribution per elevation bin, the final preprocessing step performs some corrections.

yr^{-1} K^{-1}]. Both μ^* and residual bias β^* [mm/yr] are parameters that originate from the automated calibration procedure of the model, which is used by default in OGGM. All the parameters are kept constant over time, so the sensitivity of the glacier to temperature does not change over time.

The temperature sensitivity of a glacier, μ^*, can be estimated when using a climate time series in combination with the mass balance measurements. One of the glaciers in the CAA that has a glacier mass balance record is White Glacier (WGMS, 2017), which will be used here as an example (Fig 1.3). The values for μ can be computed by assuming that the glacier mean specific mass balance, over a 31-year period centred around year t, is zero. For each t there is a candidate μ(t) for the temperature sensitivity (Fig 2.3). During the computation of μ the glacier geometry is kept constant. This geometry is determined by the digital elevation model (DEM) and the RGI outline (Fig. 2.2). The method assumes that in one of these years the glacier was near equilibrium with the climate and that therefore the computed μ is close the actual μ. The next step is that the model runs for the years with a mass balance record, using the different μ candidates.

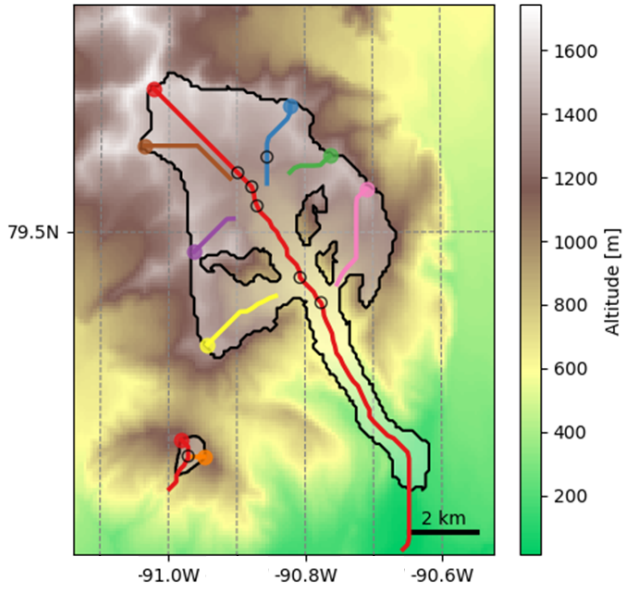

Figure 2.2: Example glaciers. The outlines of White Glacier (in the centre) and Baby Glacier (bottom left) and their flowlines, in different colors on top of the local topography (DEM3 dataset post-processed by OGGM). The filled circles indicate the origin of the flowlines and the empty circles indicate the locations where one flowline connects to another; in other words, the point where the flux of the upstream flowline is added. (This figure has been produced with one of the graphics functions from OGGM.)

The computed mass balance is compared with the mass balance record, resulting in a mean bias that is based on the years with mass balance measurements (Fig 2.3). The μ that has the smallest corresponding bias is μ^*. For White Glacier this results in a μ^* of 177 mm yr^{-1} K^{-1} and a bias of 48 mm/yr.

Many glaciers do not have a mass balance record. Globally there are about 200,000 glaciers in the RGI. Only 254 of those glaciers have mass balance measurement time series in the WGMS data base that can be used for the calibration of OGGM (Maussion et al., 2019a). The μ^* differs from glacier to glacier. Neighbouring glaciers can have a very different μ^*, as this value is mostly dependent on glacier-specific characteristics, such as topographical shading and clouds. Baby glacier has a μ^* of 728 mm yr^{-1} K^{-1}, which is roughly 4 times larger than the μ^* of its neighbour White Glacier (Fig 2.2). Because μ^* is so glacier-specific, it is not being spatially interpolated between glaciers. Instead t*, the year that μ^* originates from, and the corresponding bias are spatially extrapolated. For White Glacier and Baby Glacier t* is respectively, 1982 and 1924 CE. For the glaciers without a mass balance record, μ^* is computed in t*. Cross-validation has shown that this method gives better results than the interpolation of μ^* (Marzeion et al., 2012). For the example glaciers, it is clear that extrapolating t^* would have led

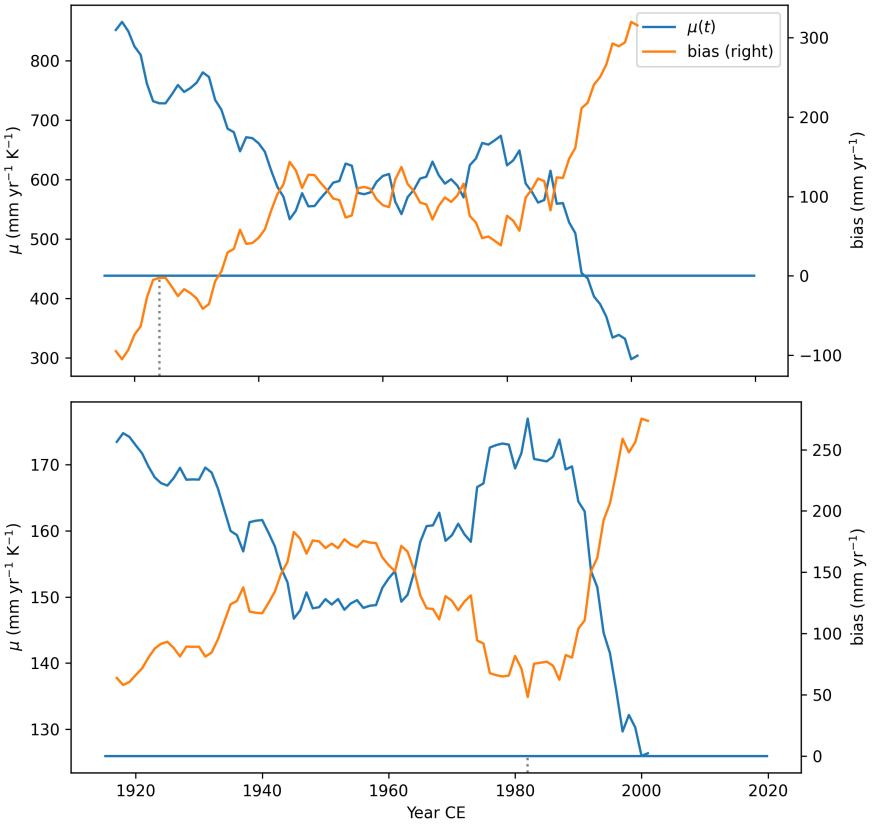

Figure 2.3: The μ candidates with their corresponding bias for two example glaciers with a mass balance record. Baby Glacier in the upper and White Glacier in the lower plot. The dashed line indicates t*, the year from which μ^* and its respective bias has been selected by the calibration procedure.

to a much better approximation of μ^* than extrapolating μ^*, in the event that one of the glaciers would have lacked a mass balance record. Though t* is very different for both glaciers, the μ candidate of White Glacier for the t* of Baby glacier is with 167 mm yr^{-1} K^{-1} a way better approximation of White Glaciers μ^* than taking Baby glaciers μ^*, which are respectively 177 mm yr^{-1} K^{-1} and 728 mm yr^{-1} K^{-1}. The μ candidate of Baby Glacier in the t* of White Glacier is 649 mm yr^{-1} K^{-1}. This underestimates μ^* with 11% instead of 76 %.

By default Climatic Research Unit (CRU) climate data is used in OGGM both for the calibration procedure and for doing model simulations. Before the calibration procedure takes place, the CRU monthly climate data of the last century (CRU TS, Harris et al., 2014) is down scaled to the CRU 1961-1990 CE climatology (CRU CL, New et al., 2002). The down scaling is done with the delta method, for each month separately (e.g. all the Julys receive the same correction). The temperature, T, is computed by applying

temperature anomalies:

$$T = CRU_{TS} - \overline{CRU_{TS(1961-1990)}} + CRU_{CL}.$$

The monthly precipitation, P, is being scaled to the CRU CL:

$$P = \frac{CRU_{TS}}{\overline{CRU_{TS(1961-1990)}}} \cdot CRU_{cl}.$$

The CRU CL has with 0.167° a higher resolution than the 0.5° resolution of CRU TS. However, the main advantage of applying the delta method in this case is the gain of elevation data, which is required for computing the mass balance. The CRU CL data set contains heights, while the CRU TS does not. (See Marzeion et al., 2012 and Maussion et al., 2019a and `https://docs.oggm.org/en/v1.1/mass-balance.html` for more information on both the calibration procedure and the mass balance model).

2.1.2 Ice thickness and dynamics

The ice thickness inversion, h[m], in the model is based on the method of Farinotti et al. (2009), using an ice density, ρ, of 900 kg/m^3. There is no distinction made between ice, firn and snow. In the Ice Thickness Models Intercomparison eXperiment (ITMIX), OGGM ranked among the best models (Farinotti et al., 2017). The inversion method makes use of the DEM, the glacier outline and the calibrated mass balance model. The method assesses how thick the glacier needs to be in order to retain its shape with the glacier dynamics that the model has under the average mass balance in the 31 years centered around t*. The default glacial bed shape in OGGM is a parabola; however, there are some exceptions to this. In the case that a section along the flowline is touching a neighboring catchment or ice divide, than the shape of that section will be rectangular. This is also the case for the terminus of a tidewater glacier, however those will not be considered in this thesis.

The glacier geometry gets updated once a year based on the glacier mass balance and the ice dynamics. The ice flux q [m^3/s]:

$$q = uS,$$

is a function of the velocity of the ice, u [m/s], and through area S [m^2], which is the

section perpendicular to the flowline. The ice velocity is computed with the shallow ice approximation (Hutter, 1983):

$$u = \frac{2A}{n+2} h \tau^n,$$

which neglects lateral drag. Here Glen's A is the creep parameter (A = 2.4*10^{-24} s^{-1} Pa^{-3}) and n Glen's flow law exponent (n = 3). The basal shear stress τ is computed as follows:

$$\tau = \rho g h \alpha,$$

where g is the gravitational acceleration (9.81 m/s^2) and α the surface slope along the flowline. The ice flux is computed on a staggered grid using a forward finite difference scheme. The spacing between the grid points, dx [m], of the respective glacier is based on area [km^2] of the respective glacier in the RGI,

$$dx = d1 * area^2 + d2,$$

where d1 is 14 and d2 is 10 by default. The grid spacing is clipped to a maximum of 200 m. To ensure numerical stability the ice flux computation uses an adaptive time stepping scheme following the Courant-Friedrichs-Lewy (CFL) condition:

$$\Delta t = \gamma \frac{dx}{max(u)},$$

where Δt [s] is the time step. The CFL number, γ, ranges from 0.1 in the ambitious set-up and to 0.01 in the conservative set-up. Δt is being clipped to a set minimum and maximum depending on the set-up. By default the time step can be as large as 15 days in the ambitious set-up to as small as 6 minutes in the most conservative set-up. The time step clipping to a minimum is being done to avoid very long computation times. However when the glaciers encounter an error during the simulation, it will automatically be simulated again using more conservative time stepping. In the set-up that was used in this thesis, the first attempt was to use the default CFL number of 0.05, followed if

needed two successive times with increasingly smaller time stepping being allowed. If the third simulation attempt would fail, it would raise an error and move on with the next glacier. As of OGGM version 1.3 an improved numerical solver is being used. The glacier length decreases once all the glacier ice at the glacier snout, the most downstream point along the glacier flowline, has melted away. The glacier grows in length once the snow in front on the glacier survived for a year. At that point this snow is considered glacier ice and a part of the glacier (for more information see Maussion et al., 2019a and `https://docs.oggm.org/en/v1.1/ice-dynamics.html`).

2.2 Climate forcing

In the framework of the Coupled Model Intercomparison Project phase 5 and the Paleo Model Intercomparison Project phase 3 (CMIP5/PMIP3) different model groups preformed the transient simulations over the last millennium with fully coupled general circulation models (GCMs) using the same experimental set-up (Taylor et al., 2012). Otto-Bliesner et al. (2016) expanded on this with the CESM-LME by generating an ensemble of transient last millennium simulations, using the CESM1.1 (Hurrell et al., 2013). The study used the fully coupled CESM, with a $\sim 2^{\circ}$ resolution of the atmosphere and the land component and a $\sim 1^{\circ}$ resolution in the ocean and sea ice component. The CESM-LME was done to study natural climate variability, including internal climate variability, making it a very suitable dataset to use in this study. In CESM the glaciers are prescribed and not dynamically modelled, hence this model by itself provides no insight into the influence of natural climate variability on glacier mass balance in the CAA.

The CESM-LME consist of both fully forced, single forced and control simulations. The two control simulations have a constant forcing throughout the simulation. The 850 CE control simulation is branched off the 1850 CE control simulation after 650 model years. The 850 CE control simulation is used to branch all the other simulations from. For all simulations this is done after 200 model years, except the ozone-aerosol single forced simulations, which branch 1000 years later. References in this thesis to the CESM-LME control simulation are to the 850 CE control simulation from the point that most simulations are branched from onwards, thereby excluding the first 200 model years of the simulation.

The fully forced simulations are forced with the same volcanic, solar, orbital, ozone, aerosol, land use and land cover change (LULCC) and greenhouse gas (GHG) forcing. Up to 1850 CE the forcings are similar to those in the Last Millennium simulation that has been done with the Community Climate System Model 4 (CCSM4, Landrum et al.,

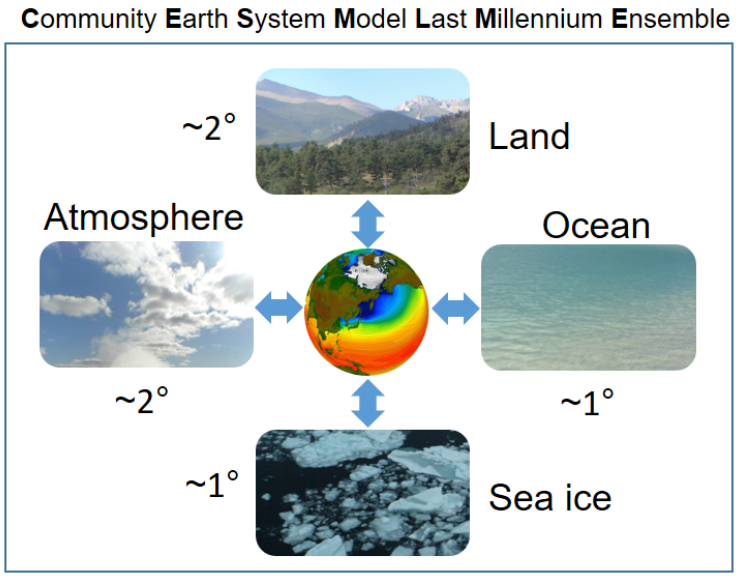

Figure 2.4: A schematic of the CESM-LME. For the CESM-LME the fully coupled version of CESM was used, meaning that the four model components interacted together via coupler. The resolution of different model components is noted next to the respective model component.

2013) and after that to those in the CESM Large Ensemble (CESM-LE, Kay et al., 2015). The changes over time in the LULCC forcing are based on reconstructions of crops and pastures by Pongratz et al. (2008) and Hurtt et al. (2011). The solar forcing is based on the reconstruction by Vieira et al. (2011) and an 11-year solar cycle has been superimposed (for more details see Schmidt et al., 2011). The ozone and aerosol forcing is the only forcing that is fixed at its control values up to 1850 CE and evolves over time for the remainder of the simulations (Otto-Bliesner et al., 2016). These are anthropogenically induced changes ozone and aerosols (Huang et al., 2018). The volcanic forcing is based on the reconstruction by Gao et al. (2008) and during the 20^{th} century, like in CMIP5, on the dataset of Ammann et al. (2003). The orbital forcing is calculated following Berger (1978) and Berger et al. (1993) and the GHG concentrations are based on Antarctic ice cores (Schmidt et al., 2011).

The 13 fully forced simulations only differ from each other because of a tiny perturbation in the initial condition of the air temperature. As a result, the differences within the ensemble are solely caused by internal variability of the climate system. Four of these simulations are extended under the RCP8.5 scenario up to 2100. This extension has not been done under other scenarios. The single forced simulations have only one forcing that changes over time. The other forcings are fixed at their initial values in 850 CE, except for the ozone-aerosol forcing that has 1850 CE as initial year. Like with the fully

forced simulations, also for the single forced set-up, a couple of simulations have been done with the same forcing: volcanic (5), orbital (3), solar (4), LULCC (3), ozone-aerosol (4) and GHG (3). As a result the simulations in the respective single forced ensembles also only differ from each other due to internal climate variability (Otto-Bliesner et al., 2016).

3 Recent glacier mass loss in the Canadian Arctic Archipelago in a last millennium perspective

3.1 Introduction

Between 1961 and 2016 the glacier and ice caps in the CAA contributed 1,485 Gt (4.1 mm) to global sea level rise and recently (over the period 2006-2016 CE) CAA was the region with the largest non ice sheet glacier mass loss (Zemp et al., 2019). The aim of this chapter is to place the recent mass loss in the perspective of the glacier mass loss in the region over the last millennium and investigate how this might evolve under a high emission scenario. For this purpose model experiments have been done with OGGM driven by the climate of the CESM-LME (Maussion et al., 2019a; Otto-Bliesner et al., 2016), hereby being the first study to use OGGM for millennium long transient simulations on a regional scale. Though OGGM has been used before for last millennium transient simulations, none of these simulated glaciers are in the CAA (Goosse et al., 2018; Parkes and Goosse, 2020). This is one of the reasons the sensitivity study was needed, leading up to the experimental set-up for the last millennial fully forced glacier simulations that were used to put the recent mass loss into perspective.

3.1.1 Sensitivity study

Internal climate variability and temperature fluctuations have an influence on the glacial volume of the Greenland Ice Sheet (Tsai et al., 2017; Mikkelsen et al., 2018). However previous glacier studies have mainly focused on the influence of a change in the mean climate on the mass balance, while little is known about the influence of changing climate variability on glacier mass balance. Nonetheless temperature variability on time scales shorter than the glacier response time can have a strong influence on glacier mass balance (Farinotti, 2013). Because melting occurs above a threshold temperature, the number of positive degree days (and therefore glacier mass balance) is influenced by both the mean temperature and temperature variability. Hence zero-mean temperature

variability can have a non-zero-mean effect on mass balance, due to the mass balance asymmetry between warm and cold years as a result of the mass balance profile (Malone et al., 2019). Some studies showed that climate variability can have a significant influence on glacier length (Roe and O'Neal, 2009; Roe, 2011; Farinotti, 2013; Goosse et al., 2018; Huston et al., 2021). However, these studies were done for a relatively small number of well observed glaciers, mostly on a short time scale. Aside from the study by Huston et al. (2021), none of these studies included glaciers in the CAA. Though it has been observed that one year with a very negative mass balance can reverse many years of positive mass balance (Koerner, 2005). The goal of the sensitivity study is to asses the role of the amplitude of the internal variability within the forcing climate data on the glacier mass balance in the CAA during the last millennium, while specifically focussing on the effect of ensemble mean forcing. In this context some additional experiments were preformed to asses the role of the mass balance - elevation feedback in the sensitivity experiment and the amplitude of the temperature variability. Based on these results adjustments have been made to the experimental set-up for the transient fully forced glacier simulations.

3.1.2 Fully forced transient simulations - 850-2100 CE

The transient fully forced simulations have been validated with the in situ mass balance measurements (WGMS, 2017), the present day glacier covered area (RGI Consortium, 2017), the present day inverted glacier volume (Maussion et al., 2019a) and modeled SMB derived from the Regional Atmospheric Climate Model (RACMO2.3) starting in 1958 CE (Noël et al., 2018). In order to make a comparison with the RACMO2.3 SMB that is not hampered by the natural year-to-year climate variability, simulations were branched off the transient fully forced simulations and from there on forced with the CERA-20C and CRU TS (Laloyaux et al., 2018; Harris et al., 2014).

The transient fully forced simulations have been extended under the RCP8.5 scenario, the only scenario under which the CESM-LME simulations have been extended (Otto-Bliesner et al., 2016). These projections are used to give an upper boundary for the future mass loss, to indicate what would be the earliest moment when the mass loss for the region becomes unprecedented for the last millennium. However there is no consensus on how the RCP8.5 scenario should be valued. According to Hausfather and Peters (2020), the RCP8.5 scenario should be seen as a worst case and unlikely scenario. However an even more recent study by Schwalm et al. (2020) showed that between 2005 and 2020 RCP8.5 scenario was close to the actual emissions. Even though the RCP8.5 overestimates the current emissions and stated policies up to 2050, it is still the best matching RCP scenario up to the middle of the century and contains highly plausible

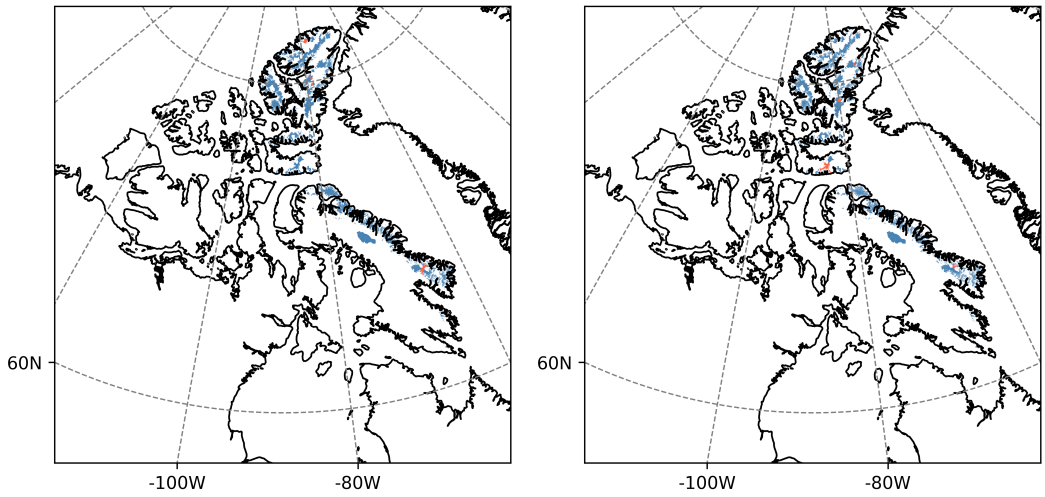

Figure 3.1: The Domain: land-terminating glaciers in the CAA. In blue the ones that were successfully simulated in the transient simulations and in red the ones that failed. On the left side the domain for the sensitivity study (RGI Consortium, 2015) and on the right domain of the fully forced transient simulations (RGI Consortium, 2017). Note there are are many small glaciers in the region, that are not visible due to the size of the map.

CO_2 levels for the end of the century (Schwalm et al., 2020).

3.2 Method

3.2.1 Sensitivity study

Model set-up

For the sensitivity study OGGM v1.0.3. is being used (Maussion et al., 2019a). The domain is set to the land-terminating glaciers of the CAA North and South, as defined by the RGIv5 (Fig. 3.1). The model has been initialized with its default settings, with an increased border parameter to allow the glaciers to advance further when evolving over time. Since the geometry of CAA glaciers is poorly known in the year 850 CE, ice volume and extent were initialized based on their present day state. Therefore they do not account for the glaciers that were present during the last millennium, but had already disappeared around 2003, i.e. the year of which most of the RGI glacier outlines are based.

The total initial glacier volume, that has been inverted with the default method in

OGGM, is 19796 km^3 (Maussion et al., 2019a). This volume does not include tidewater glaciers and 142 other glaciers (1.9% total area) that are not included due to errors during the simulations. A part of the errors occur during initialization of the model and a part of the errors are caused by glaciers that exceed the domain boundary. More information about why in rare occasions glaciers can not be modelled with OGGM can be found in Maussion et al. (2019a). When an error occurs for a glacier in one simulation, all the results for that glacier are removed for the respective experiment, the transient simulations or the temperature variability sensitivity experiment. This does not affect our conclusions, because these glaciers only make up for a small part of the total and are expected to behave in a similar manner as the other glaciers.

Transient simulations - 850-2005 CE

The goal of this sensitivity study is to investigate the influence of the amplitude of climate variability in the forcing climate on the glaciers in the CAA during the last millennium, while specifically focussing on the effect of ensemble mean forcing. Here our first step is to generate an ensemble where the ensemble members only differ from each other as a result of internal climate variability. In our simulations OGGM was driven with the temperature and precipitation of the fully forced CESM-LME simulations (Otto-Bliesner et al., 2016). To force OGGM, the CESM-LME timeseries are bias corrected to the glacier scale with a relatively simple but robust statistical method similar to the "delta-method" (e.g. Ramirez-Villegas and Jarvis, 2010) applied with CRU (New et al., 2002; Harris et al., 2014) as a reference climate. The monthly mean 2-m air temperature of each of the ensemble member ($CESM_m$) was used to calculate the temperature time series (T_m) in the following way:

$$T_m = CESM_m - \overline{CESM_{ens}} + \overline{CRU_{cl}},$$

where the bar denotes the monthly time average over the period 1961-1990 CE (i.e. one average for each calendar month) and $CESM_{ens}$ denotes the monthly average over all ensemble members. This "ensemble reference climatology" was subtracted from each ensemble member to generate the temperature anomalies, which are then applied to the CRU CL dataset (monthly climatology for 1961-1990, New et al., 2002). In practice, this applies a monthly bias correction while keeping the variability of each member unchanged. The reason we used the ensemble mean instead of each member's temporal mean (the "standard delta method") was because of the significant difference of the 30-year averages between the ensemble members. Treating the ensemble members separately would therefore have increased the ensemble spread and introduced a systematic bias, by generating ensemble members that are systematically warmer/colder than the

other ensemble members.

The total monthly precipitation was down scaled similarly to temperature, but here we use scaled anomalies instead:

$$P_m = \frac{CESM_m}{\overline{CESM_{ens}}} \cdot \overline{CRU_{cl}}$$

We use scaled anomalies because the standard anomaly procedure could lead to negative precipitation in some cases. This down scaling procedure is the same as the one that is used by default in OGGM with the CRU TS dataset, or to GCM data in Marzeion et al. (2012, 2014, 2018). The only difference is that the ensemble mean is used instead of each member independently as explained above. The influence of internal climate variability in the forcing climate on the glacier mass balance in the Canadian Arctic has been further investigated by reducing the internal climate variability. In this "reduced variability experiment", OGGM was forced with the ensemble average instead of each ensemble member independently, which leads to a great reduction of interannual climate variability in the forcing climate.

Mass balance - elevation feedback

Typically the mass balance rate increases with altitude. This is caused by the temperature lapse rate and the generally increasing amount of precipitation with altitude (Oerlemans, 2008). When a glacier has a positive mass balance, the surface of the glacier increases. This increased surface elevation will have a higher surface mass balance than it would have had with its previous geometry, in this way generating a positive feedback loop. Even though there is no precipitation gradient implemented in the model set-up, there is still a positive feedback due to the temperature lapse rate. For this reason the transient simulations that are described in the previous paragraph have been repeated with this feedback turned off in the model, to get an insight into how much the differences between the simulations are being enhanced by this mechanism. Turning the mass balance - elevation feedback off in the model means that the height at which the mass balance is calculated for a point along the glacier flowline stays constant throughout the simulation. This configuration allows the glacier geometry still to evolve over time, only the altitude at which the mass balance is computed along the flowline stays the same as in the first model year and is thus after that first year not necessarily equal to the altitude of the glacier surface at that point.

Sensitivity experiment: Temperature variability

The CAA is cold, with annual mean 2-m air temperatures ranging from -20 °C on central Ellesmere Island to -10 °C on southern Baffin Island (Sharp et al., 2014). Due to the short melt season in the region a change in the summer climate can have a significant influence on the glacier mass balance in the region (Bradley and England, 1978b; Koerner, 2005). The glacier mass balance is strongly correlated with the summer temperature and this does not seem to be much influenced by winter precipitation (Bradley and England, 1978a; Koerner, 2005; Gardner and Sharp, 2007). Therefore it was chosen to investigate further the impact of temperature variability on the glacier mass balance in the region, hereby looking at the frequency modes and the magnitude of the variability. This was done by changing the amplitude of the temperature anomalies. In a first experiment, we repeated the ensemble member 6 T_m and P_m time series of the period 1950-2000 CE for 2000 years. Ensemble member 6 was chosen for this sensitivity experiment, because it represents the median of the ensemble for that period and we therefore assumed that it will give a general picture that is representative for the ensemble. The temperature anomalies of this time series were then scaled as follows:

$$T_{m,scaled} = sc_f(T_m - \overline{T_{m(1950-2000)}}) + \overline{T_{m(1950-2000)}}$$

The following scaling factors (sc_f) have been used: 0.5, 0.75, 1 (no scaling), 1.5 and 2. In a second experiment, the role of temperature variability has been further tested by using a moving average with different window (boxcar) sizes: 1 (no moving average), 3, 10, 25 and 50 years. The yearly temperature cycle was kept intact by using the moving average for each month separately. Except for the different time series that were used to force OGGM, the set-up of the model was the same for the sensitivity experiments as for the transient simulations. In addition to the sensitivity experiments where either the temperature anomalies were scaled or smoothed, an experiment of 250 model years was done with all 25 combinations of window sizes for smoothing and the different scaling factors. Effectively this results in 21 different combinations, as there is no net difference between the runs with a window size for smoothing over 50 years for the different scaling factors. The climate time series that is repeated has in that case the same length as the smoothing window, so each year ends up having the same temperature cycle. All these simulations for the sensitivity experiment were started from the same 5000 year long spin-up run, with a repeated forcing of the 1950-2000 CE climate. This spin-up simulation was, like the transient simulations, started from present-day glaciers.

3.2.2 Glacier evolution 850 - 2100 CE

Model set-up

Based on results of the sensitivity study slight adjustments have been made to the model set-up with regard to the climate forcing for the experiments in the second part of this chapter (Table 3.1). In addition more recent versions of OGGM (v1.1.) and the RGI (v6) are being used here.

Climate forcing

To simulate SMB and ice volume over the last millennium, we used the 13 CESM-LME fully forced simulations to drive the OGGM (Maussion et al., 2019a). Four of these last millennium simulations continue under the RCP8.5 scenario until 2100 CE (Otto-Bliesner et al., 2016). In those cases the full length of the extended simulations has been used to force OGGM. This ensemble of simulation will be referred to as the *fully forced simulations*.

Based on the results of the sensitivity study, the temperature anomalies were scaled to the CRU TS (Harris et al., 2014) by using the standard deviation over the reference period. The monthly scaling factor is again based on the whole ensemble and applied to the individual ensemble members. This correction was applied, because of the higher year-to-year temperature variability in the CESM-LME compared to the CRU TS (Fig. 3.12), to which the mass balance of CAA glaciers is very sensitive (Chapter 3.3). Due to the temperature threshold for melting, temperature variability also has an influence on the positive degree days and therefore the mass balance (Farinotti, 2013). The temperature variability also influences the variability of the ELA, which is important for the mass balance, as upward and downward shifts of the mass balance gradient of the same magnitude do not have the same effect as keeping it constant, due to the glacier geometry and the shape of the mass balance gradient. Through asymmetry between the mass balance in warm and cold years the magnitude of inter-annual air temperature variability can influence the glacier mean state (Malone et al., 2019). Not correcting this effect would in this case lead to a significant underestimation of the glacier volume in the CAA (Chapter 3.4).

Sensitivity to initial conditions

It is a big assumption to initialize the simulations with present-day glaciers. Therefore sensitivity tests were performed to asses the implications of this assumption. As a first

	part 1	part 2
	Sensitivity study	Glacier evolution 850-2100 CE
OGGM version	1.0.3.	1.1.
RGI version	5	6
scaled temperature anomalies	False	True

Table 3.1: The differences in the model set-up between the part 1, the sensitivity study, and 2, the fully forced transient simulations, of this chapter. Scaled temperature anomalies refers to the scaling of temperature anomalies in the transient simulations, not to the temperature variability sensitivity experiment (Chapter 3.2.1)

test the model was initialized with the highest and lowest regional glacier volume state from the regular transient runs and forced with the climate that resulted in those states, respectively CESM-LME ensemble member 10 and 3. Another simulation was started from a state without glaciers, which is extreme and unrealistic, and forced with CESM-LME ensemble member 10. To get more insight into the influence of the initial conditions on the glacier evolution, an additional 6-millennium long run was done to see how long a difference in glacier volume can persist. One of these simulations starts from the same initial conditions as the fully forced transient simulation, while the other one starts from zero glacier volume. Both these simulations were forced with the last 6 ka of the CCSM Simulation of Transient Climate Evolution over the Last 21,000 Years (TraCE-21ka: He, 2011; Liu et al., 2014).

Validation

For local validation of the simulations observations were used. The simulated area at present day was compared to the glacier area according to the RGI (RGI Consortium, 2017). The present-day simulated volume was compared to the initial volume that was obtained by the glacier bed inversion of present day glaciers (Maussion et al., 2019a; Farinotti et al., 2019). The simulated glaciers with a SMB record in the World Glacier Monitoring Service (WGMS) of at least 5 years were compared to those records.

On a regional scale, the SMB of glaciers that were successfully modelled with OGGM were validated by using the corresponding SMB derived from the regional climate model RACMO2.3 (Noël et al., 2018). RACMO2.3, forced by ERA-40 (1958-1978; Uppala et al., 2005) and ERA-Intenim (1957-2015; Dee et al., 2011) reanalysis products, runs

at an 11 km spatial resolution for the period 1958-2015 CE, and is further statistically down scaled to a 1 km grid (Noël et al., 2018). Due to the internal variability of the climate system, there is a spread in the transient simulations. In order to make a better comparison, between our simulations and the RACMO2.3 SMB, additional simulations were preformed. A part of these simulations were branched of the 13 ensemble members in 1957 CE and than forced with the CRU TS anomalies (Harris et al., 2014; New et al., 2002). The other part of the simulations were branched of the transient fully forced simulation that resulted in median regional volume in the year prior to the start of the RACMO2.3 data, 1957 CE, and forced from there with the Coupled Ocean-Atmosphere Reanalysis of the 20th Century ensemble (CERA-20C, Laloyaux et al., 2018) scaled climate anomalies with respect to CRU timeseries (1961-1990 CE). These 23 simulations together will be referred to as the climate data forced simulations.

3.3 Sensitivity study - Results

3.3.1 Transient simulations

From the start of the transient simulation the total glacier volume in the region declines (Fig. 3.2). This decline continues throughout the Medieval Warm Period (MWP[3], here defined as 950-1250 CE, e.g.: Masson-Delmotte et al., 2013) and into the LIA (here defined as 1450-1850 CE, e.g.: Masson-Delmotte et al., 2013), until it reaches its lowest point in 1584 CE with an ensemble mean of 12,748 km^3. However for individual ensemble members the time of reaching the lowest volume ranges from 1252 to 1729 CE, with volumes ranging from 11,490 to 13,370 km^3. The ensemble mean volume starts to increase during the LIA towards a maximum of 13,929 km^3 in 1918 CE. The different ensemble members reach a maximum between 1787 and 1990 CE, with a volume ranging from 13,183 to 15,529 km^3. After that, it decreases again to a mean volume of 13,297 km^3, range 12,486-14,471 km^3, in 2005. This present day simulated volume is below the present day volume that was used for initialisation.

The mean simulated equilibrium line altitude (ELA) of the ensemble is 909 m, ranging from 896 to 919 m for the different ensemble members, and it has a mean standard deviation of 190 m. The mean ELA of the glaciers is on average higher during the MWP (941 m), lower during the LIA (878 m) and high in recent times (950 m for the period 1950-2005 CE). The ELA for the simulation that was forced with the CESM-LME ensemble mean is lower and much less variable; this pattern is consistent throughout the region (Fig. 3.3). This simulation has a mean ELA of 879 m and a standard deviation of 74 m. It has an average ELA of 912 m during the MWP, 848 m during the LIA and 921 m for the period 1950-2005 CE. The total glacier volume in that simulation is significantly larger and outside the range of the ensemble.

The results of the transient simulations show different patterns of glacier evolution for different glaciers. Baby Glacier and White Glacier, a respectively small and larger sized glacier, were chosen to use as an example of individual glacier results (Fig. 2.2). The choice of these glaciers was based on the fact that they have a relatively long mass balance record and are therefore better known and studied than other glaciers of similar size (e.g. Thomson et al., 2017). The glaciers are located near to each other on Axel Heiberg Island. Baby glacier is with 0.72 km^2 quite representative in size for the region, as it is in the 44^{th} area percentile. Due to the large amount of small glaciers and a small amount of very large glaciers the distribution is skewed, with a glacier mean size of 12 km^2 (88^{th} area percentile). White Glacier is on the other hand with 40 km^2 (96^{th} area percentile)

[3]This period is also being referred to as the Medieval Climate Anomaly (MCA).

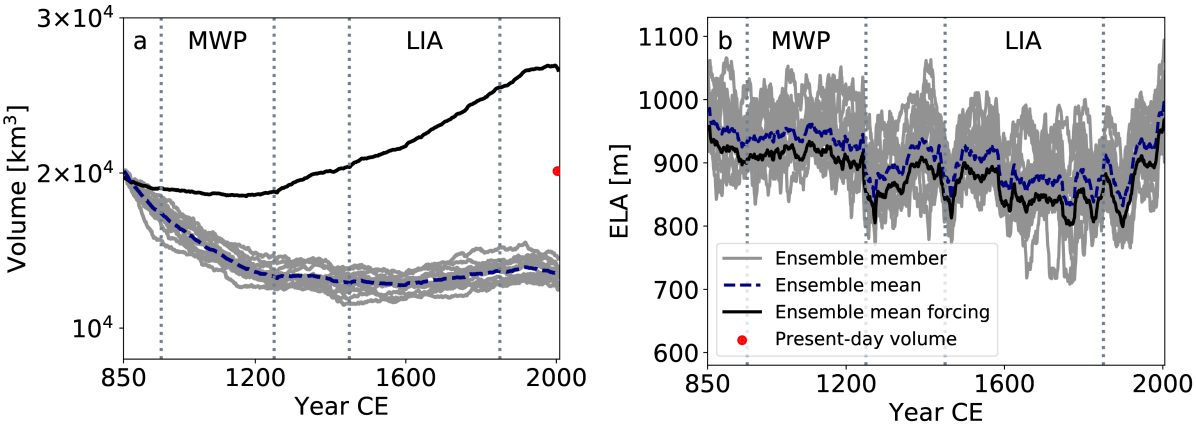

Figure 3.2: Glacier evolution in simulations forced with the CESM-LME. (a) Total CAA glacier volume of the transient simulations. The model is initialised with present day glaciers, the red dot indicates this volume at present day. (b) The average equilibrium line altitude presented with a 31-year average smoothing of the simulated glaciers in the region. The vertical dashed lines indicate the LIA and MWP (e.g. Masson-Delmotte et al., 2013). The ensemble mean, the blue dashed line, refers to the mean of the 13 simulations forced with the temperature and precipitation of the different CESM-LME ensemble members, that are presented in grey. Ensemble mean forcing, solid black line, refers to the simulation that is forced with the CESM-LME ensemble mean climate. This simulation has therefore been driven with a climate that has reduced internal climate variability compared to those that were driven by the different ensemble members. (Note that there is one legend for both panels.)

less similar to the typical glacier in the region (RGI Consortium, 2015). However, it is the bigger glaciers which contain the largest part of the region's glacier volume (Fig. 3.4).

White Glacier shows a similar glacier evolution pattern as was shown for the whole region (Fig. 3.5). Its volume decreases at the start of the simulation and during the MWP. Unlike the total glacier volume, the volume of White Glacier starts to increase right after the MWP. Then it increases until it starts to decrease again in recent times. Baby Glacier on the other hand, shows a very different pattern. The volume of Baby Glacier decreases after the start of run drastically and disappears completely. For both Baby Glacier and White Glacier the volume for the simulation that was forced with the ensemble mean is larger than the mean volume of the ensemble and outside the ensemble range. For Baby Glacier this simulation was relatively much further from the ensemble range.

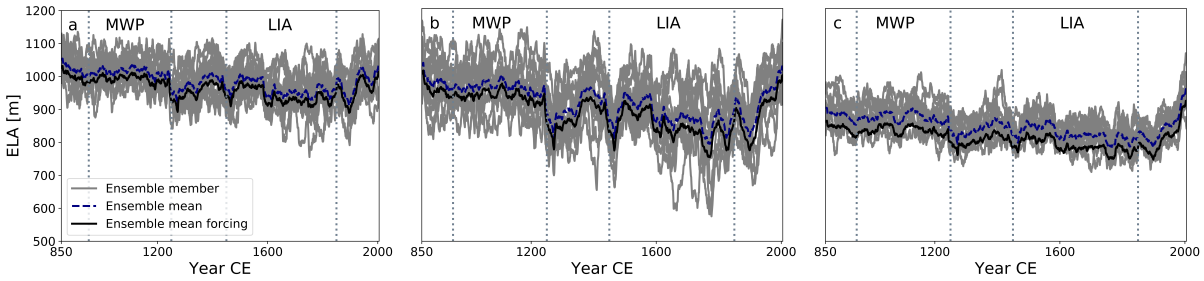

Figure 3.3: Simulated ELA per latitude band. a) South of 70°N. b) between 70 °N and 75°N. c) North of 75°N.

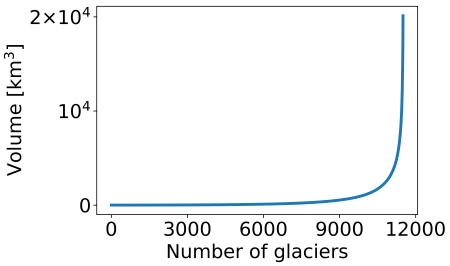

Figure 3.4: Cumulative initial volume distribution of the simulated glaciers in the CAA.

Mass balance - elevation feedback

The difference between the regular transient simulations and the one that is forced with the CESM-LME ensemble mean climate, is heightened by the mass balance elevation feedback (Fig. 3.6). Without this feedback the regular simulations would have resulted in a slightly higher volume and the simulation with the reduced climate variability in a lower volume. Still the later simulation resulted in a significantly higher glacier volume, outside the ensemble range. Therefore the large difference between the these simulations (Fig. 3.2) can only partly be attributed to the mass balance elevation feedback.

3.3.2 Sensitivity to temperature variability

The sensitivity to temperature variability is tested through equilibrium simulations that start from a 5000 year long spin-up run (Fig. 3.7a). In some cases an equilibrium is not reached within the 2000 year long simulation (Fig. 3.7b,c). Still it is clearly visible that larger temperature variability results in a smaller total glacier volume in the CAA (Fig. 3.7b). After 500 years of simulation the largest part of the deviation between the simulations with the different scaling factors already happened. Doubling the amplitude

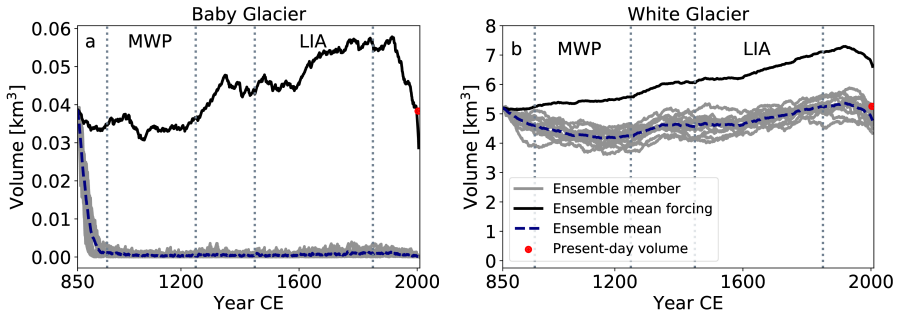

Figure 3.5: Glacier evolution of the example glaciers in simulations forced with the CESM-LME. Glacier volume of Baby Glacier (a) and White Glacier (b) in the transient simulations. (Note the different vertical axis scales. See the caption of Fig. 3.2 for more information.)

of the temperature anomalies resulted in 73 % reduction in glacier mass and reducing the anomalies by half resulted in 31 % higher volume, with respect to the simulation without adjusted temperature anomalies by the end of the simulation. These differences are not just existing for the large glaciers that dominate the signal in the total glacier volume. Smaller glaciers are even more affected by changes in the amplitude of the temperature variability than the larger ones, as these disappear with higher temperature variability while larger ones just shrink (Fig. 3.8).

Smoothing out the temperature variability over time results in a higher glacier volume in the region, the larger the window for smoothing the higher the glacier volumes (Fig. 3.7c). The largest difference occurs in the step from no smoothing to a 3-year window, resulting in a 16 % larger volume and highlighting the role of temperature variability on the inter-annual time-scale. Using a 50-year window results in a 27 % volume increase, with respect to no smoothing, after 500 years. The results of the simulations where the inter-annual variability is reduced by a moving average and the temperature anomalies are scaled by different factors are shown in figure 3.9. The larger the temperature variability the larger the difference in volume between different experiments. The largest scaling factor in combination with no smoothing of the temperature anomalies over time results in the smallest glacier volume. The largest total glacier volume is simulated in the simulation with the largest moving average window, the simulation where each year has the same temperatures.

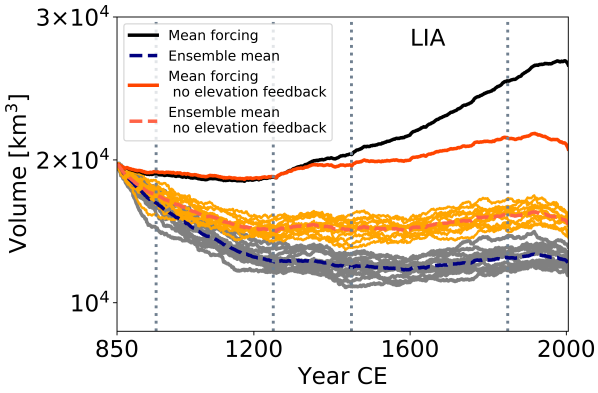

Figure 3.6: The sensitivity of glacier evolution to the mass balance - elevation feedback in OGGM, in transient simulations of the CAA. This figure shows results presented in figure 3.2a and the results of the same experiment with the mass balance - elevation feedback turned off. In the latter experiment the height at which the mass balance was computed stayed constant throughout the whole simulation. This allowed for the glacier to evolve, while keeping the height at which the SMB was computed constant over time.

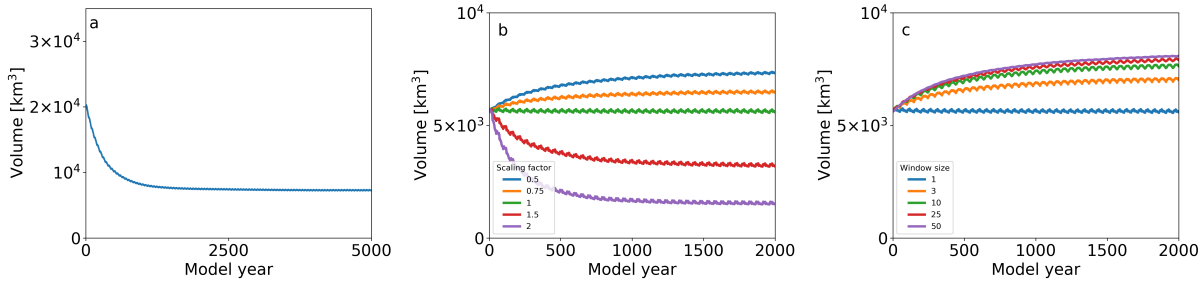

Figure 3.7: Glacier response to varying temperature anomalies. The total glacier volume in simulations forced with a repeated climate, ensemble member 6 of the CESM-LME (1950-2000), with varying temperature anomalies. (a) The spin-up simulation of this sensitivity experiment. (b) The total glacier volume in the model experiments with scaled temperature anomalies, with different scaling factors. (c) The total glacier volume in the model experiments with smoothed temperature anomalies, with different size moving boxcar average smoothing.

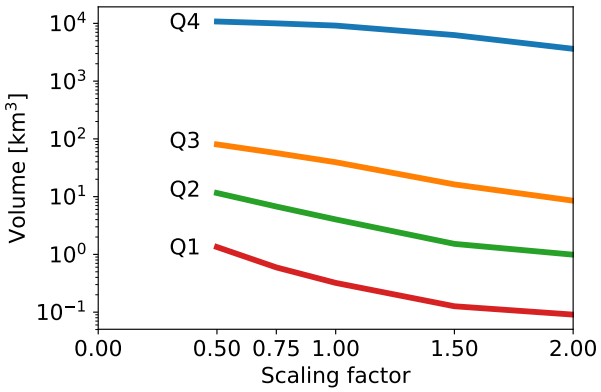

Figure 3.8: The sensitivity of glaciers of different sizes to the temperature anomaly amplitude. Total glacier volume after 500 years of simulation with repeated climate forcing and varying scaled temperature anomalies. Based on the initial area, the glaciers are divided into quantiles. Q1, Q2, Q3 represent respectively the 25^{th}, 50^{th}, 75^{th} percentile and Q4 the total glacier volume.

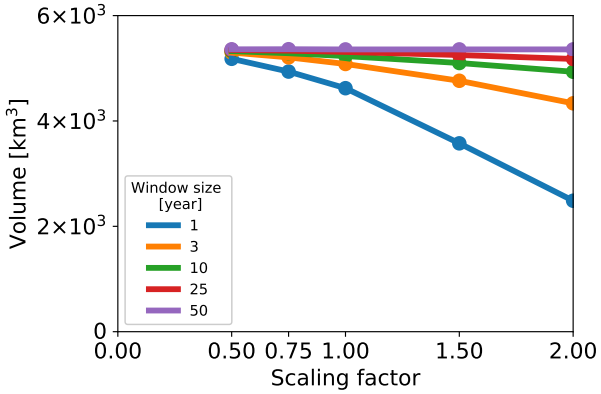

Figure 3.9: Total glacier volume after 250 years of simulation, forced with a repeated climate with varying temperature anomalies. The climate of CESM-LME ensemble member 6 (1950-2000) is repeated. The temperature anomalies in the downscaled time series are smoothed with different moving average windows and scaled with different scaling factors.

3.4 Sensitivity study - Discussion

The sensitivity study shows that even though the climate forcing for the different transient glacier simulations only differs from each other due to the internal climate variability, they resulted in different glacier volumes over time (see ensemble spread Fig. 3.2). That is similar to what was found for the Greenland Ice Sheet (Tsai et al., 2017) and for the length of well measured European glaciers (Goosse et al., 2018; Reichert et al., 2002). Reducing the amplitude of the internal climate variability in the forcing climate of the simulations by forcing the glacier model with the ensemble mean climate results in a lower ELA than the mean of the ensemble and a significantly larger glacier volume. By taking the mean of the climate ensemble both the variability in precipitation and temperature are reduced. A decreased variability in the air temperature reduces the exceedance of the threshold temperature for melting, resulting in the lower ELA and a larger glacier volume, like in the study by Farinotti (2013). This larger volume is not just seen for the few large glaciers in the region that make up the majority of the signal, but also for the smaller glaciers.

The reduction of the mean ELA that is caused by using the CESM-LME ensemble mean as forcing, instead of the CESM-LME ensemble members, is relatively small (Fig. 3.14b) compared to the increase in glacier volume that is generated in that simulation (Fig. 3.14a). The mean ELA of the different ensemble members has a range of 23 m, while the lowest mean ELA of the ensemble and the mean ELA of the simulation that was forced with the CESM-LME ensemble mean differ only by 17 m (Fig. 3.2b). However the ensemble spread of the total glacier volume is much narrower than the difference between the ensemble maximum and the volume of the simulation that is forced with the CESM-LME ensemble mean, respectively 1,985 km^3 vs 12,175 km^3 in 2005 (Fig. 3.2a). This points towards the lowered mean ELA, as result of the reduced climate variability, not being the full explanation for the increased glacier volume in the simulation with the CESM-LME ensemble mean forcing. Other indicators for this can be found when comparing the simulations in more detail. The mean ELA and the ELA of the simulation with the mean forcing covary, while being constantly relatively close to each other (Fig. 3.2b). The amplitude of their variance is larger than their difference to each other, showing that there are occasions where just based on the mean ELA there should be a volume decrease while there is an increase in the simulation with CESM-LME mean forcing (Fig. 3.2a). Though the difference between these simulations is enhanced by the mass balance - elevation feedback, it can only partly be explained by this feedback (Fig. 3.6). This indicates again that not only the reduced mean ELA is responsible for the high glacier volume in the simulation with the ensemble mean forcing.

In addition to lowering the ELA, its variability gets reduced when using the ensemble mean instead of the different ensemble members to force OGGM. The variability of the ELA can have an influence on the glacier volume due to the glacier geometry (glaciers are commonly wider in the accumulation area than ablation area) in combination with the surface mass-balance gradient, as the mass balance gradient is typically steeper below the ELA than above. Moving the ELA up by a certain amount results in more mass loss than the mass gain that results from moving it down by the same amount. This causes White Glacier, for example, to lose more mass with a more variable ELA (Fig. 3.5b & 3.10). This mechanism is in line with observations that have been done in the region, showing that a year with very negative mass balance can cancel out the effect of several positive mass balance years (Bradley and England, 1978a; Koerner, 2005).

As temperature variability influences both the mean ELA and the variability of the ELA, one cannot fully disentangle the influence that the two have on the glacier volume. However the data can be used to get an insight into the correlation of both the mean ELA and its variability with the volume change. In this analysis, the comparison is being made between selections of regular transient simulations, where either the mean ELA is the same or its variability is the same as in another ensemble member over a 10-year time slice. The correlation between the difference in mean ELA and the difference in volume change is higher than that of the difference in ELA variability and the difference change in glacier volume (Fig. 3.11). The mean ELA also seems to have a stronger influence than variability of the ELA on the glacier volume, where relative rates differ for different selections of data (e.g. by region/ glacier). Nonetheless the reduction in variability of the ELA seems to be the main reason for the significantly larger glacier volume in the simulation that is forced with the ensemble mean. That is because using the ensemble mean reduces the ELA variability much more than its mean.

The glaciers are at the start of the transient simulations not in equilibrium with the climate, although neither would the real glacier have been during that period. As a result part of the response of the glacier to the climate is therefore due to this disequilibrium. Even though transient simulations have present day glaciers as initial conditions, at the end of the millennium long transient runs the total glacier volume is lower than the initial glacier volume. Though this could have many reasons there is one straight forward explanation. Summer air temperature variability in the CESM-LME ensemble members is higher than in the CRU TS dataset for the CAA (Otto-Bliesner et al., 2016; Harris et al., 2014) and the glacier volume in the CAA is very sensitive to temperature variability (Fig. 3.7 and 3.12). Our sensitivity experiment showed that doubling the temperature anomalies results in 73% smaller glacier volume after 2000 years, with respect to not adjusting the anomalies. As higher temperature variability results in a higher and more variable ELA and therefore a lower glacier volume in the CAA, it is

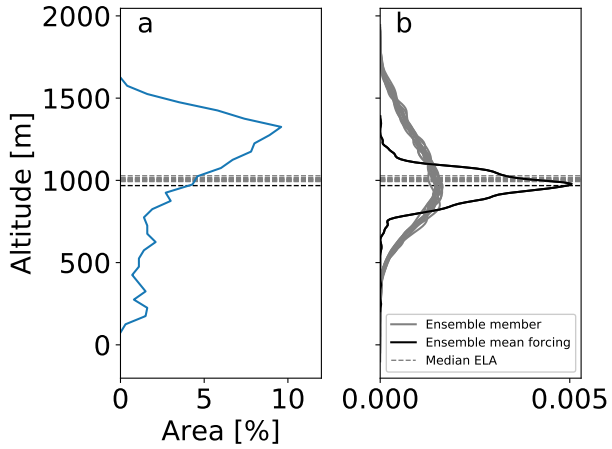

Figure 3.10: The hypsometry and ELA distribution of White Glacier. a) The glacier area per altitude bin of 50 meters. b) The ELA height distribution of the ensemble members and the simulation with ensemble mean forcing. The horizontal lines indicate the median simulated ELA.

no surprise that the total glacier volume is underestimated at the end of the transient simulations.

The average standard deviation of the CESM-LME temperature over the months June, July and August in the period 1950-2005 is ∼37% higher than in the CRU TS dataset. This overestimation of temperature variability is in the same order of magnitude as was found in a comparison between the CESM-LE and observations (McKinnon et al., 2017). CESM-LME has model settings that are very similar to that of the CESM-LE (Kay et al., 2015; Otto-Bliesner et al., 2016). McKinnon et al. (2017) found that the near surface internal temperature variability in the winter months 1966-2015 is by 32% overestimated by the CESM-LE for North America compared to observations. The results of our sensitivity experiment indicate that this amount of increased temperature variability is in the right order of magnitude to cause the underestimation of the present-day glacier volume by ∼34%. Using the standard deviation of the monthly temperature anomalies of the CESM-LME and scaling those to that of the CRU TS could solve this issue. This has been confirmed with the fully forced transient simulations (Chapter 3.5).

Though temperature index models are commonly used, in the end temperature is a proxy for the ablation within the model. In the calibration procedure of OGGM, a sensitivity factor to the temperature above the melting threshold is determined for each glacier. A limitation of this study is that this sensitivity parameter μ^* is constant over time. Biases in μ^* resulting from a changing sensitivity to temperature over time or the calibration, are likely having an influence on the magnitude of the sensitivity to temperature variabil-

ity. Using monthly climate forcing instead of a daily one might have introduced another unknown bias. However it is common practice to use monthly climate data in the global glacier modelling community (e.g. Zekollari et al., 2019) and the model used monthly climate forcing for the calibration of μ^*, so this is at least partly being accounted for the lack of sub-monthly variability. Though refreezing is a large component in the surface mass balance in the CAA (Noël et al., 2018), in our experiments it was not separately accounted for. When refreezing would be separately included, the influence that temperature variability has on the glacier mass in the simulation could be different. However the sign of this difference is uncertain. On one hand it would result in a higher calibrated sensitivity parameter, while on the other hand the capacity of the glaciers to store and refreeze melt water could decrease the sensitivity of the mass balance to temperature variability. Once the maximum water retention capacity is reached, the glacier could become more sensitive to temperature variability, because the temperature sensitivity parameter would be larger in that case.

In a case study of Rhonegletscher, Farinotti (2013) found that day-to-day, month-to-month and year-to-year air temperature variability has an influence on the number of positive degree days and therefore on the glacier evolution. We showed here that temperature variability also has a large influence on the evolution of glaciers in the Canadian Arctic and explained this by the influence temperature variability has on the mean ELA and its variability. Here the mean ELA and its variability should be seen as measures. Both above and below the ELA, temperature variability has for the same reasons an effect on the surface mass balance. Changing the temperature variability while keeping the mean temperature the same has a large influence on the equilibrium volume of the glaciers. This shows that caution should be taken when using an ensemble mean temperature as forcing in a glacier model, but perhaps it is also of significance for other processes. In addition it highlights the importance of representing the temperature variability in climate models well when these will be used to force a glacier model. Neglecting or underestimating a change in air temperature variability in a warming climate could lead to glacier mass losses being overestimated or underestimated in future projections.

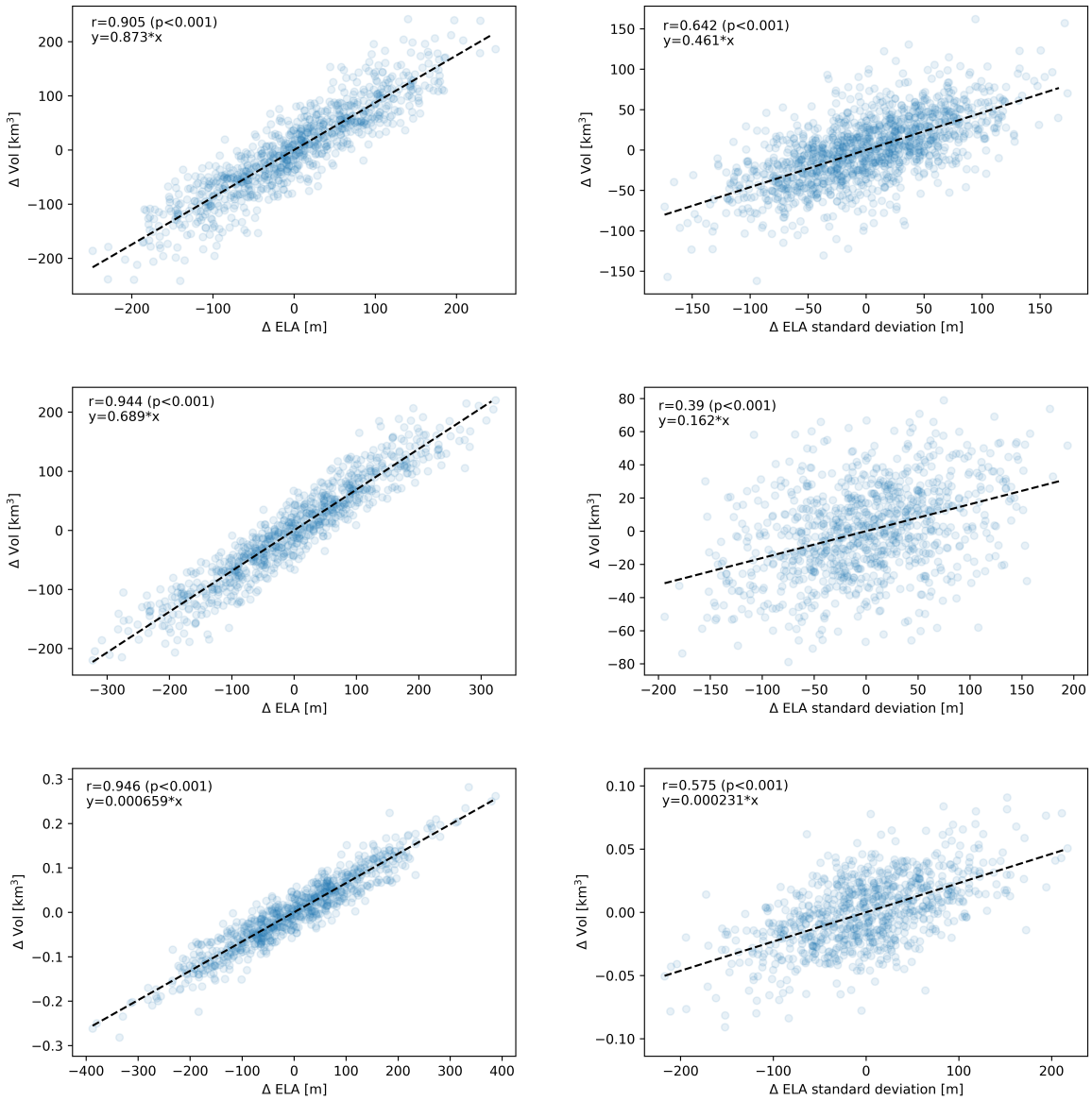

Figure 3.11: The influence of ELA mean and variability on the glacier mass balance. 10-year time windows from the regular transient simulations with roughly the same mean ELA or ELA variability (the threshold is set to respectively 0.5 m and 1 m difference) over that time window are being compared to each other. For each time slice with a match the difference in volume change is shown against the difference in standard deviation for the Northern CAA (top), Southern CAA (middle) and White Glacier (bottom). In this analysis the first 150 years of the simulation are excluded.

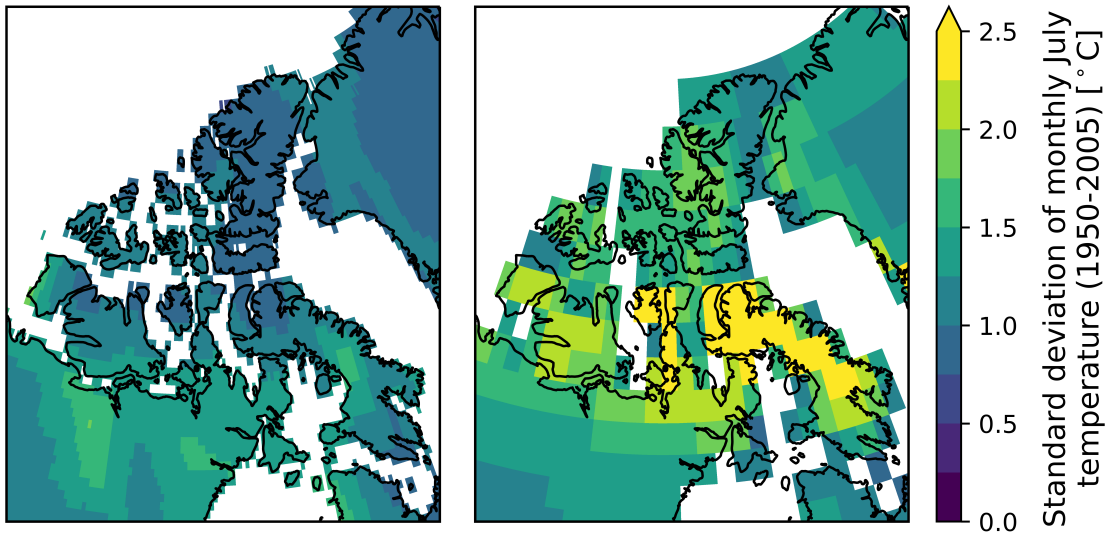

Figure 3.12: July monthly mean temperature variability 1950-2005. (Left) Standard deviation of the monthly mean July CRU temperature. (Right) The mean standard deviation of the monthly mean July CESM-LME members temperature.

3.5 Glacier Evolution - Results

The focus of the second part of the chapter is on placing the recent mass loss of land-terminating glaciers in the perspective of the last millennium. In this context fully forced transient simulations are being presented and evaluated. Based on the first part of this chapter (3.3 and 3.4), the experimental set-up has been improved for the simulations that are being presented here, in this second part of the chapter (table 3.1). The major change that has been made in the model set-up is that the temperature anomalies have been scaled when applying the anomalies method (3.2.2). This has been done to adjust for the difference in temperature variability between the CESM-LME fully forced simulations (Otto-Bliesner et al., 2016) and the CRU TS (Harris et al., 2014). Without this adjustment the regional glacier volume ends up being too low as a result of the sensitivity to the higher temperature variability seen in CESM-LME than in the CRU TS.

3.5.1 Model-observation comparison for present day

The model is initialized with present-day glacier extent and volume. Even though some glaciers completely disappear before present day in the simulations (Fig. 3.13), e.g. Liaka, Meville and St. Patrick glacier, the total initial volume is within the range of the present-day simulated volume (Fig. 3.14). The glacier covered area is, unlike the volume, underestimated at present day. The simulated glacier area is 90 % of that derived from the RGI (RGI Consortium, 2017), while for 49 % of the glaciers their present-day area according to the RGI lies within their ensemble spread. For the glacier volume that is the case for 66 % of the glaciers. SMB from RACMO2.3 for both the Canadian Arctic North and South fall well within the ensemble range of the fully forced simulations, exempt for 1 year in the northern and 2 years in the southern part of the region (Fig. 3.15), though the variability of the SMB in RACMO2.3 is lower than that of our simulations. The climate data forced simulations, showed an even more similar pattern as the RACMO2.3 SMB for both for the CAA North and South (Fig. 3.16). However the SMB variability is also higher there than in the RACMO2.3 data.

Since White Glacier has the most observations available in the WGMS database (thanks to F. Müller, J. Cogley, L. Thomson and many others), this glacier is being compared to the simulations in more detail and used as an example glacier (WGMS, 2017). Model performance for other glaciers with SMB data in the WGMS database can be found in Table 3.2. White Glacier is located on Axel Heiberg Island and is with 40.5 km^2 average in size for the region (RGI Consortium, 2017). This glacier's volume falls also within the simulated range. Its simulated glacier covered area is slightly overestimating the WGMS

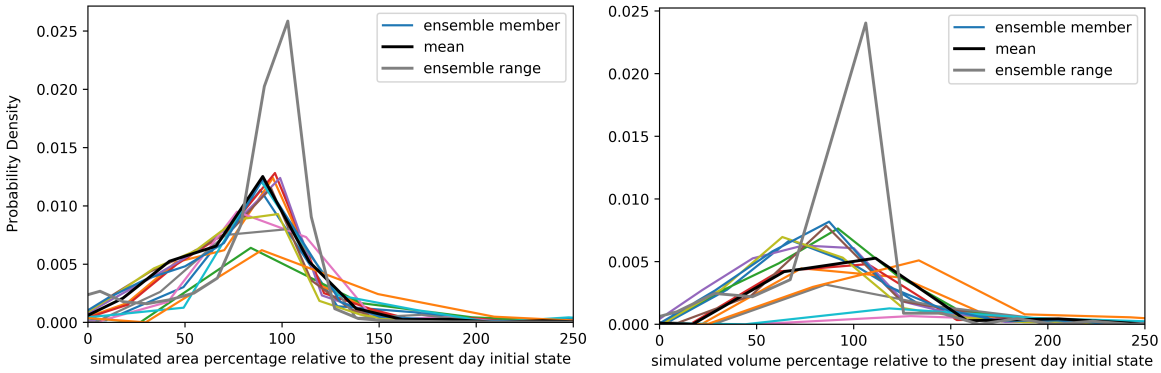

Figure 3.13: Present day performance of the simulations presented in distribution graphs. The initial glacier volume and glacier covered area (which is based on present day glaciers) are compared here with the present day simulated glaciers. For the ensemble range 100% means that the respective area or volume are within the range of the simulated ones at present day. When the volume is outside that range, the percentage is based on the nearest outer bound of the range. (e.g. In the case of an underestimation simulated volume the highest simulated volume is being used to calculate to percentage.)

area records and that of the RGI in the simulations (Fig. 3.17). 85 % of the WGMS SMB observations lie within the ensemble range (Cogley et al., 1996, Fig. 3.18). Most of the WGMS ELA records for White glacier lie inside the ensemble. Note that although the average ELA seems to be comparable, the variability of the WGMS record is larger, 156 m and 250 m, respectively.

3.5.2 Simulations

From the start of the glacier simulation, in 850 CE, the ensemble shows a loss in regional volume (Fig. 3.14). This decrease in glacier volume continues throughout the MWP. During the LIA the volume increases, until it starts to decrease again in recent times. This decrease continues during the 21^{st} century under the RCP8.5 scenario, with a sharp increase in the rate at which the mass loss occurs. This pattern matches the simulated ELA, which is higher during the MWP than during the LIA and shows a steep increase during the 21^{st} century (Fig. 3.19).

The trajectory of the simulated glacier volume is dependent on the prescribed initial conditions (Fig. 3.20). In some cases, simulations with a different initial condition diverge, however in most cases they converge. While the simulated glacier volume converges, the total regional simulated volume remains different throughout the millennium. This is from the perspective of absolute simulated glacier volume in the region. When looking

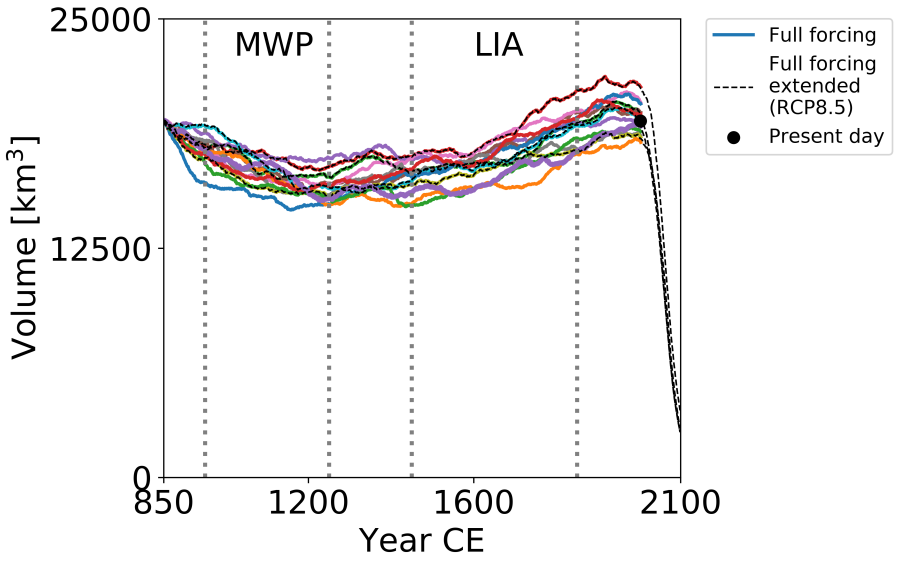

Figure 3.14: Glacier evolution in simulations forced with scaled anomalies of the CESM-LME full forced simulations with respect to CRU. Total CAA glacier volume of the transient simulations. The model is initialised with present day glaciers, the black dot indicates this volume at present day. The vertical dashed lines indicate the MWP and the LIA (e.g. Masson-Delmotte et al., 2013).

into the difference in volume change the simulations with changed initial conditions converge at an earlier stage (Fig. 3.21). The difference between simulations with a different initial condition turns out to be smaller than discrepancies caused by the internal climate variability, when excluding the simulation that was initialized with no glaciers present.

The total glacier volume in the region is very sensitive to the initial conditions of the glaciers (Fig. 3.20). The TraCE-21ka (He, 2011; Liu et al., 2014) forced sensitivity experiment showed that even after a 6-millennium long run with the same forcing there is a difference in glacier volume in the CAA. It takes about 4 millennia before these simulations become very similar (Fig. 3.22). The differences between the two simulations become negligible, but the simulated volume never becomes identical over the course of the simulation.

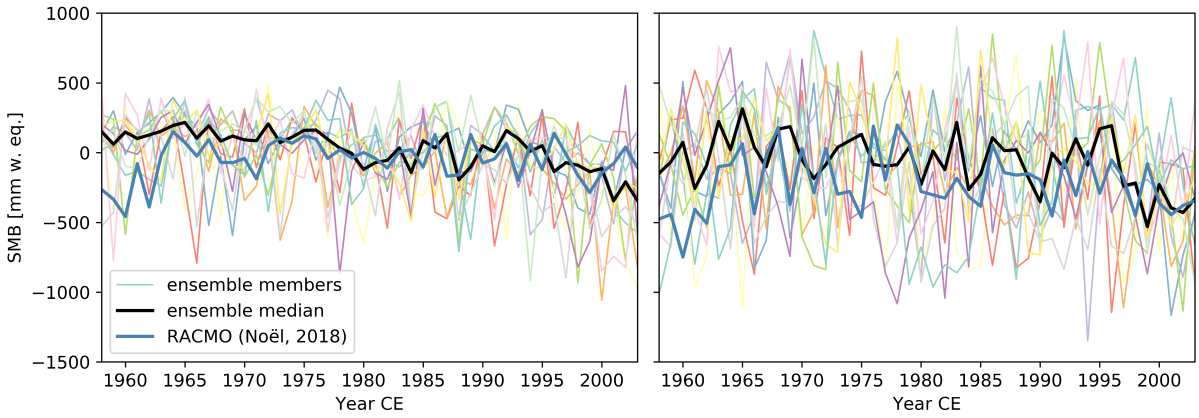

Figure 3.15: Surface mass balance comparison of the fully forced simulations with RACMO. On the left the Canadian Arctic North (RGI region 3) and on the right the Canadian Arctic South (RGI region 4).

Glacier	RGI ID	Volume	Area	SMB range
Baby Glacier	RGI60-03.00840	40 %	90 %	100 %
Barnes	RGI60-04.06187	76 %	51 %	80 %
Decade	RGI60-04.03082	100 %	100 %	100 %
Ward Rise	RGI60-03.04079	15 %	79 %	9 %
White glacier	RGI60-03.04539	100 %	101 %	85 %

Table 3.2: Evaluation of simulations of individual glaciers. In the first column their name and in the second the RGI ID. In the third and fourth column the present day simulated volume and area are compared to the initial glacier volume and RGI area (for more information see fig 3.13). In the last column it is indicated how much percent of the WGMS SMB observations lie within the ensemble.

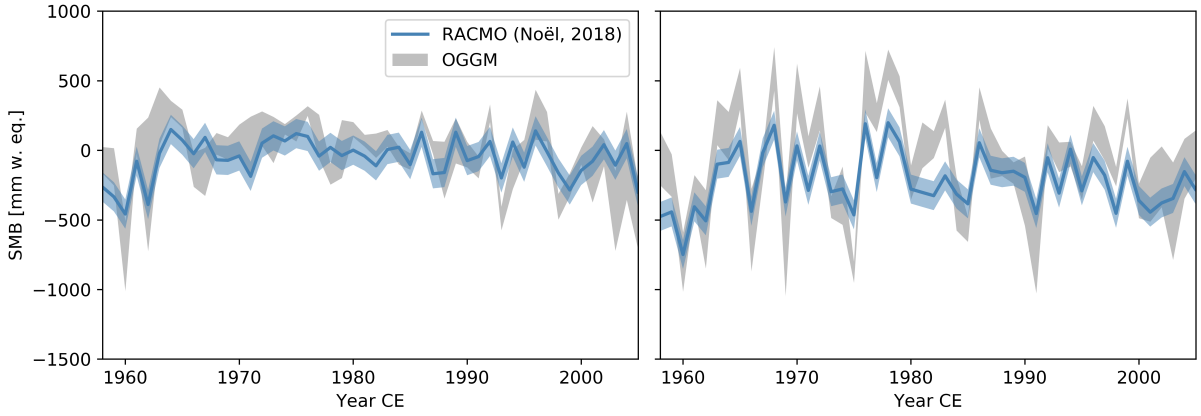

Figure 3.16: Surface mass balance comparison of the climate data forced simulations and RACMO2.3. Ten simulations were branched of the simulation that was forced with CESM-LME ensemble member 5 in 1957 CE, the year prior to the start of the RACMO2.3 simulation, and forced with CERA-20C scaled anomalies with respect to the CRU TS dataset (1961-1990). In addition a simulation was branched of each of the individual CESM-LME forced simulations and then forced with the CRU TS climate. Together these simulations are the ensemble created with OGGM, which is shown next to the RACMO2.3 simulation with its uncertainty. On the left the Canadian Arctic North (RGI region 3) and on the right the Canadian Arctic South (RGI region 4).

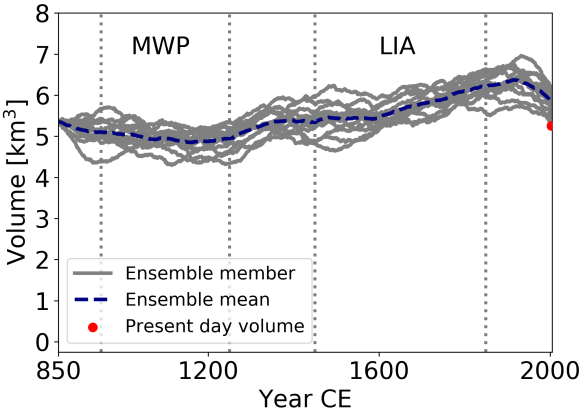

Figure 3.17: The evolution of White Glacier in simulations forced with scaled anomalies of the CESM-LME full forced simulations with respect to CRU. The initial conditions of the glacier are based on the glacier at present day. The red dot indicates that volume at present day.

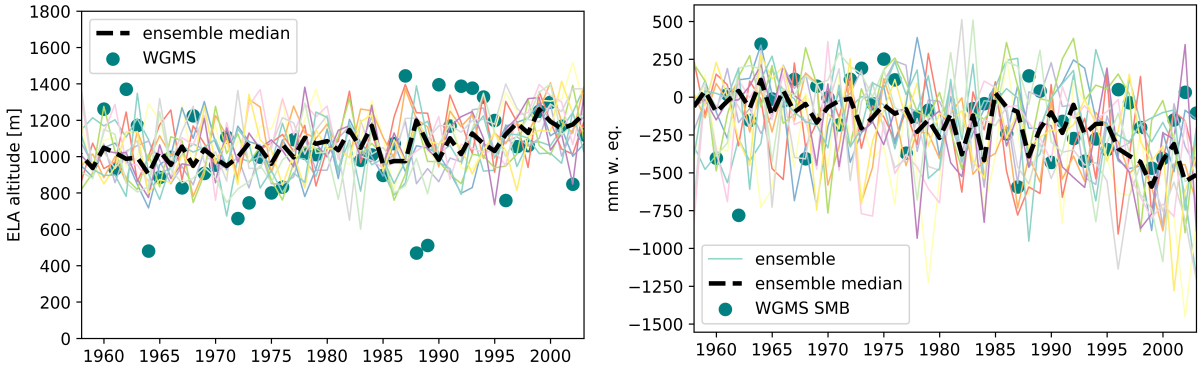

Figure 3.18: Simulated White Glacier compared to observations. left) The equilibrium line altitude. right) The surface mass balance.

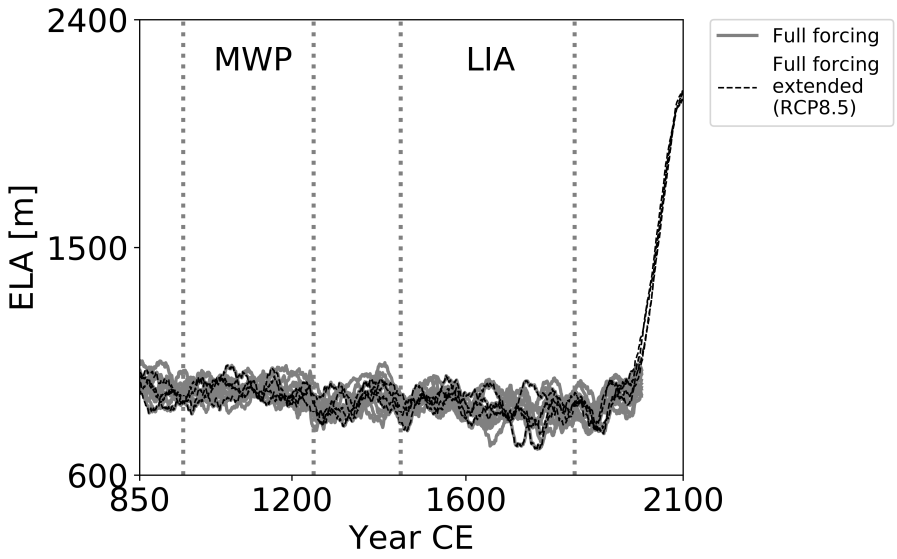

Figure 3.19: The mean ELA in simulations forced with scaled anomalies of the CESM-LME full forced simulations with respect to CRU.

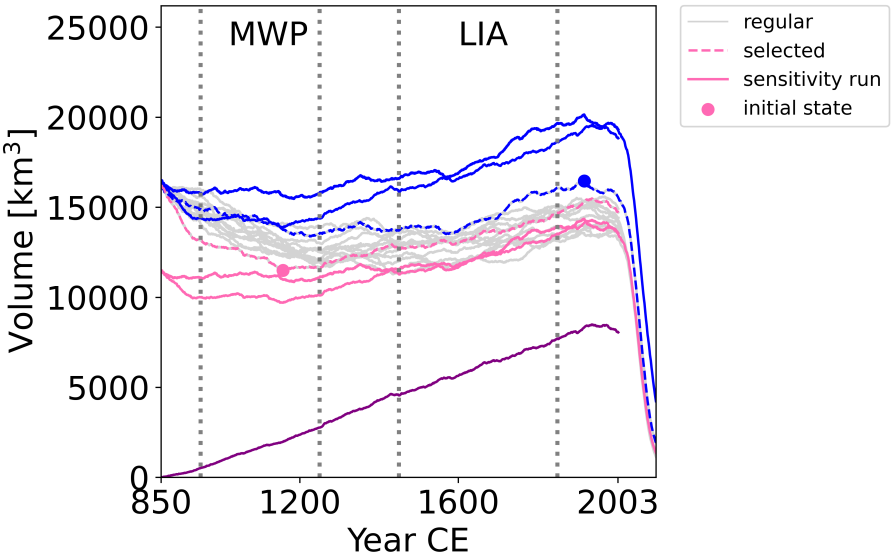

Figure 3.20: Sensitivity of the regional glacier evolution to the initial glacier state. The gray lines present the simulations forced with the fully forced CESM-LME simulations, that started from a present-day state (Fig. 3.14 minus some of the glaciers that grew out of the domain boundary in the sensitivity experiment). The dashed lines indicate the simulations that contain either the maximum (blue dot) or the minimum (pink dot) volume. The simulations presented in pink start from the state at the pink dot and the blue ones with the state at the blue dot. These runs have the same forcing as those with the dashed line of the respective colour. The purple simulations started from zero glacier volume and has the same forcing as dashed simulation with the highest glacier volume.

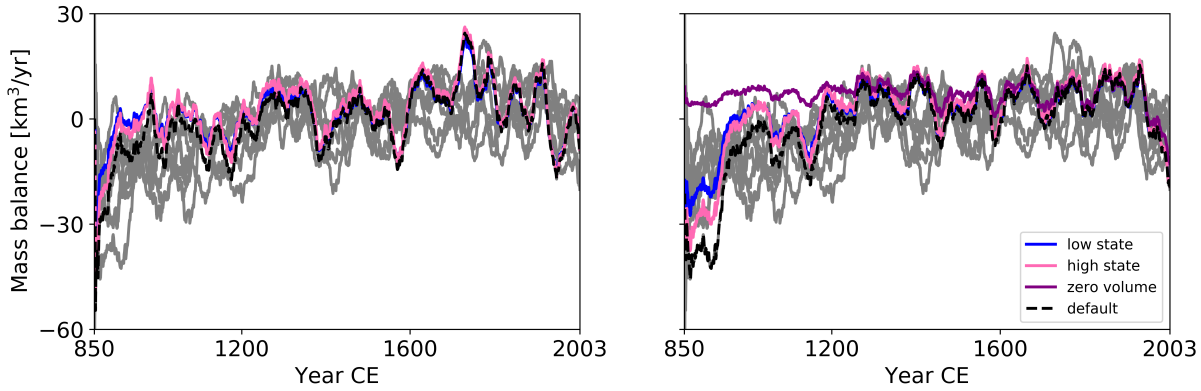

Figure 3.21: Mass balance sensitivity to the initial glacier volume. Yearly mass change plotted with a 31-year moving average smoother [boxcar]. These plots present the same simulations as figure 3.20. On the left the simulations that are forced with the run that resulted in the highest regional volume state and on the right the one that resulted in the lowest volume state. In grey the regular transient simulations.

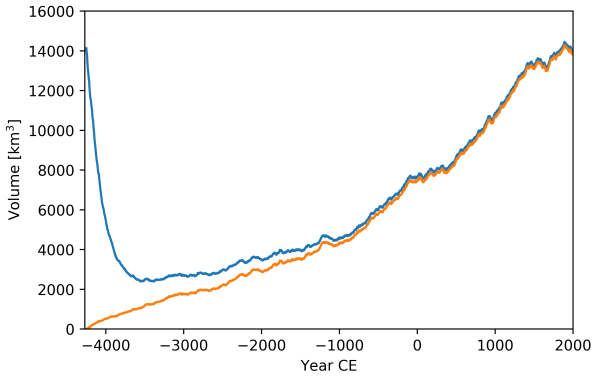

Figure 3.22: Total regional glacier volume in simulations forced with TraCE 21k (He, 2011; Liu et al., 2014). In blue the simulation started from present day glacier states and in orange the simulations started from zero glacier volume.

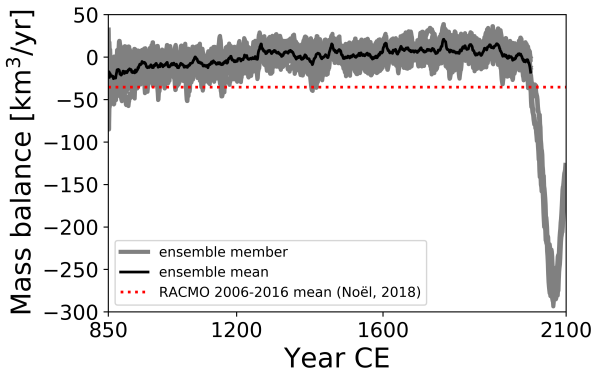

Figure 3.23: Glacier mass balance 851-2099 CE. The mass balance is presented with a 10-year moving average smoother [boxcar] to put the mass balance of 2006-2016 CE into perspective. Like in the previous plots the presented RACMO2.3 data is a selection based on the glaciers that are also modelled in our simulations. In addition the RACMO2.3 SMB has been converted to a volume by using the same ice density (900 kg/m^3) as was used in OGGM.

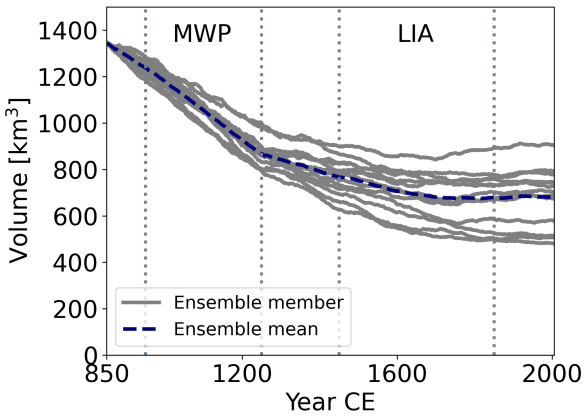

Figure 3.24: Simulated evolution of Barnes Ice Cap. (RGI entity RGI60-04.06187 & RGI60-04.06188)

3.6 Glacier Evolution - Discussion

3.6.1 Initial conditions

It is clearly visible that total regional volume is sensitive to the initial glacier volume from which the simulations were started (Fig. 3.20). Over the course of the last millennium the simulations with different initial conditions do not fully converge and in some cases even diverge (Fig. 3.20). It was expected upfront that unlike in the Alps (Goosse et al., 2018; Eis et al., 2019), it might take a couple of centuries for these different simulations to converge due to the cold and dry climate that causes a low mass turnover rate. In the end, full convergence does not happen within the time span of the experiment. An additional sensitivity experiment, forced with the last 6 ka of the TraCE 21k (He, 2011; Liu et al., 2014, Fig. 3.22), shows that roughly four millennia are required for the simulations to converge, but within the time span of the simulations the state does not become identical (Fig. 3.22). This small remaining difference, can be ascribed to two mechanisms: First, for certain climates there are two stable states, one with a glacier and one without, as a result of the temperature-elevation feedback (Oerlemans, 2008). In such cases, the presence of a glacier reinforces its own existence by maintaining surface area above the ELA, and a new glacier will not grow from scratch as a result of having a too low surface elevation. The second mechanism, which occurs only on very rare occasions, is numeric instability. Together these mechanisms prevent full convergence, however the differences occur only for a few glaciers and are, with 1 % difference in total volume, negligible on a regional level. The newly implemented numerical scheme in OGGM v1.3 should solve the issue of these very rare cases of numerical instability. These sensitivity experiments show the importance of proper initial conditions when doing simulations for this region with the purpose of looking into absolute glacier volume, while for the mass balance initialisation is less important provided that the simulation starts from a reasonable estimate of the initial glacier states (Fig. 3.21). For the mass balance, the resulting difference is in that case smaller than the differences that are caused by the internal variability of the climate system.

3.6.2 Model-data comparison

Some of the data that were used for evaluating the simulations were not independent. The RGI area, the present-day glacier volume and the WGMS SMB were also used for setting up OGGM, either for the initialisation or the calibration procedure. Keeping this in mind, the comparison still gave some interesting insights, as the model was calibrated and initialized using data of the past century while the simulations start one millennium earlier. The RACMO2.3 SMB is on the other hand independent from our simulations and

the two data sets show very good agreement (Noël et al., 2018). The RACMO2.3 SMB falls within the ensemble spread of our CESM-LME forced simulations and is for most years close to the ensemble median (Fig. 3.15). Due to the relatively large difference between this median and RACMO2.3 estimates in the first years of the comparison, it could be argued that they might represent a different trend. However the negative SMB might be slightly overestimated in RACMO2.3 during those years, due to a potentially too low bare ice albedo in RACMO2.3 for those years, i.e. based on MODIS albedo records averaged over the period 2000-2015. These years were relatively warm with large mass loss, so if brighter snow or ice was actually exposed at the surface in this early period, the downscaled RACMO2.3 product would overestimate the runoff as a result of a too low prescribed ice albedo. Due to this potential bias in combination with the fact that the SMB lies within the ensemble spread, we do not speculate further on this topic. Another difference stems from the fact that RACMO2.3 SMB shows less variability than that of our ensemble of simulations. A possible reason for this is that refreezing is simulated in RACMO2.3, while refreezing in OGGM is only indirectly taken into account as a part of the sensitivity parameter μ^*, therefore not representing the year-to-year buffering effect of meltwater refreezing can have, which dampens the SMB inter-annual variability.

3.6.3 Comparison to reconstructions

Vegetation that recently emerged from underneath retreating glaciers, at some sites on Baffin Island, has been dated by the use of ^{14}C, indicating the date that specific location must have been ice free at that point in time. Based on the lack of such vegetation kill dates it is suggested that the period ∼1000-1250 CE was a period of glacier retreat or stable state (Anderson et al., 2008; Margreth et al., 2014). Ice growth began abruptly between 1275 and 1300 CE (Miller et al., 2012). The period 1280-1450 was marked with oscillations of advance and retreat associated with an overall advancing trend (Anderson et al., 2008). This period was followed by extensive ice expansion (Anderson et al., 2008), that started between 1430-1455 CE (Miller et al., 2012). The lack of samples younger than 1650 CE indicates an extensive ice cover until the recent warming (Anderson et al., 2008). The maximum ice extent was reached around 1900 CE (Pendleton et al., 2017). The pattern described above, which is based on reconstructions of different sites in the CAA, is also visible on a regional level in our simulations (Fig. 3.14). However there is a moraine chronology for Naqsaq valley, Baffin Island, that puts the glaciers at their maximum extent during the MWP. Young et al. (2015) and Blake Jr (1981) suggested that there was a glacier advance around 1050 CE. These patterns are both not visible on a regional level in our regular transient simulations (Fig. 3.14), but individual glaciers can behave differently than the regional pattern. For instance Barnes Ice Cap has continuously been retreating throughout the Holocene (Koerner and Fisher, 2002).

This means that for Barnes ice cap the simulations were initialized with a too small ice extent, as all simulations were started from present day glacier states. Even though the absolute volume is not correct this pattern of retreat is visible during the last millennium in Barnes' simulations (Fig. 3.24). A multi proxy study shows clear evidence of regional LIA glacier expansion until the late 19^{th} century, followed by variable glacier retreat, whereupon some glaciers have remained at their LIA maximum, but most retreated significantly (Miller et al., 2005). This is again in line with our simulations.

3.6.4 Present and future mass losses compared to past mass losses

Ice core melt records suggest that the Canadian Arctic ice caps are currently losing mass faster than at any time in the last four millennia (Fisher et al., 2012). However at first sight it seems like the recent glacier mass loss on a regional level in the CAA is not exceptional in the region for the last millennium. At the start of the simulations the mass loss is higher than over the last years of our regular simulations (Fig. 3.21). This is both the case when comparing the ensemble mean as when looking at the lower boundary of the ensemble range. However the sharp increase in mass loss from 31 $\pm$ 8 Gt/yr from the period 2004-2006 CE to 92 $\pm$ 12 Gt/yr over 2007-2009 CE (Gardner et al., 2011) is not covered in the regular simulations, which stop in 2004 CE. So the period, 2006-2016 CE, over which the CAA is known to be the region with the largest non-ice sheet mass loss is only a part of the simulations that are extended under the RCP8.5 scenario. Therefore the mass loss based on the RACMO2.3 SMB of Noël et al. (2018) over that period was compared to our SMB of the last millennium (Fig. 3.23). Though the 10-year ensemble mean SMB is never as negative throughout the last millennium as the RACMO2.3 2006-2016 CE SMB, in the ensemble it is not unprecedented. Up to 1200 CE the 10-year mean RACMO2.3 SMB lies about half of the time within the ensemble spread. When excluding the first decade of the simulation only three out of the thirteen ensemble members, that only differ from each other due to internal climate variability, do not exceed this minimum. This indicates that the 2006-2016 CE mass loss for the region might not be unprecedented for the last millennium.

Under the RCP8.5 scenario the mass loss will reach a level during the next decade that was unprecedented during the last millennium. The mass loss rate keeps increasing up to roughly 2065 CE, after which it starts to decrease again. While the mean specific glacier mass balance continues to increase, the decrease in total mass loss rate is caused by a decrease in glacier covered area in the region as a result of the glacier retreat. Even though the mass balance becomes less negative towards the end of the 21^{st} century, it stays more negative than it has been in the region during the last millennium. As a result

the glacier volume decreases in the 21^{st} century to below a level that has been seen in the last millennium (Fig. 3.14). With 14.5 ± 1.8 % of its glacier volume remaining at the end of the 21^{st} century that is significantly less than the 18 % total mass loss projected by Lenaerts et al. (2013) for the RCP4.5 scenario for the region as a whole. The RCP scenario is the largest source of uncertainty of the total glacier mass loss by the end of the century in CAA according to the Glacier Model Intercomparison Project (GlacierMIP) study by Marzeion et al. (2020). Either way the simulated remaining glacier volume relative to present day, is also well below the presented ensemble range (mean ± 1 standard deviation) of the RCP8.5 forced simulations in the GlacierMIP (Marzeion et al., 2020). A significant part of these differences is could be caused by our simulations excluding the tidewater glaciers. The tidewater glaciers in the region tend to be larger than the land terminating ones and are therefore expected to respond slower in the simulations to a warming climate. In addition, the use of other climate forcing and different initial conditions, could have contributed to this difference too.

4 Contribution of individual forcings to the glacier mass balance in the Canadian Arctic Archipelago

4.1 Introduction

The glacier mass loss of land-terminating glaciers in the CAA over the period 2006-2016 CE was extremely large for the region. However, this mass loss might not have been unprecedented for the last millennium (Chapter 3). Nevertheless, the CAA has recently been the region with the largest non ice sheet glacier mass loss both according to geodetic measurements (Zemp et al., 2019) and gravimetry (Wouters et al., 2019; Ciracì et al., 2020). The glacier volume in the region is both influenced by internal climate variability (Chapter 3.5, 3.6) and external forcing. The external forcing includes both natural forces (e.g. orbital) and anthropogenic influence (e.g. changes in land use and land cover). The different forcings act on different time scales, where the orbital forcing is a slowly and constantly changing climatic diver that acts on a multi-millennial timescale and the volcanic forcing is an event-based interannual to decadal phenomenon. A recent global study of the length of 76 glaciers over the last millennium shows that glaciers with longer response times are more influenced by external forcing than internal climate variability (Huston et al., 2021). Due to the cold and dry climate glaciers in the CAA have relatively long response times. The ice caps in the region, that make up for the largest part of the regional volume, have estimated response times of 250 to 1000 years (Patterson, 1994). As a result, it can be expected that external forcing might have a relatively large influence on the CAA glacier volume too. This raises the question: *What is the long-term contribution of individual forcings to the recent glacier mass loss?*

This chapter is about the influence different external forces have on the glacier mass balance of land terminating glaciers in the CAA, namely: the volcanic, orbital, solar, land use and land cover change (LULCC), ozone-aerosol and GHG forcing (Chapter 2.2). These factors are the focus in determining what led to the build up of glacier volume during the LIA and the recent mass loss, addressing both the influence of those different forces and the natural vs anthropogenic forcing. Therefore, these millennium-long simu-

lations also give additional insights on the last century compared to historical (1850 CE - present) simulations (Marzeion et al., 2014). This is not the first study addressing the influence that different forces have on the glaciers mass balance in the region. Marzeion et al. (2014) and Slangen et al. (2016) studied the influence that anthropogenic vs natural forces have had on the global glacier mass balance had, since 1850 CE and 1900 CE, respectively, with the model from Marzeion et al. (2012). Roe et al. (2021) does take into account the last millennium in their assessment of the relative anthropogenic contribution to the glacier mass loss. However, the model from Marzeion et al. (2012) and Roe and Baker (2014), that is being used by Huston et al. (2021) and Roe et al. (2021), make use of estimated glacier response times for the glacier evolution, while here we use OGGM which includes ice dynamics (Maussion et al., 2019a).

4.2 Method

4.2.1 Simulations

The fully forced transient simulations that have been presented and evaluated in the previous chapter serve here as a base to investigate the role of individual forcings on the glacier mass loss in those simulations. Here OGGM has been forced with the single forced simulations of the CESM-LME (Maussion et al., 2019a; Otto-Bliesner et al., 2016; Chapter 2.2). The temperature and precipitation of the CESM-LME single forced simulations were treated in the same way as those in the fully forced transient simulations (Chapter 3). However, bias correcting the single forced simulations with their own climatology and scaling factor, would remove the difference between these simulations that are caused by having a different forcing. In order to preserve these differences, the ensemble mean climatology and the scaling factors of the fully forced transient simulations are applied to bias correct the single forced simulations.

To be able to attribute glacier mass change to the different forcings, an ensemble was made of the CESM-LME 850 CE control simulation (Otto-Bliesner et al., 2016). The 850 CE control simulation has a constant forcing with all forcings fixed at their 850 CE levels. The years from this simulation were randomly and uniquely sampled from the last millennium. For this procedure, the RandomMassBalance function in OGGM was used, which takes care of this random sampling before passing the climate on to the part of the model that computes the actual mass balance (Maussion et al., 2019b). For the sampling seed 1 to 13 were used, meaning that for each respective ensemble member all glaciers experience the climate from the same year. Additionally, the simulations can be replicated, as the order of the randomized climate time series is fixed for each seed. Like

in the fully forced transient simulations all single forced simulations and the control simulations are initialized with present-day glacier conditions, except for the ozone-aerosol experiment. The CESM-LME ozone-aerosol simulations only start in 1850 CE, therefore our simulations that are forced with this climate forcing do not start from the present-day condition, but are branched off the original control simulation in their starting year.

4.2.2 Analysis

In the process of analysing the influence that the different climate forcings have on the glacier mass in the region, a trend test has been applied to the climate time series. This was done to later assess if the differences in glacier volume between the ensemble members by the end of the simulations can be explained by different trends in the climate. To test for trends in the temperature and precipitation time series a variation of the Mann-Kendall test (Mann, 1945; Kendall, 1948) has been used. The Mann-Kendall test is non-parametric, meaning that the data that it is being applied to does not need to be normally distributed. The test is rank based, which makes it less sensitive to outliers. The robustness with regards to the distributional shape of the time series is an advantage for analysing climate data (Mudelsee, 2013). However, data that is serially correlated, which is likely the case for climate data, can result in a significant trend even when none is present (Hamed, 2009). There are two ways to address this problem. It is an option to remove the serial correlation, a method commonly referred to as 'pre-whitening', before applying the Mann-Kendall test (Mudelsee, 2013). However, according to a study by Sang et al. (2014), pre-whitening does not improve the detection of trends. Therefore it was decided to apply an adjusted version of the Mann-Kendall trend test that accounts for serial correlation. The method of Yue and Wang (2004) was used, as implemented in the Pymannkendall package (Hussain and Mahmud, 2019). By taking into account the effective sample size, the method reduces the influence of auto correlation on the Mann-Kendall test (Yue and Wang, 2004). The CAA is a very cold region, with a yearly mean temperature that is far below the freezing point for all the different simulations. Because the melt season is short and the temperature during this time of the year does not necessarily follow the yearly trends (Koerner, 2005), the trend test has been applied to the July monthly mean temperature. The trend analysis has also been applied to the total yearly precipitation. This has the advantage of not having a seasonal cycle in the time series, as seasonality can also negatively impact the Mann-Kendall test (Shao and Li, 2011).

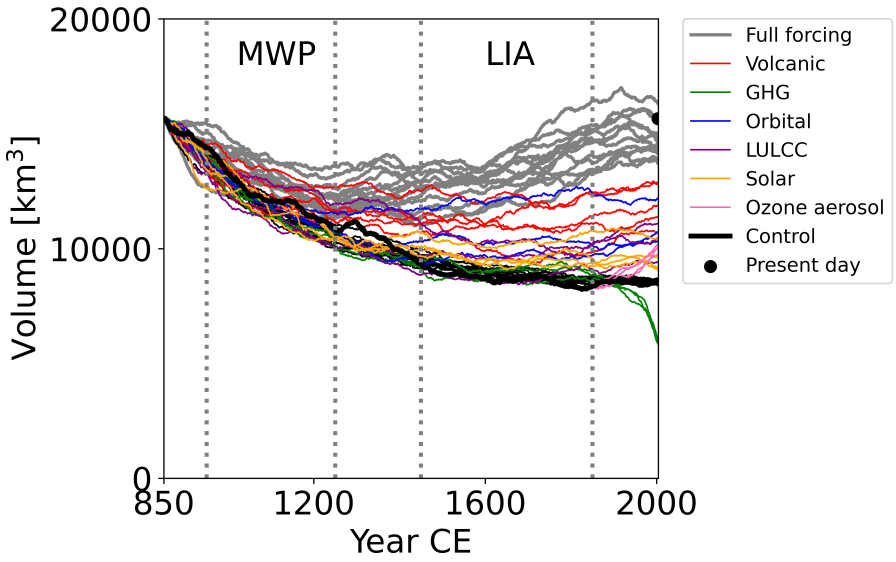

Figure 4.1: Glacier evolution under a range of climate forcings over the past millennium. The model has been initialised with present-day glaciers, the black dot indicates this volume at present day. The thick black line represents the simulation that has been forced with the original 850 CE control simulation and the thin ones the control simulations that have been sampled from that. The vertical dashed lines indicate the MWP and the LIA (e.g. Masson-Delmotte et al., 2013).

4.3 Results

Of all the land-terminating glaciers 93.4 % (83.7 % of the land-terminating glacier covered area) was successfully simulated for all the fully forced, single forced and control simulations (Fig. 4.1). These are 24 (0.2 %) less successfully simulated glaciers than in the fully forced transient simulations (Chapter 3). To assess the influence of the individual forcings on the glacier mass balance, the glacier volume in the single forced simulations with respect to that of the mean of the control simulation ensemble have been added up. This results in an ensemble of 2160 combinations (Fig. 4.3). These are different combinations that can be made when adding up the anomalies of the single forced simulations (5 (volcanic) * 3 (orbital) * 4 (solar) * 3 (land use) * 4 (ozone-aerosol) * 3 (GHG) = 2160 combinations). This ensemble will be referred to as the *single forced totals*.

4.3.1 Single compared to fully forced glacier volume evolution

It is clearly visible that the initial glaciers, that are based on present-day states, were out of balance with the 850 CE control simulation climate. The glacier volume decreases

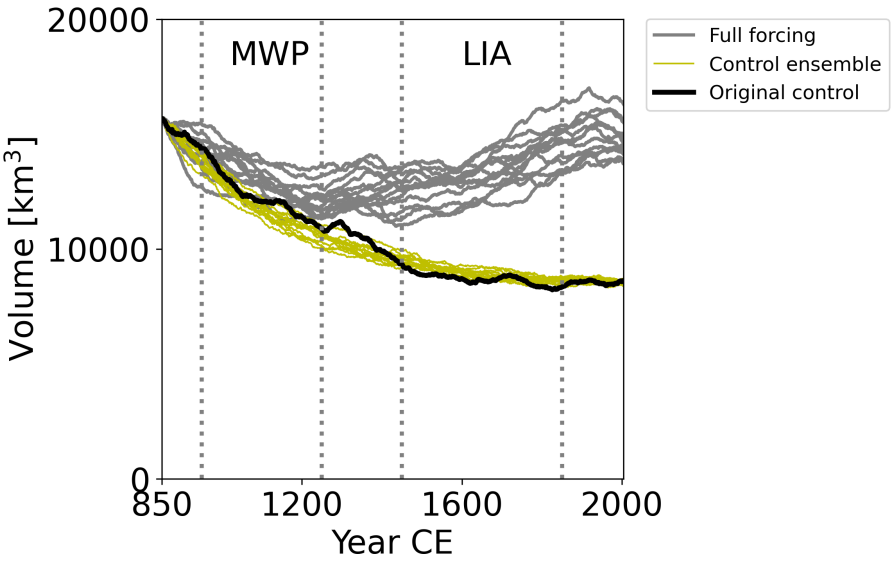

Figure 4.2: Glacier volume evolution in the control ensemble. The vertical dashed lines indicate the MWP and the LIA (e.g. Masson-Delmotte et al., 2013).

from the start of the simulation, both in the original control simulation as in the control ensemble. The original 850 CE control simulation lies largely within the control ensemble (Fig. 4.2). From the control simulations it is not clear if glaciers are in equilibrium with the climate by the end of the control simulation. Based on the difference in glacier volume between the beginning and the end of the simulation the regional glacier volume in the simulations has an e-folding response time[1] of at least 150 years.

The glacier volume in the fully forced transient simulations increases with respect to the control ensemble from the beginning of the simulations until a peak is reached between 1849 and 1999 CE. The range of these volume anomalies is much larger for the single forced totals, where this peak occurs as early as 1755 CE and in some cases does not happen before the end of the simulation. Its median peak occurs 1965 CE, which is well within the range of the fully forced maxima, and only 20 years after its median maximum in 1945 CE (Fig. 4.3). The median of the single forced totals lies largely within the ensemble spread of fully forced transient simulations and is not distinguishably different in magnitude compared to the fully forced anomalies. In other words, adding up the effect that the single forces have on the glacier volume, is not distinguishably different in magnitude than the effect they have when being combined in the fully forced exper-

[1]The term response time has been used with different definitions throughout the literature (Benn and Evans, 2010). The e-folding response time is the time it takes to reach $\frac{1}{e}$ of the change. This is a different definition than Patterson (1994) used in his response time calculations. Thus the e-folding response time should not be compared with the values that are cited in the introduction of this chapter.

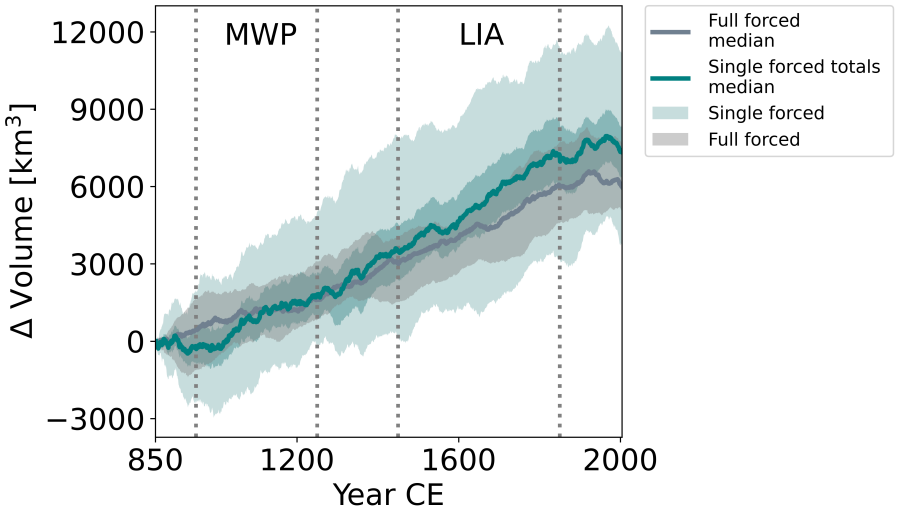

Figure 4.3: Contribution of individual forcings to the glacier evolution. The glacier volume evolution relative to the control ensemble is shown here, both for the fully forced simulations and the single forced totals. In light shading is the whole ensemble range and in darker shading is the interquartile range for the single forced totals.

iment. This implies that there is no interaction between the forcings and that they do add up linearly. The single forced simulations therefore can provide further insight into the mechanisms that shape the fully forced runs.

By the year 1800 CE all forcings contributed to a net increase in glacier volume compared to the initial conditions and with respect to the control simulations (Fig. 4.4). From that point onwards the volume in the GHG forced simulations starts to decrease. Even though the glacier mass balance gets increasingly more negative in the GHG simulations (Fig. 4.5), the total glacier volume still increases in both the fully forced transient simulations as it does in the single forced totals. From 1850 CE onwards, changes in the ozone-aerosol forcing gets included, which has a strong positive influence on the glacier mass balance. In this way it partly counter balances the negative influence of the GHG. By the end of the simulations all forcings except the GHG contributed to a net gain in mass since 850 CE with respect to the control simulations. Although there is some uncertainty as a result of internal variability, it seems that the changes in volcanic and orbital forcing since 850 CE contributed the most to the gain, with respect to the control simulations, in glacier volume in the region (Fig. 4.4). The changes in land use and land cover might have contributed significantly to the build up of ice volume during the LIA. In two of the three ensemble members, there is a relatively large gain in glacier volume over this period, 1117 km^3 and 1378 km^3. However, such a contribution of the LULCC to the glacier volume increase during the LIA is not at all certain from our results, as in the other ensemble member the glacier volume decreased by 92 km^3 over this period.

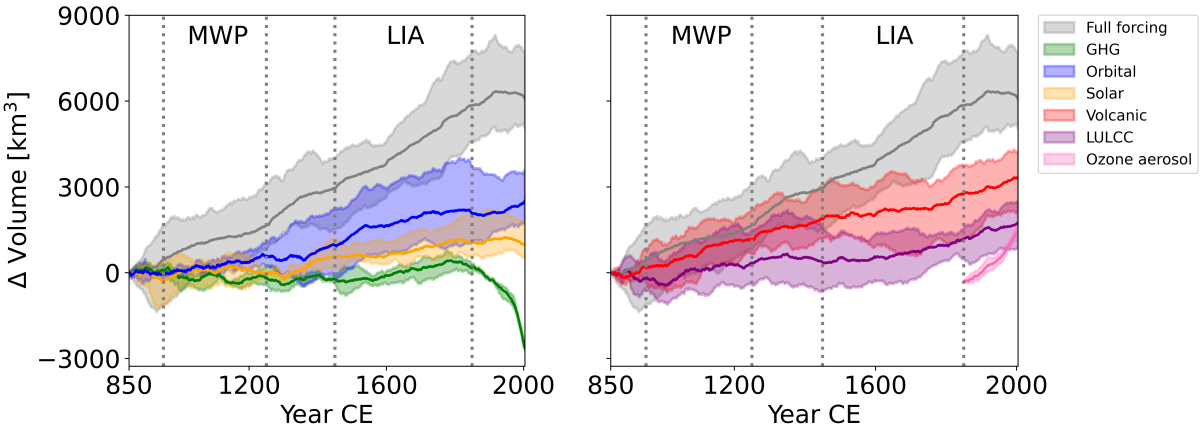

Figure 4.4: Contribution of individual forcings to the glacier evolution. Each color represents simulated volume for each single forcing with respect to the control ensemble. The ensemble range is shaded and the mean is given by the bold lines.

4.3.2 Climate forcing and present-day glacier volume

The simulated mass balance is a function of the precipitation and the temperature (e.g. Chapter 2.1). The glacier volume at the end of the simulations is highly correlated with the simulated mean ELA over the entire simulation (Fig. 4.6). This result combined with the relatively slow glacier response in the region (e.g. Chapter 3) indicates that it might be valuable to study the whole climate time series, when assessing the differences in present-day simulated volume between simulations.

The differences in mean precipitation over the whole time series between the simulations are relatively small, ranging from 253 mm/yr in one of the ozone-aerosol simulations to 265 mm/yr for one of the GHG simulations (Table 4.1). The total precipitation over the simulation cannot explain the difference in glacier evolution in the simulations (Fig. 4.7). On the contrary, the millennium-long simulations with a large glacier volume at the end were forced with less precipitation than the simulations that resulted in a lower volume at present-day. Neither can this pattern, in present-day simulated glacier volumes, be explained by trends in the precipitation (Fig. 4.8). The trends in regional precipitation are either not present in the time series or are opposite of what would be needed to explain the difference in glacier volume at present-day (Table 4.1). The yearly ensemble mean precipitation in the volcanic single forced simulations has a decreasing trend for instance, though it results in a relatively high glacier volume (Fig. 4.4). This is the opposite for the GHG single forced simulations, where the ensemble mean annual

precipitation shows an increasing trend in precipitation, while the simulated volume at the end of the simulation is relatively low.

The annual mean temperature is far below the freezing point in the simulations. We therefore compare the trends of July temperature in the CESM-LME ensemble members with the total glacier volume at the end of the simulation. The trends in the ensemble mean temperature of the respective forcings line up for all forcings except for the LULCC forcing (Fig. 4.9). The LULCC forcing has a stronger negative trend in the July temperature than the volcanic forcing; however, results in a lower glacier volume (Fig. 4.4). The trends in the July temperature do therefore not, or at least cannot fully, explain the differences in simulated glacier volume. This pattern also holds when looking at the individual ensemble members and is not just a result of analysing the ensemble mean trends (Table 4.1). However, the simulated glacier volume at present-day does correlate to a high degree with the mean July temperatures over the entire simulation (Fig. 4.10). The differences in regional mean July temperatures in the CESM-LME ensemble members is an explanation for the resulting differences in glacier volume between the simulations. The negative relation between the increase in precipitation and simulated glacier volume can be explained by the correlation between the mean July temperatures and the mean yearly precipitation (Fig. 4.11). The temperature change seems to have a larger effect on the glacier volume than the change in precipitation.

Ensemble member		Volume	ELA	July Temperature		Precipitation	
Forcing	**no.**	total	mean	mean	trend	mean	trend
		km^3	m	°C	°C/yr	mm/yr	mm/yr
full	3	16295	887	-1.67	-0.00040	257	-0.00891
full	6	15527	895	-1.66	-0.00034	256	-0.00809
full	10	15511	892	-1.65	-0.00063	258	-0.00785
full	13	15019	894	-1.66	-0.00038	257	-0.00545
full	5	14839	900	-1.60	-0.00037	258	no trend
full	2	14768	899	-1.64	-0.00036	257	no trend
full	9	14604	898	-1.58	no trend	258	-0.00451
full	1	14419	905	-1.57	-0.00043	258	-0.00549
full	4	14257	905	-1.59	no trend	258	-0.00514
full	7	14232	903	-1.56	-0.00029	257	-0.00655
full	12	14111	907	-1.60	-0.00063	258	-0.00759
full	11	13816	907	-1.54	-0.00052	258	-0.00581
full	8	13727	910	-1.55	-0.00035	258	no trend
volcanic	2	12876	920	-1.55	no trend	260	no trend
volcanic	1	12778	917	-1.52	-0.00048	259	no trend
orbital	3	12216	921	-1.48	-0.00029	260	no trend
volcanic	3	11867	926	-1.45	no trend	258	no trend
volcanic	4	11396	929	-1.43	-0.00042	260	-0.00553
LULCC	1	11070	939	-1.38	no trend	262	-0.00555
volcanic	5	10765	939	-1.37	-0.00026	261	-0.00446
orbital	2	10753	938	-1.32	-0.00027	261	no trend
LULCC	2	10477	944	-1.34	-0.00051	261	-0.00741
solar	1	10377	945	-1.34	no trend	261	-0.00485
orbital	1	10359	945	-1.24	-0.00024	261	no trend
ozone-aerosol	2	10207	821	-2.09	-0.00598	253	-0.10646
ozone-aerosol	3	10077	840	-1.98	-0.01479	256	-0.15453
ozone-aerosol	1	10069	839	-1.92	-0.00947	255	-0.13094
ozone-aerosol	4	9762	861	-1.86	-0.00910	256	-0.14025
solar	3	9620	949	-1.30	no trend	262	no trend
LULCC	3	9406	955	-1.27	-0.00050	261	-0.00479
solar	5	9168	959	-1.28	no trend	261	no trend
solar	4	9044	956	-1.25	no trend	262	no trend
GHG	3	5981	978	-1.09	0.00034	265	0.00487
GHG	2	5905	982	-1.08	0.00044	264	no trend
GHG	1	5831	980	-1.11	0.00055	264	0.01084

Table 4.1: Trends in the climate forcing. For the different forcings the ensemble members climate characteristics are presented for the region (Otto-Bliesner et al., 2016). This regional selection has been made in the same way as for figure 4.7. The results are ordered by present-day simulated glacier volume. The trend analysis that is presented here was done with a modified version of the Mann-Kendall test (Yue and Wang, 2004; Hussain and Mahmud, 2019). "No trend" indicates that no significant ($p<0.05$) trend was found with the trend test.

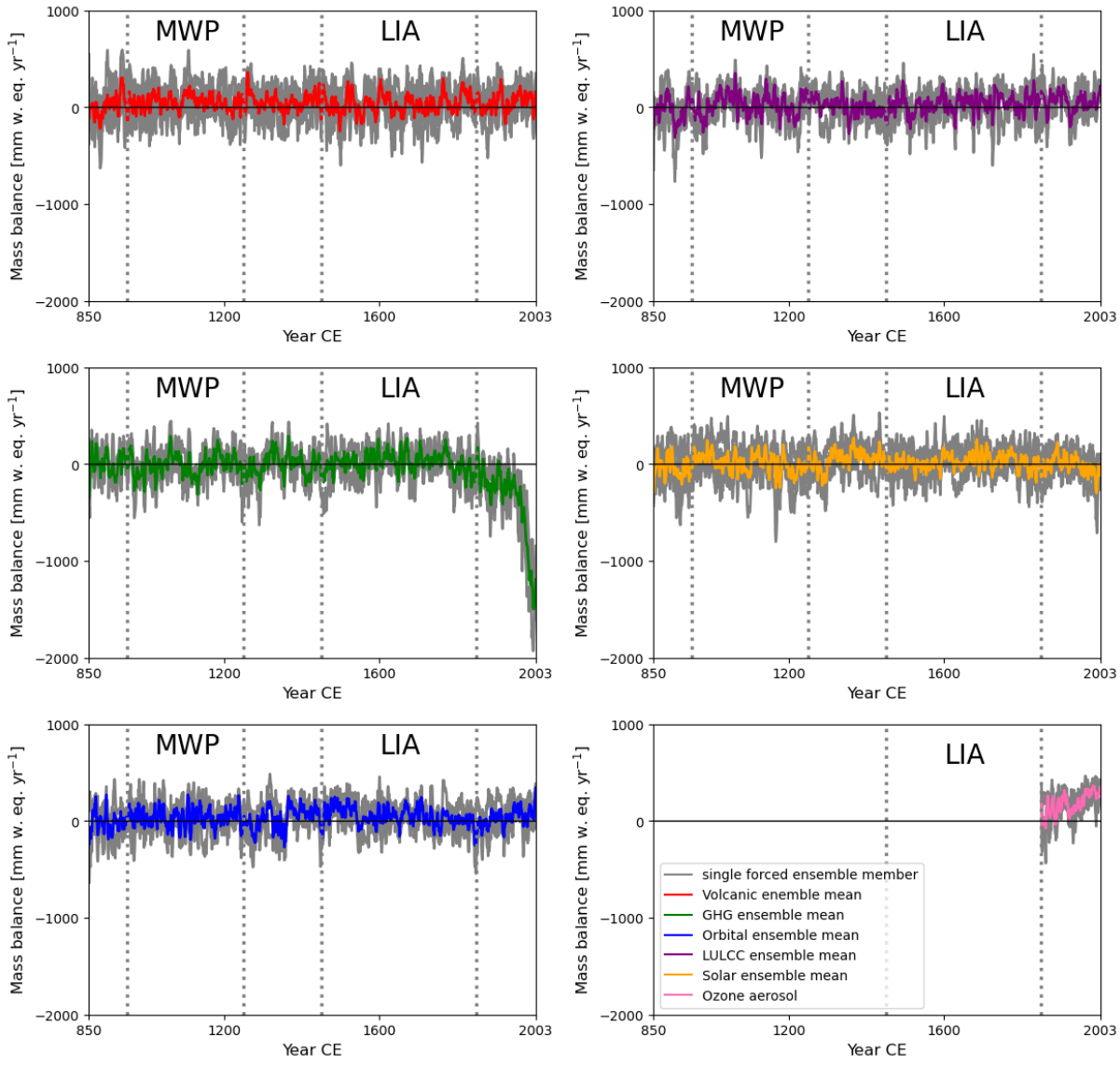

Figure 4.5: SMB in the single forced simulations with respect to the control ensemble, shown here with a 5-year moving average. The coloured lines indicate the ensemble mean of the single forced simulations, and the grey lines the respective single forced ensemble members.

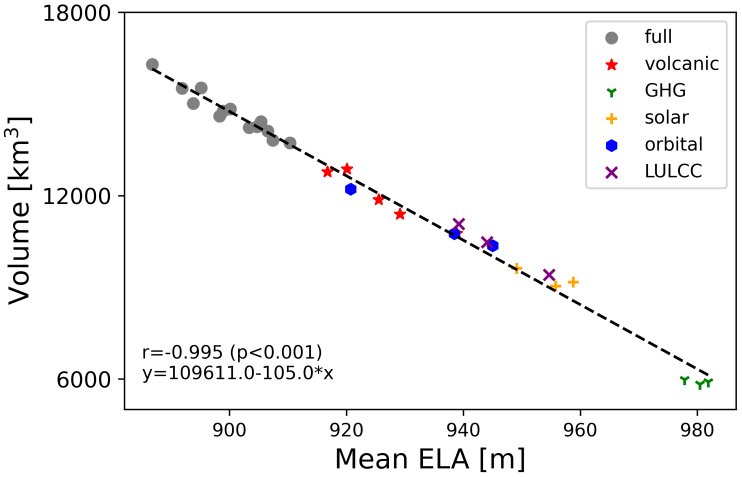

Figure 4.6: Total glacier volume at the end of the simulations vs mean ELA. The mean ELA that is presented here is the mean ELA of all successfully simulated glaciers, which are not being corrected for the glacier size. The ozone-aerosol single forced simulations have been excluded from this figure, because of the shorter duration of those simulations.

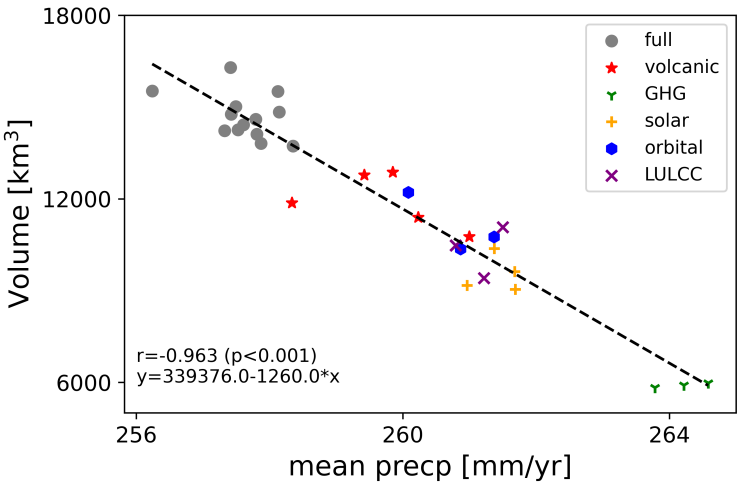

Figure 4.7: Total glacier volume at the end of the simulations vs mean precipitation. The mean precipitation shown here is the mean precipitation of the CESM-LME (Otto-Bliesner et al., 2016) over the area where land-terminating glaciers are present in the CAA based on the RGI v6. This selection has been made with the salem python package (Maussion et al., 2019c) and includes all the CESM-LME grid points that contain a glacier. The results of the ozone-aerosol forcing are not shown here because these simulations have a shorter duration. (Note that the anomaly method, that is used in the preprocessing step before forcing OGGM, has not been applied on the precipitation data that is being presented here.)

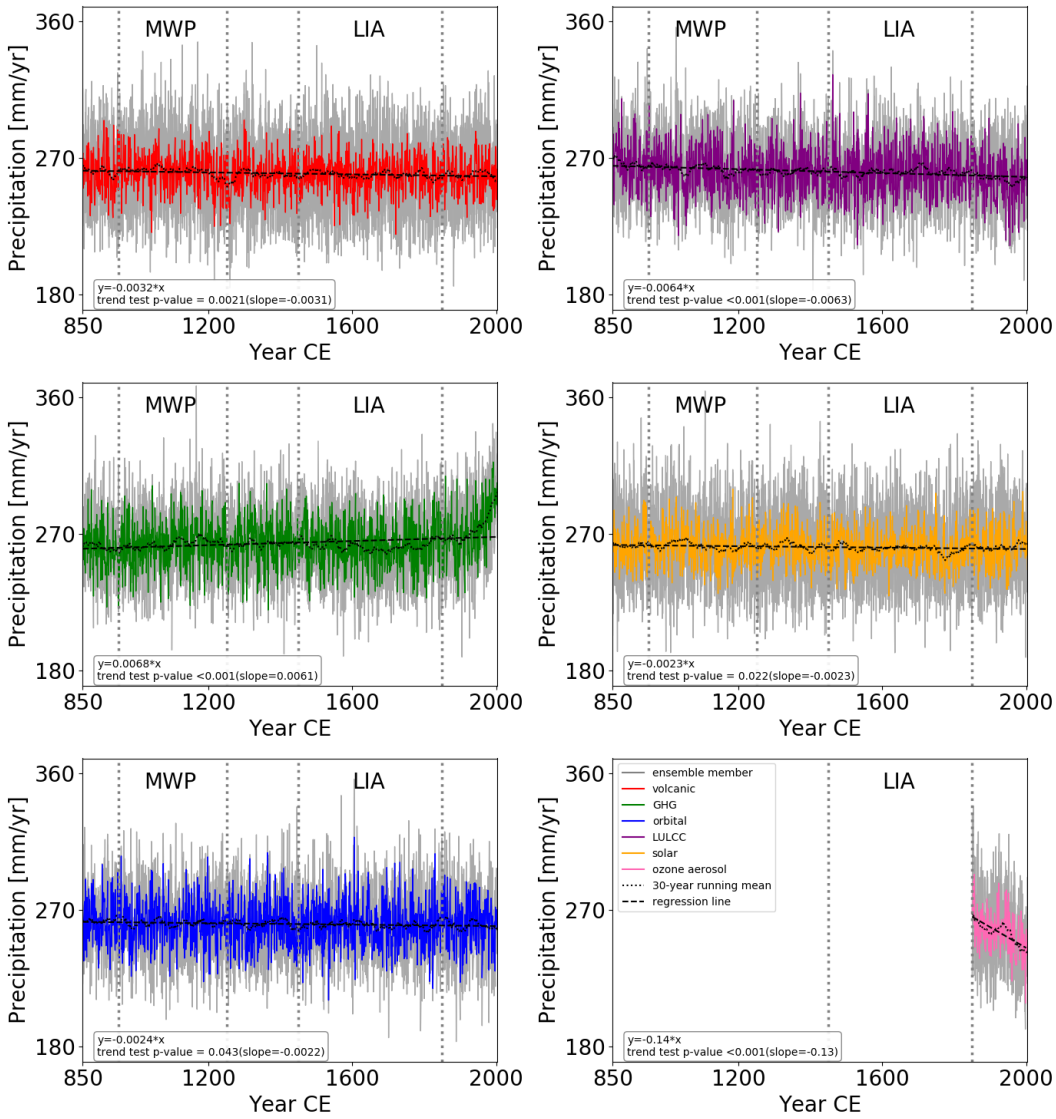

Figure 4.8: Yearly mean precipitation under different climate forcings. The CESM-LME precipitation time series that are presented here are based on the same selection as in figure 4.7 (Otto-Bliesner et al., 2016). The trend analysis was done with a modified version of the Mann-Kendall test on the ensemble mean from each of the different forcings (Yue and Wang, 2004; Hussain and Mahmud, 2019).

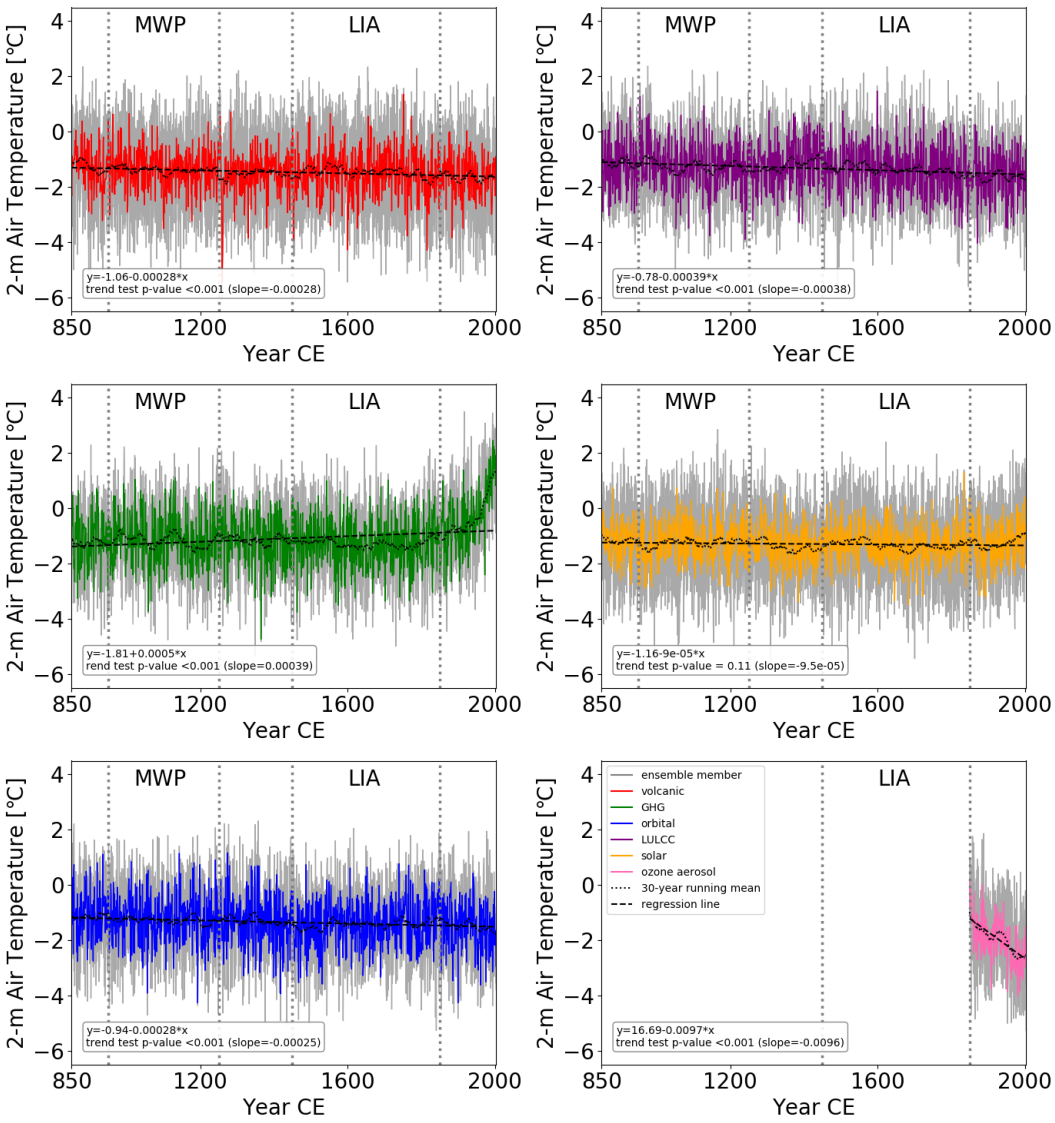

Figure 4.9: July temperature trends under different climate forcings. The CESM-LME timeseries that are being presented here are based on the same selection as in figure 4.7 (Otto-Bliesner et al., 2016). The trend analysis was done with a modified version of the Mann-Kendall test on the ensemble mean from each of the different forcings (Yue and Wang, 2004; Hussain and Mahmud, 2019).

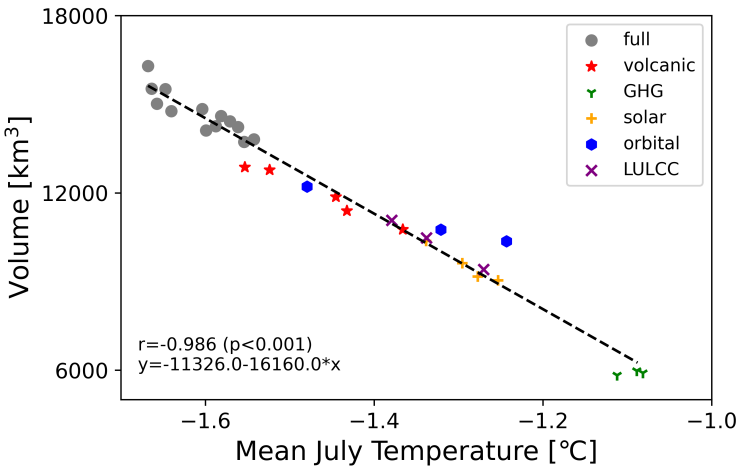

Figure 4.10: Total glacier volume at the end of the simulations vs mean July temperature. The selection of the CESM-LME temperature data has been done in the same way as in figure 4.7 (Otto-Bliesner et al., 2016). Also here the ozone-aerosol single forced simulations have been excluded from the plot because of their shorter duration.

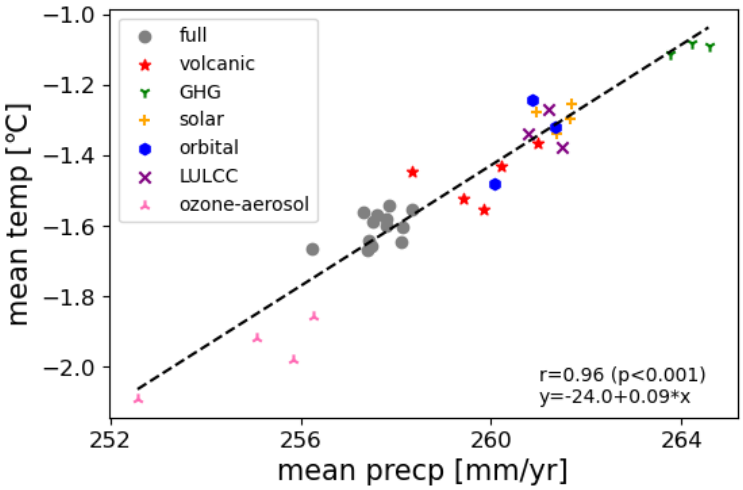

Figure 4.11: Mean precipitation vs mean July temperature. The selection of the CESM-LME temperature data has been plotted similarly as figure 4.7 (Otto-Bliesner et al., 2016).

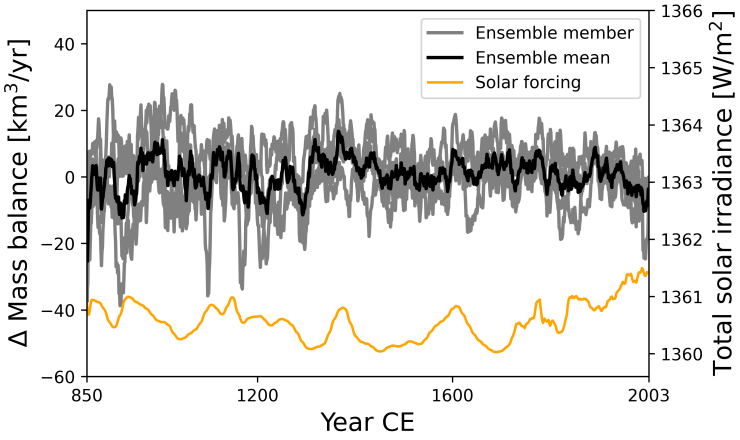

Figure 4.12: SMB and solar forcing. The SMB is of the solar single forced simulations and the solar forcing that was used in the CESM-LME (Vieira et al., 2011; Schmidt et al., 2011), are presented here with an 11-year moving average to filter out the 11-year solar cycle.

4.3.3 The influence of solar forcing

There is no significant trend in the July temperature of the solar single forced simulations (Table 4.1). However, the solar forcing fluctuated over the last millennium and a trend test does not capture such influence. Therefore the correlations between the solar forcing and July temperature, precipitation and the SMB are given here for the solar single forced experiment. In all these cases the time series have been smoothed with an 11-year running mean, to filter out the effect of the 11-year solar cycle, before computing the correlation (Fig. 4.12). The preprocessed climate time series have been weighted here by the glacier area at the respective time step in order to use a time series that is representative of the area covered by land-terminating glaciers and account for the fact that most glaciers are very small (Fig. 3.4). There is no significant correlation between the solar forcing and the simulated SMB in the solar single forced simulations. This correlation ranges from r=-0.188(p=0.441) to r=0.019(p=0.920) for the ensemble members. Also the ensemble mean SMB shows no significant correlation with the solar forcing, r=-0.185(p=0.265). Neither is there a significant correlation between the climate data that is being used to force the model. The correlation between the solar forcing and the July temperature ranges from r=0.015(p=0.947) to r=0.090(p=0.722) for the ensemble members and is r=0.081(p=0.683) for the ensemble mean. For the yearly precipitation this ranges from r=-0.035(p=0.673) to r=0.055(p=0.447) for the ensemble members and r=0.017(p=0.790) is for the ensemble mean.

4.3.4 The influence of volcanic forcing

The volcanic forcing has a strong positive influence on the total glacier volume in the region. Because the forcing is event based, we look here in more detail at what the influence of the volcanic forcing is on the July temperature and the SMB. For this purpose the ten eruptions with the largest aerosol load in the Northern Hemisphere have been selected (Fig. 4.13). A one-tailed student's t-test was used to test if the July temperature and SMB before the eruption was significantly different from the year of eruption onward (Fig. 4.14 and 4.15). The 15 years before the event were compared to the following 15 years (Fig. 4.16) to assess the influence of the eruption on a time scale that is longer than the event itself. Because of the length of these samples two eruptions had to be excluded from the analysis, due to their overlapping time window. The 5 volcanic single forced ensemble members and 8 eruptions result in 40 time slices. In 11 of those 40 cases the temperature is significantly ($p<0.05$) colder in July in the 15 years from the year of the eruption onwards than in the 15 years before. This percentage in slightly higher when the test is applied to the ensemble mean, leading to significantly colder temperatures 3 out of 8 times. When instead of assessing the ensemble members individually the t-test is applied to the whole ensemble, increasing the sample size 5 times, 4 out of 8 eruptions result in significantly colder July temperatures. These numbers are slightly lower for the more positive SMB after the eruptions. In the volcanic single forced simulations, the SMB is in 8 out of 40 cases significantly lower after the respective events. When applying the same test to the ensemble mean, 2 out of the 8 eruptions (1238 and 1761 CE) result in a significantly more positive mass balance. There is one additional eruption, 1600 CE, that results in a significantly more positive SMB when the t-test is applied to the ensemble. These results indicate that in some cases the signal in the individual ensemble members is not significant as a result of internal climate variability. When applying the same test to the 104 time slices (13 ensemble members * 8 eruptions) of July temperature and the SMB in the fully forced simulations, the result is in the same order of magnitude for the individual volcanic single forced ensemble members: in 21% of the events there is a significantly lower July temperature and 25% of the cases have a significantly more positive SMB. However when analysing ensemble mean the number increase to 100% for the July temperature and 38% for the SMB. For the ensemble as a whole, these values are respectively 63% and 88%. The higher numbers for the ensemble mean and the ensemble as a whole for the full forced experiment, compared to the volcanic single forced experiment, are likely the result of the larger ensemble size.

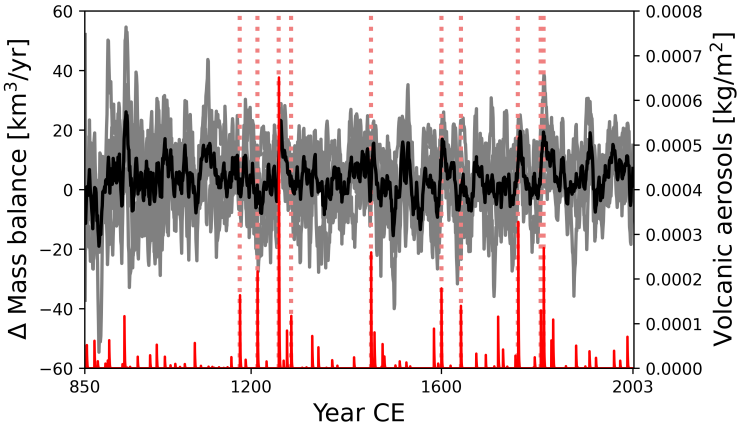

Figure 4.13: SMB and volcanic forcing. The SMB of volcanic single forced simulations is presented here with a 5-year moving average. The yearly mean values for the Northern Hemisphere volcanic forcing as used in the CESM-LME (Gao et al., 2008; Ammann et al., 2003), are shown here in red. The dashed lines indicate the dates of the 10 largest eruptions in the Northern Hemisphere that occurred during the last millennium.

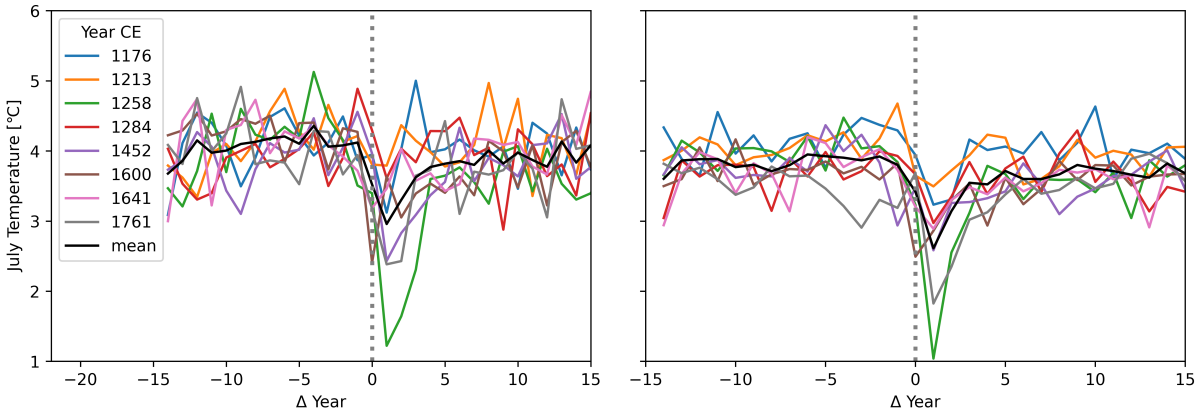

Figure 4.14: Ensemble mean July temperature before and after the 8 selected volcanic eruptions. On the left the volcanic single forced and on the right the fully forced temperature.

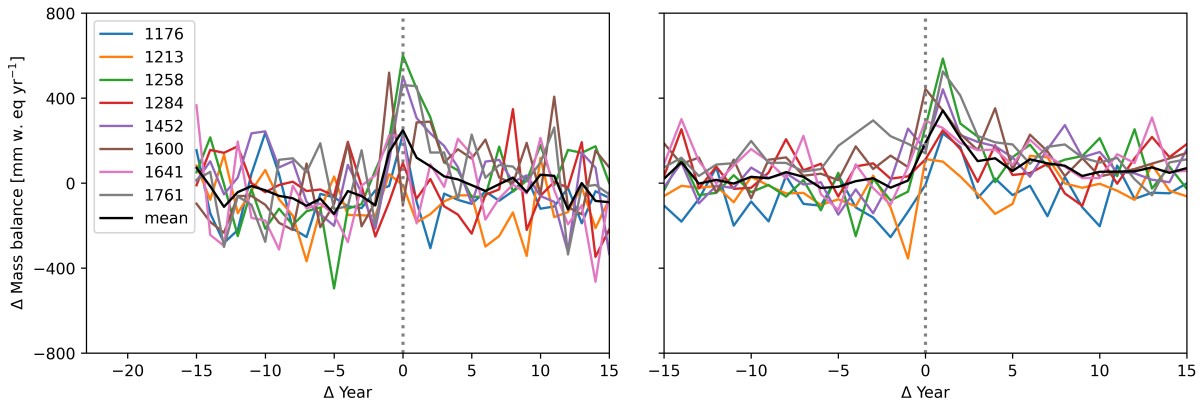

Figure 4.15: Ensemble mean SMB before and after the 8 selected volcanic eruptions. On the left the volcanic single forced and on the right the fully forced SMB.

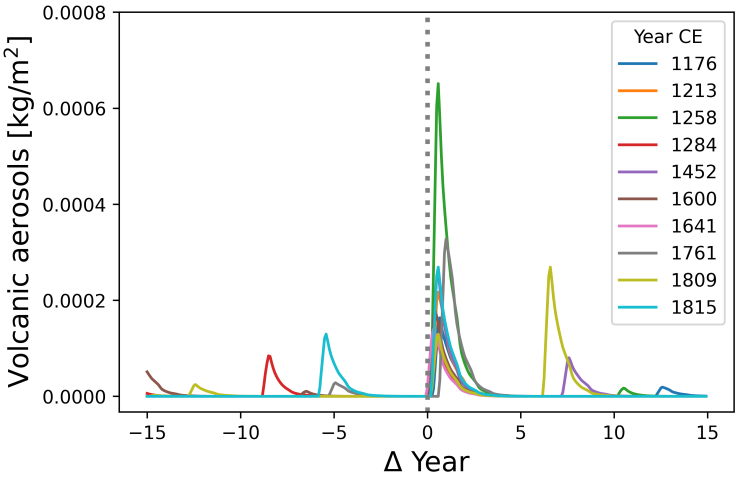

Figure 4.16: The volcanic eruption with the largest load of volcanic aerosols for the Northern Hemisphere in the forcing of the CESM-LME simulations (Gao et al., 2008; Ammann et al., 2003). The volcanic load is presented with respect to the year of the volcanic outburst.

4.4 Discussion

It is known that the glacier mass balance in the CAA strongly depends on the summer temperature and not on the precipitation (e.g. Koerner, 2005). Lower melt season temperatures favour glacier growth and that is also seen in our simulations, where glacier volume strongly correlates with the mean July temperature (Fig. 4.10). More precipitation could favour larger glaciers, however in our experiments the total precipitation in the climate forcing is negatively correlated with the simulated glacier volume (Fig. 4.7). This is a result of the strong correlation between July temperature and precipitation (Fig. 4.11). Bintanja and Selten (2014) found a 4.5 % increase in precipitation per degree warming for the whole Arctic, in CMIP5 21^{st} century simulations. This very comparable with the 10.7 mm/°C relationship between the mean July temperature and mean precipitation, over the last millennium in the CESM-LME for the different simulations in the region (Fig. 4.11), which corresponds to roughly 4.1%/°C. A decreasing sea ice extent has been linked with increasing precipitation in the Arctic, resulting from both increased evaporation in the region and increased meridional moisture transport (Bintanja et al., 2020). However Arctic summer sea ice extent over the last 1450 years correlates poorly with the surface atmospheric temperature, suggesting changes in sea ice extent were driven by a combination of different forces (Kinnard et al., 2011).

There are small changes in the GHGs due to natural feedbacks prior to 1800 CE (Landrum et al., 2013). Up to 1800 CE our GHG single forced simulations follow as a result a comparable trajectory as the control ensemble (Fig. 4.4). However, a small increase in glacier volume occurs during the LIA. This is in line with the reduced GHG emissions during this period. The reduction in GHG concentrations are caused by reduced emissions by the terrestrial biosphere as a results of colder temperatures during that time (Macfarling Meure et al., 2006). From 1800 CE onwards anthropogenically induced changes in GHGs become apparent (Landrum et al., 2013) and the decline in glacier volume starts. This trend is comparable to the influence the GHG has on the sea ice extent in the Northern Hemisphere, which shows an increasing trend up to the mid 19^{th} century before it starts to decline rapidly in the GHG single forced simulations (Otto-Bliesner et al., 2016). For comparison purposes we will therefore treat the GHG single forced simulations as the anthropogenic forcing together with the ozone-aerosol and land use and land cover change single forced simulations (Fig. 4.17).

The volcanic, solar and orbital single forced simulations are grouped together as the natural forced simulations (Fig. 4.17). The change in glacier volume due to solar forcing might be underestimated in our simulations, because the CESM-LME does not include the mechanism through which variations in solar intensity can influence the stratospheric

ozone and through this the climate (Gray et al., 2010; Varma et al., 2012). Even though this mechanism is also lacking in the HadCM3 simulations, Schurer et al. (2014) concluded based on fingerprinting that the solar forcing probably had a minor influence on the Northern Hemisphere climate during the last millennium. As a result the solar forcing also has a relatively small influence on the glacier evolution during the last millennium in our simulations (Fig. 4.4). The volcanic cooling, on the other hand, is generally stronger in the CESM-LME than in reconstructions (Otto-Bliesner et al., 2016), like in the HadCM3 simulations by Schurer et al. (2014). The gap between the PMIP3 simulated volcanic and the reconstructed cooling can partly be assigned to missing nonlinear aerosol microphysics in the models and partly to the reconstructions (Stoffel et al., 2015). The simulated glacier volume and the volcanic contribution to that, are potentially slightly overestimated as a consequence (Fig. 4.4). This does not take away that there was a significant influence by volcanism on the climate (Schurer et al., 2014). There are clear indications that two major volcanic eruptions were followed by ice growth and intensification of that growth (Miller et al., 2012; Anderson et al., 2008). Though volcanic aerosols stay briefly in the atmosphere, the continued cold summers can be explained by sea-ice ocean feedbacks during a northern hemispheric summer insolation minimum that was driven by orbital forcing (Miller et al., 2005, 2012). This supports the pattern of sustained significantly colder July temperatures and subsequently more positive SMB after large volcanic eruptions. The declining summer insolation over the last millennium also explains the lower summer temperatures in the orbital single forced simulations (Fig. 4.9) and the increasing glaciers volumes as a result (Fig. 4.4). Additionally, signs for a positive influence by volcanism on the mass balance of Devon Ice Cap have been found based on instrumental records (Bradley and England, 1978b). Our results are also in line with the study by Huston et al. (2021) on the influence of different forcings on global glacier length. This model study of 76 glaciers shows that most of the pre-industrial last millennium forced response of the glaciers is a result of the volcanic forcing (Huston et al., 2021).

From the onset of the LIA onwards the ensembles of anthropogenic forced and fully forced total do not overlap. The fully forced ensemble is located within the spread of the natural forced ensemble throughout the simulated period. The natural forced simulations show a very similar pattern as the fully forced simulations and do not seem to be distinctly different (Fig. 4.18). Although the glacier volume keeps increasing in the natural forced simulations, it starts to decrease in the fully forced simulations in recent times. With respect to the control simulations, the total of the single forced simulations result in the highest glacier volume, with a slightly higher volume than the natural forced totals from the early LIA onwards (Fig. 4.17). This indicates that the anthropogenic forcing contributed to the build-up of the glacier volume over the last millennium in the region, prior to contributing to the decline in recent times. Even though the anthropogenic forcing as

a whole contributed to the recent decline in glacier volume, its net contribution at the end of the simulation might still be positive. This positive net contribution is, however, not at all certain and maybe even unlikely. Firstly, as with the volcanic aerosols, CESM is likely oversensitive to the indirect effect of anthropogenic aerosols, resulting in a cold bias (Otto-Bliesner et al., 2016). This cold bias would result in an overestimated glacier volume. Secondly, both the GHG and the ozone-aerosol forced experiments both have a relatively narrow ensemble spread compared to the LULCC simulation (Fig. 4.3). The ensemble spread of the anthropogenic forced totals is for that reason largely a result of the ensemble spread on the change in LULCC (Fig. 4.17, 4.18). The LULCC ensemble consists of only 3 members, meaning the lower range of the ensemble is not necessarily an unlikely scenario. Neither is the increasing glacier volume as a result of LULCC required to explain the increase in glacier volume during the LIA. This means these results should be seen as a range of possible scenarios, without necessarily a large decrease in likelihood toward the boundaries of the range. Thirdly, the strong negative mass balance in the last century under the GHG single forcing is likely an underrepresented effect in the anthropogenically forced totals. As the glacier volume decreases under the GHG single forcing, it leaves less that can be melted. By the end of the GHG forced simulation, the ensemble mean volume is only 40% of the fully forced one. Applying the same forcing on these larger glaciers in the fully forced simulations would very likely have resulted in a more negative mass balance. Though this is an issue that could have influenced all single forced simulations, it may disproportionately affected the GHG single forced simulations as a result of the huge mass loss during the last century. Lastly, the positive mass balance during the LIA in the GHG single forced simulation is a result of the decreasing GHG concentrations. The reduced GHG concentrations during this period, measured in ice core samples, have been ascribed to be a natural response to the colder climate (Macfarling Meure et al., 2006). However, in our comparison the GHG forced simulation contains the added effects of anthropogenic and natural GHG forcing, thereby creating a positive bias.

The cooling effect that the LULCC has in the permafrost regions is caused by an increase in albedo due to the change from forest, grassland and shrubs to cropland (Peng et al., 2020). The positive influence that the LULCC as a result has on the glacier volume in the simulations might be bound to the region, because the summer cooling that occurred because of LULCC is stronger for the permafrost regions than in the remaining part of the Northern Hemisphere (Peng et al., 2020). On the other hand, the cooling effect of the LULCC could have a significant effect on the glaciers in other regions, as the cooling in summer is relatively weak compared to the cooling in other seasons. Not only does the mean temperature go down in the LULCC simulations, but there is also a cooling of daily cold and warm extremes in these simulations (Chen and Dirmeyer, 2019). Though this is not taken into account in the glacier simulations, as they are forced with monthly

mean temperature, the reduced extreme temperatures could have an additional positive effect on the glacier volume. However, there are inconsistencies in warm season temperature changes as a result of LULCC between different models (Lejeune et al., 2017). So in addition to the difference between the ensemble members due to internal climate variability, the impact that LULCC has in the simulations might be very different when using another GCM to force the simulations.

Marzeion et al. (2014) showed a decline in glacier volume in the CAA since 1850 CE, the start of their transient simulations based on full forcings from CMIP5. This decline in glacier volume starts on average later in our fully forced simulations, however in one of our ensemble members peak volume occurs one year prior to the start of the simulations by Marzeion et al. (2014). On the other hand there is a larger difference between the natural forced simulations, as our simulations show a growing glacier volume, while their mean glacier volume declines. This difference might be caused by the fact that we present our results with respect to the control ensemble and/or the glaciers that we take into account in our simulations (Fig. 4.17). The advantage of analysing the glacier simulations with respect to the control simulation, is that the results are not affected by adjustments to the climate prior to the start of the simulations. Such a disequilibrium with the climate would be removed when subtracting the control simulation, making the observed signals more robust. However at the same time this introduces a source of error in the comparison that is being made in this paragraph. The mass balance sign might change (e.g. from a negative to positive mass balance when close to zero) in the simulations of Marzeion et al. (2014) once presented with respect to a control run. Either way our simulations show that without anthropogenic influence the glacier volume in the region would still be growing instead of decreasing, and this can be ascribed to the strong influence of GHGs (Fig 4.19, 4.20).

Slangen et al. (2016) did perform a control simulation for their CMIP5 forced global glacier simulations over the period 1900-2005. Like in our results, their simulations show a negative mass balance under the anthropogenic forcing, where the anthropogenic aerosols partly counter balance the effect the GHG has. However unlike in our simulations, their results show a pattern of globally retreating glaciers under natural forcing as a result of LIA relaxation (Slangen et al., 2016). Hirabayashi et al. (2016), on the other hand, did describe a pattern of increasing glacier in their natural forced experiments of 85 Northern Hemisphere glaciers and retreating glaciers under full and natural forcing since the 1980's. Our results are also largely in line with the findings of Roe et al. (2021), who found, for larger ice caps with multi-century response times like those that determine the regional signal in the CAA, that anthropogenic forces likely contributed to 85 to 180 % of the mass loss since 1850 CE. Even though there is a chance that the net influence of the anthropogenic contribution to the glacier volume in the region is

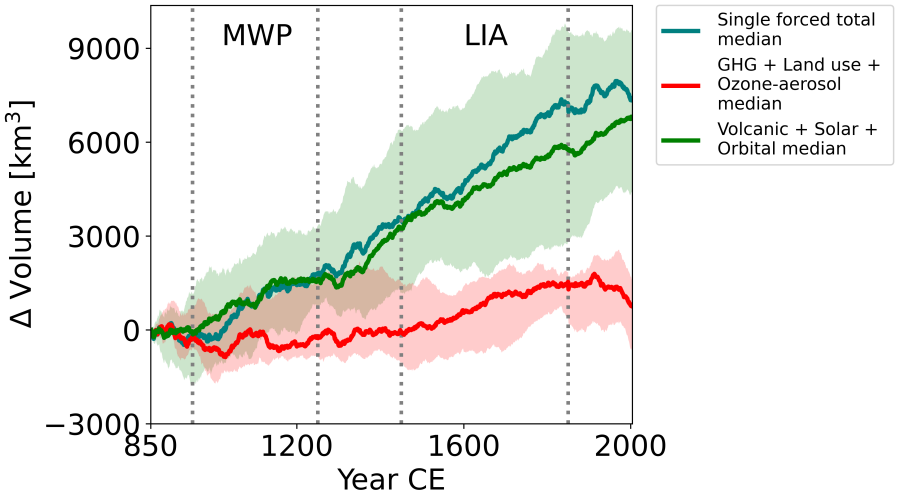

Figure 4.17: The contribution of grouped forcings to the glacier evolution. The glacier volume is presented with respect to the control ensemble. The red line represents the anthropogenic forcing, the green line the natural forcing and the blue line all forcing combined. Shaded is the ensemble range of the respective ensemble. (For the ensemble of the single forced totals see Fig. 4.4.)

maybe still net positive today, it does not mean that there is anthropogenic glacier mass "credit" left that could be spent before hitting the zero net anthropogenic influence bar for these glaciers. Glaciers respond slowly to a changing climate and a part of the mass loss is therefore already committed (Marzeion et al., 2018).

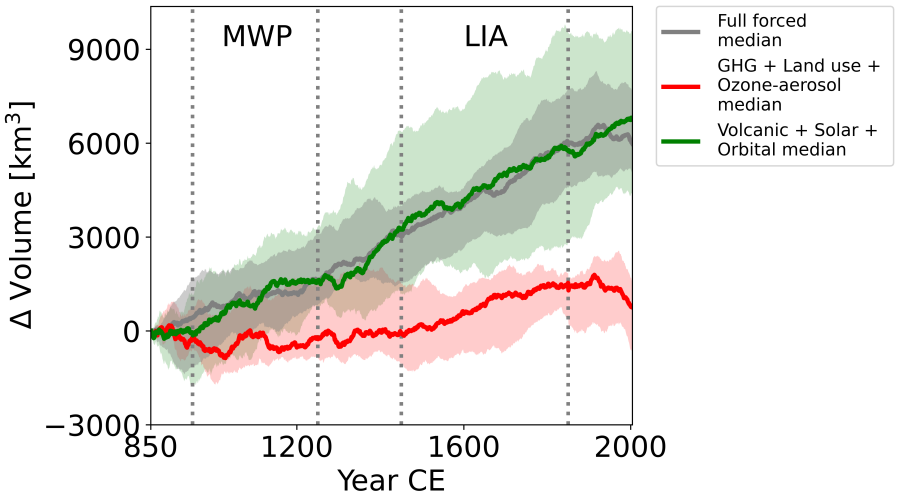

Figure 4.18: The contribution of the full, natural and anthropogenic forcing to the glacier evolution. The glacier volume is presented with respect to the control ensemble. The red line represents the anthropogenic forcing, the green line the natural forcing and the grey line the full forcing. Shaded is the ensemble range of the respective ensemble.

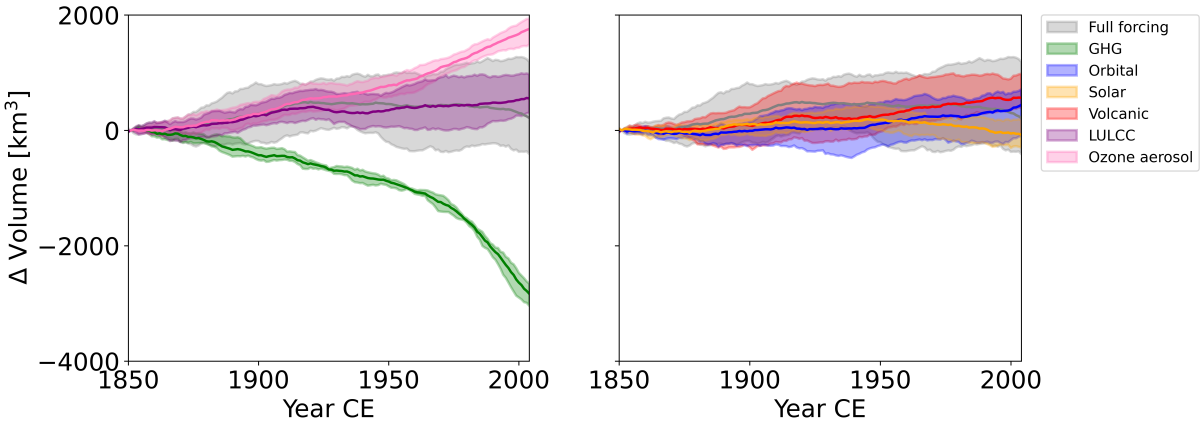

Figure 4.19: Contribution of individual forcings to the glacier evolution over the last 153 years. The simulated volume with respect to the control ensemble as presented in figure 4.4. In this case, the individual forcings were also set to zero in 1851 CE. The shading indicates the ensemble range and the solid line the respective mean.

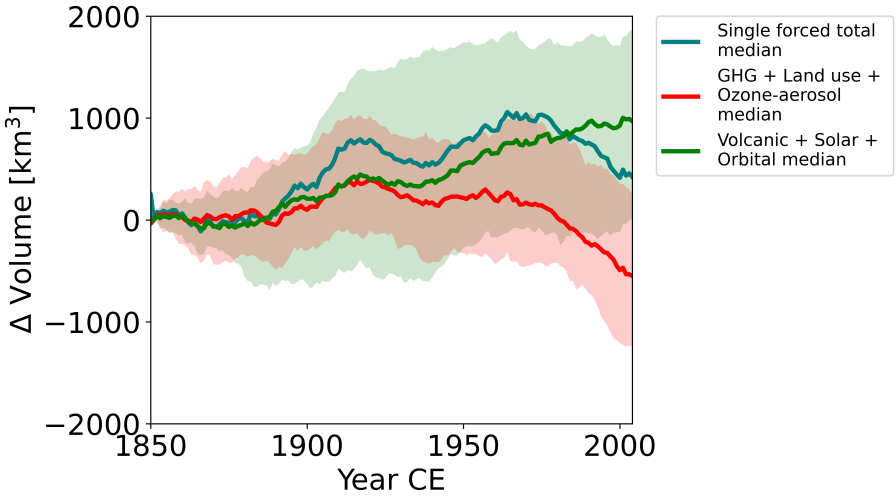

Figure 4.20: The contribution of grouped forcings to the glacier evolution over the last 153 years. The glacier volume with respect to the control ensemble is presented relative to the simulated volume in 1851 CE. The red line represents the anthropogenic forcing, the green line the natural forcing and the blue line all forcing combined. The shaded areas resemble the ensemble range of the respective ensemble. (For the ensemble of the single forced totals see Fig. 4.4.)

5 Conclusions and outlook

The sensitivity study showed that the simulation that was forced with the average of the fully forced ensemble members, and therefore has a reduced amplitude of the internal variability within the climate forcing, has much higher glacier volumes that are well outside the, by internal climate variability generated, ensemble range of the regular fully forced simulations. The amplitude of the climate variability has an influence on both the mean ELA and its variability, resulting in an influence on evolution of glaciers in the CAA. Because a decreased variability in the air temperature reduces the exceedance of the threshold melting temperature, it results in a lower ELA. In addition decreased air temperature variability decreases the variability of the ELA, together causing larger equilibrium volumes in the region, because of the typical glacier geometry and shape of the mass balance gradient. When not taking into account a changing air temperature variability, glacier mass losses might be biased in future projections with a changing climate. Therefore temperature variability cannot be neglected when assessing long-term glacier changes in the Canadian Arctic. This has implications for any glacier modelling study that is driven by climate model output and calls for careful treatment when downscaling gridded data to a glacier scale. Though it goes beyond the scope of this study, this finding might be relevant for other disciplines that make use of climate model output too.

The evolution of the total glacier volume in the region is very sensitive to the initial glacier states in the simulations. However irrespective of the initial conditions the regional volume increases during the LIA, after which it starts to decrease. The regional glacier mass balance is on the other hand not as sensitive to the initial glacier states, enabling us to put recent mass loss in perspective. On a regional level the recent CAA mass loss (2006-2016 CE) might not be unprecedented in the last millennium. Ten out of the thirteen fully forced simulations exceed the recent mass loss during the last millennium. This suggests that with the climate forcing of the last millennium, similar as recent or even more negative mass balance rates could have occurred, but not necessarily did occur.

Under the high emission scenario RCP8.5, the volume loss strongly increases in the 21^{st} century and becomes unprecedented compared to the last millennium within the next decade. The volume loss rate increases up to 2065 CE, after which it decreases. Also after 2065 CE the mass loss stays larger than at present day. The decreasing glacier

volume loss is a result of a decreasing glacier covered area and not of a specific mass balance that becomes less negative. On the contrary, the specific mass balance continues to become more negative up to 2080 CE after that it stays around the 2080 CE values for the remainder of the century. By the end of the century only 14.5 ± 1.8 % of the initial glacier volume remains in the simulations.

Since 850 CE all the different climate forcings, except maybe for the GHG, contributed to a net build up of the glacier volume of land-terminating glaciers up to the end of the LIA. Though there is quite some uncertainty as a result of internal climate variability, the volcanic and orbital forcing seem to be the largest contributors to long term volume build up in the region by the end of the simulation. They are followed by LULCC and the ozone aerosol forcing, of which the later one, though only included for the last 155 years, has a net comparable effect as the LULCC. As a result of the ensemble spread caused by internal climate variability it is not detectable if GHG made net positive contributions to the total volume at the end of the LIA. Around 1800 CE a change in this trend starts and throughout the following 200 years the net contribution of GHG to the glacier volume becomes increasingly more negative. At first the regional volume still grows as a result of the other forcings, in which the anthropogenic ozone aerosol forcing plays a large role from 1850 CE onwards. All together the anthropogenic influence on the glacier volume might have been net positive over the last millennium, thought there are large uncertainties associated with this. Either way, this has already begun to change as a results of both the increasing GHG emissions and glaciers that are not in equilibrium with the climate. Over the last 150 years, GHG had a negative influence on the glacier mass balance, though the impact this has on the glacier volume is at first largely counterbalanced by other forcings, most strongly by the ozone and aerosol forcing. Since the middle of the 20^{th} century, the GHG signal has become stronger than that of the other anthropogenic forcings combined, resulting in a negative anthropogenic influence on the glacier mass balance. Total anthropogenic influence has also grown in recent decades to become larger than the positive influence that the combined natural forces have. Without the recent change in GHG emissions the glacier volume in the Canadian Arctic would still be growing instead of losing large amounts of mass.

The conclusions being presented here are based on the simulations forced with the climate of one GCM in one set-up, the CESM-LME. Putting the recent glacier mass loss into perspective could be improved by repeating the fully forced transient simulations with forcings from different GCMs, e.g. CMIP6/PMIP4, and extending the simulations under different future scenarios. In this context the effect of using another baseline climate than CRU could also be tested. Though it would be interesting to include the tidewater glaciers in such simulations, it does not seem likely that this will be possible to simulate large numbers of tidewater glaciers dynamically on a millennium timescale in

the near future. Additionally the model simulations would likely be improved by including the process of melt water refreezing into OGGM, which is an important component in the SMB of CAA glaciers (Noël et al., 2018).

The glaciers in the region respond relatively slowly to a changing climate. Over the millennium long simulations, the simulated total glacier volume is very sensitive to the initial glacier conditions. The geometry of the glaciers at start of the simulations is unknown. A way to get an better estimate, could be to go further back in time and simulate glaciers over the entire Neoglacial and capture with that the build-up to the maximum extent during the LIA. The sensitivity experiment that was forced over the last 6 millennia with TraCE-21k (He, 2011; Liu et al., 2014), could be a good starting point for doing so (Fig. 3.22). The advantage of starting the simulations during the mid-Holocene would be that many of the valley glaciers were smaller during that time (Briner et al., 2009), likely resulting in a shorter impact of the initial conditions. This would result in the initial conditions no longer being relevant for many glaciers over a large time span of our simulations, on the condition that they were started from reasonable initial states. However this is not the case for all glaciers: e.g. Barnes Ice Cap is a remnant of the Laurentide Ice Sheet and has been retreating throughout the Holocene (Koerner and Fisher, 1990; Thomas et al., 2010). Besides that such simulations could give additional information about the last millennium, the simulation by itself could give valuable insight about the glacier evolution during the Neoglacial, among others because the onset of the advance seems to be asynchronous (Solomina et al., 2015).

It would also be worthwhile to expand the single forced experiment to a global domain. In this context it would however be important to re-think the way this experiment is implemented. Glaciers under the single forcing that deviated too much from the fully forced experiment, might result in misrepresenting the influence the respective forcing has on the glacier mass balance. This is likely a larger issue in regions that have a shorter response time; for instance, as a result of a warmer climate or a regional signal controlled by smaller glaciers than those in the CAA. Prescribing the glacier geometry with for instance the fully forced simulations, could be a way to deal with this issue. Such global simulations would give a global insight into what drove glacier evolution throughout the last millennium, thereby showing what caused the build-up of glacier volume during the LIA (which occurred asynchronously; Neukom et al., 2019), the recent decline, and how that differs by region. It is especially interesting to do this type of simulations on a longer time scale, as glaciers respond slowly to changing climate forcing and are therefore at any given time are also responding to previous changes when being out of equilibrium with the current climate forcing. Therefore it would also give a better insight into the influence of different forcings for the last century than shorter simulations. To our knowledge such simulations have not been done before globally for

the last millennium, which would make them particularly valuable.

Bibliography

Allen, M., Dube, O., Solecki, W., Aragón-Durand, F., Cramer, W., Humphreys, S., Kainuma, M., K. J., Mahowald, N., Mulugetta, Y., Perez, R., Wairiu, M., and Zickfeld, K. *Framing and Context. In: Global Warming of 1.5°C. An IPCC Special Report on the impacts of global warming of 1.5°C above pre-industrial levels and related global greenhouse gas emission pathways, in the context of strengthening the global response to the threat of climate change, sustainable development, and efforts to eradicate poverty*, chapter 1. in press.

Ammann, C. M., Meehl, G. A., Washington, W. M., and Zender, C. S. A monthly and latitudinally varying volcanic forcing dataset in simulations of 20^{th} century climate. *Geophysical Research Letters*, 30(12), 2003. doi: 10.1029/2003GL016875.

Anderson, R. K., Miller, G. H., Briner, J. P., Lifton, N. A., and DeVogel, S. B. A millennial perspective on Arctic warming from 14C in quartz and plants emerging from beneath ice caps. *Geophysical Research Letters*, 35(1), 2008. doi: 10.1029/2007GL032057.

Benn, D. and Evans, D. *Glaciers and Glaciation*. Hodder Education, 2 edition, 2010. ISBN 9780340905791.

Berger, A. Long-term variations of daily insolation and Quaternary climatic changes. *Journal of the Atmospheric Sciences*, 35(12):2362–2367, 1978. doi: 10.1175/1520-0469(1978)035<2362:LTVODI>2.0.CO;2.

Berger, A., Loutre, M.-F., and Tricot, C. Insolation and Earth's orbital periods. *Journal of Geophysical Research: Atmospheres*, 98(D6):10341–10362, 1993. doi: 10.1029/93JD00222.

Bintanja, R. and Selten, F. Future increases in Arctic precipitation linked to local evaporation and sea-ice retreat. *Nature*, 509(7501):479–482, 2014. doi: 10.1038/nature13259.

Bintanja, R., van der Wiel, K., Van der Linden, E., Reusen, J., Bogerd, L., Krikken, F., and Selten, F. Strong future increases in Arctic precipitation variability linked to poleward moisture transport. *Science Advances*, 6(7):eaax6869, 2020. doi: 10.1126/sciadv.aax6869.

Blake Jr, W. Neoglacial fluctuations of glaciers, southeastern Ellesmere Island, Canadian Arctic Archipelago. *Geografiska Annaler: Series A, Physical Geography*, 63(3-4):201–

218, 1981. doi: 10.1080/04353676.1981.11880035.

Box, J. E., Colgan, W. T., Wouters, B., Burgess, D. O., O'Neel, S., Thomson, L. I., and Mernild, S. H. Global sea-level contribution from Arctic land ice: 1971–2017. *Environmental Research Letters*, 13(12):125012, 2018. doi: 10.1088/1748-9326/aaf2ed.

Bradley, R. S. and England, J. Recent climatic fluctuations of the Canadian High Arctic and their significance for glaciology. *Arctic and Alpine Research*, 10(4):715–731, 1978a. doi: 10.1080/00040851.1978.12004010.

Bradley, R. S. and England, J. Volcanic dust influence on glacier mass balance at high latitudes. *Nature*, 271(5647):736, 1978b. doi: 10.1038/271736a0.

Briner, J. P., Davis, P. T., and Miller, G. H. Latest Pleistocene and Holocene glaciation of Baffin Island, Arctic Canada: key patterns and chronologies. *Quaternary Science Reviews*, 28(21-22):2075–2087, 2009. doi: 10.1016/j.quascirev.2008.09.017.

Chen, L. and Dirmeyer, P. A. The relative importance among anthropogenic forcings of land use/land cover change in affecting temperature extremes. *Climate Dynamics*, 52 (3-4):2269–2285, 2019. doi: 10.1007/s00382-018-4250-z.

Ciracì, E., Velicogna, I., and Swenson, S. Continuity of the mass loss of the world's glaciers and ice caps from the GRACE and GRACE follow-on missions. *Geophysical Research Letters*, 47(9):e2019GL086926, 2020. doi: 10.1029/2019GL086926.

Cogley, J. G., Adams, W., Ecclestone, M., Jung-Rothenhäusler, F., and Ommanney, C. Mass balance of White Glacier, Axel Heiberg Island, N.W.T, Canada, 1960–91. *Journal of Glaciology*, 42(142):548–563, 1996. doi: 10.3189/S0022143000003531.

Cogley, J. G., Hock, R., Rasmussen, L., Arendt, A., Bauder, A., Braithwaite, R., Jansson, P., Kaser, G., Möller, M., Nicholson, L., et al. Glossary of glacier mass balance and related terms. *IHP-VII technical documents in hydrology*, 86:965, 2011.

Cook, A. J., Copland, L., Noël, B. P., Stokes, C. R., Bentley, M. J., Sharp, M. J., Bingham, R. G., and van den Broeke, M. R. Atmospheric forcing of rapid marine-terminating glacier retreat in the Canadian Arctic Archipelago. *Science Advances*, 5 (3):eaau8507, 2019. doi: 10.1126/sciadv.aau8507.

Dee, D. P., Uppala, S., Simmons, A., Berrisford, P., Poli, P., Kobayashi, S., Andrae, U., Balmaseda, M., Balsamo, G., Bauer, d. P., et al. The ERA-Interim reanalysis: Configuration and performance of the data assimilation system. *Quarterly Journal of the Royal Meteorological Society*, 137(656):553–597, 2011. doi: 10.1002/qj.828.

Deevey, E. S. The human population. *Scientific American*, 203(3):194–205, 1960. doi: 10.2307/24940623.

Dutton, A. and Lambeck, K. Ice volume and sea level during the last interglacial. *Science*, 337(6091):216–219, 2012. doi: 10.1126/science.1205749.

Eis, J., Maussion, F., and Marzeion, B. Initialization of a global glacier model based on present-day glacier geometry and past climate information: an ensemble approach. *The Cryosphere*, 13(12):3317–3335, 2019. doi: 10.5194/tc-13-3317-2019.

England, J., Atkinson, N., Bednarski, J., Dyke, A., Hodgson, D., and Cofaigh, C. Ó. The Innuitian Ice Sheet: configuration, dynamics and chronology. *Quaternary Science Reviews*, 25(7-8):689–703, 2006. doi: 10.1016/j.quascirev.2005.08.007.

Farinotti, D. On the effect of short-term climate variability on mountain glaciers: insights from a case study. *Journal of Glaciology*, 59(217):992–1006, 2013. doi: 10.3189/2013JoG13J080.

Farinotti, D., Huss, M., Bauder, A., Funk, M., and Truffer, M. A method to estimate the ice volume and ice-thickness distribution of alpine glaciers. *Journal of Glaciology*, 55(191):422–430, 2009. doi: 10.3189/002214309788816759.

Farinotti, D., Brinkerhoff, D. J., Clarke, G. K. C., Fürst, J. J., Frey, H., Gantayat, P., Gillet-Chaulet, F., Girard, C., Huss, M., Leclercq, P. W., Linsbauer, A., Machguth, H., Martin, C., Maussion, F., Morlighem, M., Mosbeux, C., Pandit, A., Portmann, A., Rabatel, A., Ramsankaran, R., Reerink, T. J., Sanchez, O., Stentoft, P. A., Singh Kumari, S., van Pelt, W. J. J., Anderson, B., Benham, T., Binder, D., Dowdeswell, J. A., Fischer, A., Helfricht, K., Kutuzov, S., Lavrentiev, I., McNabb, R., Gudmundsson, G. H., Li, H., and Andreassen, L. M. How accurate are estimates of glacier ice thickness? Results from ITMIX, the Ice Thickness Models Intercomparison eXperiment. *The Cryosphere*, 11(2):949–970, 2017. doi: 10.5194/tc-11-949-2017.

Farinotti, D., Huss, M., Fürst, J. J., Landmann, J., Machguth, H., Maussion, F., and Pandit, A. A consensus estimate for the ice thickness distribution of all glaciers on Earth. *Nature Geoscience*, 12(3):168, 2019. doi: 10.1038/s41561-019-0300-3.

Fisher, D., Zheng, J., Burgess, D., Zdanowicz, C., Kinnard, C., Sharp, M., and Bourgeois, J. Recent melt rates of Canadian Arctic ice caps are the highest in four millennia. *Global and Planetary Change*, 84:3–7, 2012. doi: 10.1016/j.gloplacha.2011.06.005.

Frankcombe, L. M., England, M. H., Mann, M. E., and Steinman, B. A. Separating internal variability from the externally forced climate response. *Journal of Climate*, 28(20):8184–8202, 2015. doi: 10.1175/JCLI-D-15-0069.1.

Frankcombe, L. M., England, M. H., Kajtar, J. B., Mann, M. E., and Steinman, B. A. On the choice of ensemble mean for estimating the forced signal in the presence of internal variability. *Journal of Climate*, 31(14):5681–5693, 2018. doi: 10.1175/JCLI-D-17-0662.1.

Fretwell, P., Pritchard, H. D., Vaughan, D. G., Bamber, J. L., Barrand, N. E., Bell, R., Bianchi, C., Bingham, R., Blankenship, D. D., Casassa, G., et al. Bedmap2: improved ice bed, surface and thickness datasets for Antarctica. *The Cryosphere*, 7(1):375–393,

2013. doi: 10.5194/tc-7-375-2013.

Gao, C., Robock, A., and Ammann, C. Volcanic forcing of climate over the past 1500 years: An improved ice core-based index for climate models. *Journal of Geophysical Research: Atmospheres*, 113(D23), 2008. doi: 10.1029/2008JD010239.

Gardner, A., Moholdt, G., Wouters, B., Wolken, G., Burgess, D., Sharp, M., Cogley, J., Braun, C., and Labine, C. Sharply increased mass loss from glaciers and ice caps in the Canadian Arctic Archipelago. *Nature*, 473(7347):357–360, 2011. doi: 10.1038/nature10089.

Gardner, A. S. and Sharp, M. Influence of the Arctic circumpolar vortex on the mass balance of Canadian High Arctic glaciers. *Journal of Climate*, 20(18):4586–4598, 2007. doi: 10.1175/JCLI4268.1.

Gardner, A. S., Moholdt, G., Cogley, J. G., Wouters, B., Arendt, A. A., Wahr, J., Berthier, E., Hock, R., Pfeffer, W. T., Kaser, G., et al. A reconciled estimate of glacier contributions to sea level rise: 2003 to 2009. *Science*, 340(6134):852–857, 2013. doi: 10.1126/science.1234532.

Goosse, H., Renssen, H., Timmermann, A., and Bradley, R. S. Internal and forced climate variability during the last millennium: a model-data comparison using ensemble simulations. *Quaternary Science Reviews*, 24(12-13):1345–1360, 2005. doi: 10.1016/j.quascirev.2004.12.009.

Goosse, H., Barriat, P.-Y., Dalaiden, Q., Klein, F., Marzeion, B., Maussion, F., Pelucchi, P., and Vlug, A. Testing the consistency between changes in simulated climate and Alpine glacier length over the past millennium. *Climate of the Past*, 14(8):1119–1133, 2018. doi: 10.5194/cp-14-1119-2018.

Gray, L. J., Beer, J., Geller, M., Haigh, J. D., Lockwood, M., Matthes, K., Cubasch, U., Fleitmann, D., Harrison, G., Hood, L., et al. Solar influences on climate. *Reviews of Geophysics*, 48(4), 2010. doi: 10.1029/2009RG000282.

Hamed, K. Enhancing the effectiveness of prewhitening in trend analysis of hydrologic data. *Journal of Hydrology*, 368(1-4):143–155, 2009. doi: 10.1016/j.jhydrol.2009.01.040.

Harig, C. and Simons, F. J. Ice mass loss in Greenland, the Gulf of Alaska, and the Canadian Archipelago: Seasonal cycles and decadal trends. *Geophysical Research Letters*, 43(7):3150–3159, 2016. doi: 10.1002/2016GL067759.

Harris, I., Jones, P., Osborn, T., and Lister, D. Updated high-resolution grids of monthly climatic observations–the CRU TS3.10 Dataset. *International Journal of Climatology*, 34(3):623–642, 2014. doi: 10.1002/joc.3711.

Hausfather, Z. and Peters, G. P. Emissions–the 'business as usual' story is misleading.

Nature, 577:618–620, 2020. doi: 10.1038/d41586-020-00177-3.

He, F. *Simulating transient climate evolution of the last deglaciation with CCSM 3*. 2011.

Hirabayashi, Y., Nakano, K., Zhang, Y., Watanabe, S., Tanoue, M., and Kanae, S. Contributions of natural and anthropogenic radiative forcing to mass loss of Northern Hemisphere mountain glaciers and quantifying their uncertainties. *Scientific reports*, 6:29723, 2016. doi: 10.1038/srep29723.

Huang, W., Feng, S., Liu, C., Chen, J., Chen, J., and Chen, F. Changes of climate regimes during the last millennium and the twenty-first century simulated by the Community Earth System Model. *Quaternary Science Reviews*, 180:42–56, 2018. doi: 10.1016/j.quascirev.2017.11.019.

Hurrell, J. W., Holland, M. M., Gent, P. R., Ghan, S., Kay, J. E., Kushner, P. J., Lamarque, J.-F., Large, W. G., Lawrence, D., Lindsay, K., et al. The Community Earth System Model: a framework for collaborative research. *Bulletin of the American Meteorological Society*, 94(9):1339–1360, 2013. doi: 10.1175/BAMS-D-12-00121.1.

Hurtt, G. C., Chini, L. P., Frolking, S., Betts, R., Feddema, J., Fischer, G., Fisk, J., Hibbard, K., Houghton, R., Janetos, A., et al. Harmonization of land-use scenarios for the period 1500–2100: 600 years of global gridded annual land-use transitions, wood harvest, and resulting secondary lands. *Climatic Change*, 109(1-2):117, 2011. doi: 10.1007/s10584-011-0153-2.

Hussain, M. and Mahmud, I. pymannkendall: a python package for non parametric Mann Kendall family of trend tests. *Journal of Open Source Software*, 4(39):1556, 7 2019. ISSN 2475-9066. doi: 10.21105/joss.01556.

Huston, A., Siler, N., Roe, G. H., Pettit, E., and Steiger, N. J. Understanding drivers of glacier-length variability over the last millennium. *The Cryosphere*, 15(3):1645–1662, 2021. doi: 10.5194/tc-15-1645-2021.

Hutter, K. *Theoretical glaciology: material science of ice and the mechanics of glaciers and ice sheets*. D. Reidel Publishing Company, 1983.

Kaufman, D. S., Schneider, D. P., McKay, N. P., Ammann, C. M., Bradley, R. S., Briffa, K. R., Miller, G. H., Otto-Bliesner, B. L., Overpeck, J. T., Vinther, B. M., et al. Recent warming reverses long-term Arctic cooling. *Science*, 325(5945):1236–1239, 2009. doi: 10.1126/science.1173983.

Kay, J., Deser, C., Phillips, A., Mai, A., Hannay, C., Strand, G., Arblaster, J., Bates, S., Danabasoglu, G., Edwards, J., et al. The Community Earth System Model (CESM) large ensemble project: A community resource for studying climate change in the presence of internal climate variability. *Bulletin of the American Meteorological Society*, 96(8):1333–1349, 2015. doi: 10.1175/BAMS-D-13-00255.1.

Kendall, M. G. Rank correlation methods. 1948.

Kienholz, C., Rich, J., Arendt, A., and Hock, R. A new method for deriving glacier centerlines applied to glaciers in Alaska and northwest Canada. *The Cryosphere*, 8(2): 503–519, 2014. doi: 10.5194/tc-8-503-2014.

Kinnard, C., Zdanowicz, C. M., Fisher, D. A., Isaksson, E., de Vernal, A., and Thompson, L. G. Reconstructed changes in Arctic sea ice over the past 1,450 years. *Nature*, 479 (7374):509–512, 2011. doi: 10.1038/nature10581.

Koerner, R. M. Mass balance of glaciers in the Queen Elizabeth Islands, Nunavut, Canada. *Annals of Glaciology*, 42:417–423, 2005. doi: 10.3189/172756405781813122.

Koerner, R. M. and Fisher, D. A record of Holocene summer climate from a Canadian High-Arctic ice core. *Nature*, 343(6259):630–631, 1990. doi: 10.1038/343630a0.

Koerner, R. M. and Fisher, D. A. Ice-core evidence for widespread Arctic glacier retreat in the Last Interglacial and the early Holocene. *Annals of Glaciology*, 35:19–24, 2002. doi: 10.3189/172756402781817338.

Kulp, S. A. and Strauss, B. H. New elevation data triple estimates of global vulnerability to sea-level rise and coastal flooding. *Nature Communications*, 10(1):1–12, 2019. doi: 10.1038/s41467-019-12808-z.

Laloyaux, P., de Boisseson, E., Balmaseda, M., Bidlot, J.-R., Broennimann, S., Buizza, R., Dalhgren, P., Dee, D., Haimberger, L., Hersbach, H., et al. CERA-20C: A coupled reanalysis of the twentieth century. *Journal of Advances in Modeling Earth Systems*, 10(5):1172–1195, 2018. doi: 10.1029/2018MS001273.

Lambeck, K., Rouby, H., Purcell, A., Sun, Y., and Sambridge, M. Sea level and global ice volumes from the Last Glacial Maximum to the Holocene. *Proceedings of the National Academy of Sciences*, 111(43):15296–15303, 2014. doi: 10.1073/pnas.1411762111.

Landrum, L., Otto-Bliesner, B. L., Wahl, E. R., Conley, A., Lawrence, P. J., Rosenbloom, N., and Teng, H. Last millennium climate and its variability in CCSM4. *Journal of Climate*, 26(4):1085–1111, 2013. doi: 10.1175/JCLI-D-11-00326.1.

Lejeune, Q., Seneviratne, S. I., and Davin, E. L. Historical land-cover change impacts on climate: Comparative assessment of LUCID and CMIP5 multimodel experiments. *Journal of Climate*, 30(4):1439–1459, 2017. doi: 10.1175/JCLI-D-16-0213.1.

Lenaerts, J., Angelen, J., Broeke, M., Gardner, A., Wouters, B., and Meijgaard, E. Irreversible mass loss of Canadian Arctic Archipelago glaciers. *Geophysical Research Letters*, 40(5):870–874, 2013. doi: 10.1002/grl.50214.

Liu, Z., Lu, Z., Wen, X., Otto-Bliesner, B., Timmermann, A., and Cobb, K. Evolution and forcing mechanisms of El Niño over the past 21,000 years. *Nature*, 515(7528):550, 2014. doi: 10.1038/nature13963.

Macfarling Meure, C., Etheridge, D., Trudinger, C., Steele, P., Langenfelds, R., Van Ommen, T., Smith, A., and Elkins, J. Law Dome CO_2, CH_4 and N_2O ice core records extended to 2000 years BP. *Geophysical Research Letters*, 33(14), 2006. doi: 10.1029/2006GL026152.

Malone, A. G., Doughty, A. M., and Macayeal, D. R. Interannual climate variability helps define the mean state of glaciers. *Journal of Glaciology*, 65(251):508–517, 2019. doi: 10.1017/jog.2019.28.

Mann, H. B. Nonparametric tests against trend. *Econometrica: Journal of the Econometric Society*, pages 245–259, 1945.

Margreth, A., Dyke, A. S., Gosse, J. C., and Telka, A. M. Neoglacial ice expansion and late Holocene cold-based ice cap dynamics on Cumberland Peninsula, Baffin Island, Arctic Canada. *Quaternary Science Reviews*, 91:242–256, 2014. doi: 10.1016/j.quascirev.2014.02.005.

Marzeion, B., Jarosch, A., and Hofer, M. Past and future sea-level change from the surface mass balance of glaciers. *The Cryosphere*, 6(6):1295–1322, 2012. doi: 10.5194/tc-6-1295-2012.

Marzeion, B., Cogley, J. G., Richter, K., and Parkes, D. Attribution of global glacier mass loss to anthropogenic and natural causes. *Science*, 345(6199):919–921, 2014. doi: 10.1126/science.1254702.

Marzeion, B., Leclercq, P., Cogley, J., and Jarosch, A. Brief Communication: Global reconstructions of glacier mass change during the 20^{th} century are consistent. *The Cryosphere*, 9(6):2399–2404, 2015. doi: 10.5194/tc-9-2399-2015.

Marzeion, B., Kaser, G., Maussion, F., and Champollion, N. Limited influence of climate change mitigation on short-term glacier mass loss. *Nature Climate Change*, 8(4):305, 2018. doi: 10.1038/s41558-018-0093-1.

Marzeion, B., Hock, R., Anderson, B., Bliss, A., Champollion, N., Fujita, K., Huss, M., Immerzeel, W. W., Kraaijenbrink, P., Malles, J.-H., et al. Partitioning the uncertainty of ensemble projections of global glacier mass change. *Earth's Future*, 8(7): e2019EF001470, 2020. doi: 10.1029/2019EF001470.

Masson-Delmotte, V., Schulz, M., Abe-Ouchi, A., Beer, J., Ganopolski, A., Gonzàlez Rouco, J., Jansen, E., Lambeck, K., Luterbacher, J., Naish, T., Osborn, T., Otto-Bliesner, B., Quinn, T., Ramesh, R., Rojas, M., Shao, X., and Timmermann, A. *Information from Paleoclimate Archives*, book chapter 5, pages 383–464. Cambridge University Press, Cambridge, United Kingdom and New York, NY, USA, 2013. ISBN 978-1-107-66182-0. doi: 10.1017/CBO9781107415324.013.

Maussion, F., Rothenpieler, T., Recinos, B., Vlug, A., Dusch, M., Marzeion, B., Landmann, J., Eis, J., Oesterle, F., Bartholomew, S., Champollion, N., Gregor, P., Butenko,

A., Smith, S., and Oberrauch, M. OGGM/oggm: v1.0.3. December 2018. doi: 10.5281/zenodo.1998082.

Maussion, F., Butenko, A., Champollion, N., Dusch, M., Eis, J., Fourteau, K., Gregor, P., Jarosch, A. H., Landmann, J., Oesterle, F., Recinos, B., Rothenpieler, T., Vlug, A., Wild, C. T., and Marzeion, B. The open global glacier model (oggm) v1.1. *Geoscientific Model Development*, 12(3):909–931, 2019a. doi: 10.5194/gmd-12-909-2019.

Maussion, F., Rothenpieler, T., Dusch, M., Recinos, B., Vlug, A., Marzeion, B., Landmann, J., Eis, J., Bartholomew, S., Champollion, N., Gregor, P., Butenko, A., Smith, S., and Oberrauch, M. OGGM/oggm: v1.1. Feb. 2019b. doi: 10.5281/zenodo.2580277.

Maussion, F., TimoRoth, tbridel, Dusch, M., and Landmann, J. fmaussion/salem: v0.2.4. Mar. 2019c. doi: 10.5281/zenodo.2605265.

McKay, N. P. and Kaufman, D. S. An extended Arctic proxy temperature database for the past 2,000 years. *Scientific Data*, 1:1–10, 2014. doi: 10.1038/sdata.2014.26.

McKinnon, K. A., Poppick, A., Dunn-Sigouin, E., and Deser, C. An "Observational Large Ensemble" to compare observed and modeled temperature trend uncertainty due to internal variability. *Journal of Climate*, 30(19):7585–7598, 2017. doi: 10.1175/JCLI-D-16-0905.1.

Meredith, M., Sommerkorn, M., Cassotta, S., Derksen, C., Ekaykin, A., Hollowed, A., Kofinas, G., Mackintosh, A., Melbourne-Thomas, J., Muelbert, M., Ottersen, G., Pritchard, H., and Schuur, E. *Polar Region*, book chapter 3, pages 203–320. Cambridge University Press, Cambridge, United Kingdom and New York, NY, USA, 2019. doi: 10.1017/9781009157964.005.

Mikkelsen, T. B., Grinsted, A., and Ditlevsen, P. Influence of temperature fluctuations on equilibrium ice sheet volume. *The Cryosphere*, 12(1), 2018. doi: 10.5194/tc-12-39-2018.

Millan, R., Mouginot, J., and Rignot, E. Mass budget of the glaciers and ice caps of the Queen Elizabeth Islands, Canada, from 1991 to 2015. *Environmental Research Letters*, 12(2):024016, 2017. doi: 10.1088/1748-9326/aa5b04.

Miller, G. H., Wolfe, A. P., Briner, J. P., Sauer, P. E., and Nesje, A. Holocene glaciation and climate evolution of Baffin Island, Arctic Canada. *Quaternary Science Reviews*, 24(14-15):1703–1721, 2005. doi: 10.1016/j.quascirev.2004.06.021.

Miller, G. H., Alley, R. B., Brigham-Grette, J., Fitzpatrick, J. J., Polyak, L., Serreze, M. C., and White, J. W. Arctic amplification: can the past constrain the future? *Quaternary Science Reviews*, 29(15-16):1779–1790, 2010. doi: 10.1016/j.quascirev.2010.02.008.

Miller, G. H., Geirsdóttir, Á., Zhong, Y., Larsen, D. J., Otto-Bliesner, B. L., Holland,

M. M., Bailey, D. A., Refsnider, K. A., Lehman, S. J., Southon, J. R., et al. Abrupt onset of the Little Ice Age triggered by volcanism and sustained by sea-ice/ocean feedbacks. *Geophysical Research Letters*, 39(2), 2012. doi: 10.1029/2011GL050168.

Miller, G. H., Lehman, S. J., Refsnider, K. A., Southon, J. R., and Zhong, Y. Unprecedented recent summer warmth in Arctic Canada. *Geophysical Research Letters*, 40 (21):5745–5751, 2013.

Morlighem, M., Williams, C. N., Rignot, E., An, L., Arndt, J. E., Bamber, J. L., Catania, G., Chauché, N., Dowdeswell, J. A., Dorschel, B., et al. BedMachine v3: Complete bed topography and ocean bathymetry mapping of greenland from multibeam echo sounding combined with mass conservation. *Geophysical research letters*, 44(21):11–051, 2017. doi: doi.org/10.1002/2017GL074954.

Mudelsee, M. *Climate time series analysis*. Springer, 2013.

Neukom, R., Steiger, N., Gómez-Navarro, J. J., Wang, J., and Werner, J. P. No evidence for globally coherent warm and cold periods over the preindustrial common era. *Nature*, 571(7766):550–554, 2019. doi: 10.1038/s41586-019-1401-2.

New, M., Lister, D., Hulme, M., and Makin, I. A high-resolution data set of surface climate over global land areas. *Climate Research*, 21(1):1–25, 2002. doi: 10.3354/cr021001.

Noël, B., van de Berg, W. J., Lhermitte, S., Wouters, B., Schaffer, N., and van den Broeke, M. R. Six decades of glacial mass loss in the Canadian Arctic Archipelago. *Journal of Geophysical Research: Earth Surface*, 123(6):1430–1449, 2018. doi: 10.1029/2017JF004304.

Oerlemans, J. *Minimal glacier models*. Igitur, Utrecht Publishing & Archiving Services, 2008. ISBN 9789067010221.

Oppenheimer, M., Glavovic, B., Hinkel, J., van de Wal, R., Magnan, A. K., Abd-Elgawad, A., Cai, R., Cifuentes-Jara, M., DeConto, R. M., Ghosh, T., Hay, J., Isla, F., Marzeion, B., Meyssignac, B., and Sebesvari, Z. *Sea Level Rise and Implications for Low Lying Islands, Coasts and Communities.*, book chapter 4, pages 321–445. Cambridge University Press, Cambridge, United Kingdom and New York, NY, USA, 2019. doi: 10.1017/9781009157964.006.

Otto-Bliesner, B. L., Brady, E. C., Fasullo, J., Jahn, A., Landrum, L., Stevenson, S., Rosenbloom, N., Mai, A., and Strand, G. Climate variability and change since 850 CE: An ensemble approach with the Community Earth System Model. *Bulletin of the American Meteorological Society*, 97(5):735–754, 2016. doi: 10.1175/BAMS-D-14-00233.1.

Overland, J., Dunlea, E., Box, J. E., Corell, R., Forsius, M., Kattsov, V., Olsen, M. S., Pawlak, J., Reiersen, L.-O., and Wang, M. The urgency of Arctic change. *Polar*

Science, 21:6–13, 2019. doi: 10.1016/j.polar.2018.11.008.

Parkes, D. and Goosse, H. Modelling regional glacier length changes over the last millennium using the Open Global Glacier Model. *The Cryosphere*, 14(9):3135–3153, 2020. doi: 10.5194/tc-14-3135-2020.

Patterson, W. The physics of glaciers, 1994.

Pendleton, S. L., Miller, G. H., Anderson, R. A., Crump, S. E., Zhong, Y., Jahn, A., and Geirsdottir, Á. Episodic Neoglacial expansion and rapid 20^{th} century retreat of a small ice cap on Baffin Island, Arctic Canada, and modeled temperature change. *Climate of the Past*, 13(11):1527–1537, 2017. doi: 10.5194/cp-13-1527-2017.

Peng, X., Zhang, T., Frauenfeld, O. W., and Du, R. Permafrost response to land use and land cover change in the last millennium across the Northern Hemisphere. *Land Degradation & Development*, 2020. doi: 10.1002/ldr.3578.

Pongratz, J., Reick, C., Raddatz, T., and Claussen, M. A reconstruction of global agricultural areas and land cover for the last millennium. *Global Biogeochemical Cycles*, 22(3), 2008. doi: 10.1029/2007GB003153.

Ramirez-Villegas, J. and Jarvis, A. *Downscaling global circulation model outputs: the delta method decision and policy analysis Working Paper No. 1.* International Center for Tropical Agriculture (CIAT), 2010.

Recinos, B., Maussion, F., Rothenpieler, T., and Marzeion, B. Impact of frontal ablation on the ice thickness estimation of marine-terminating glaciers in Alaska. *The Cryosphere*, 13(10):2657–2672, 2019. doi: 10.5194/tc-13-2657-2019.

Reichert, B. K., Bengtsson, L., and Oerlemans, J. Recent glacier retreat exceeds internal variability. *Journal of Climate*, 15(21):3069–3081, 2002. doi: 10.1175/1520-0442(2002)015<3069:RGREIV>2.0.CO;2.

RGI Consortium. Randolph Glacier Inventory - a dataset of global glacier outlines: Version 5.0: Technical report, global land ice measurements from space, Colorado, USA. Digital Media. 2015. doi: 10.7265/N5-RGI-50.

RGI Consortium. Randolph Glacier Inventory - a dataset of global glacier outlines: Version 6.0: Technical report, global land ice measurements from space, Colorado, USA. Digital Media. 2017. doi: 10.7265/N5-RGI-60.

Roe, G. H. What do glaciers tell us about climate variability and climate change? *Journal of Glaciology*, 57(203):567–578, 2011. doi: 10.3189/002214311796905640.

Roe, G. H. and Baker, M. B. Glacier response to climate perturbations: an accurate linear geometric model. *Journal of Glaciology*, 60(222):670–684, 2014. doi: 10.3189/2014JoG14J016.

Roe, G. H. and O'Neal, M. A. The response of glaciers to intrinsic climate variability:

observations and models of late-Holocene variations in the Pacific Northwest. *Journal of Glaciology*, 55(193):839–854, 2009. doi: 10.3189/002214309790152438.

Roe, G. H., Christian, J. E., and Marzeion, B. On the attribution of industrial-era glacier mass loss to anthropogenic climate change. *The Cryosphere*, 15:1889–1905, 2021. doi: 10.5194/tc-15-1889-2021.

Sang, Y.-F., Wang, Z., and Liu, C. Comparison of the MK test and EMD method for trend identification in hydrological time series. *Journal of Hydrology*, 510:293–298, 2014. doi: 10.1016/j.jhydrol.2013.12.039.

Schmidt, G. A., Jungclaus, J. H., Ammann, C. M., Bard, E., Braconnot, P., Crowley, T. J., Delaygue, G., Joos, F., Krivova, N. A., Muscheler, R., Otto-Bliesner, B. L., Pongratz, J., Shindell, D. T., Solanki, S. K., Steinhilber, F., and Vieira, L. E. A. Climate forcing reconstructions for use in PMIP simulations of the last millennium (v1.0). *Geoscientific Model Development*, 4(1):33–45, 2011. doi: 10.5194/gmd-4-33-2011.

Schurer, A. P., Tett, S. F., and Hegerl, G. C. Small influence of solar variability on climate over the past millennium. *Nature Geoscience*, 7(2):104–108, 2014. doi: 10.1038/ngeo2040.

Schwalm, C. R., Glendon, S., and Duffy, P. B. RCP8.5 tracks cumulative co_2 emissions. *Proceedings of the National Academy of Sciences*, 117(33):19656–19657, 2020. doi: 10.1073/pnas.2007117117.

Shao, Q. and Li, M. A new trend analysis for seasonal time series with consideration of data dependence. *Journal of Hydrology*, 396(1-2):104–112, 2011. doi: 10.1016/j.jhydrol.2010.10.040.

Sharp, M., Burgess, D. O., Cawkwell, F., Copland, L., Davis, J. A., Dowdeswell, E. K., Dowdeswell, J. A., Gardner, A. S., Mair, D., Wang, L., et al. Remote sensing of recent glacier changes in the Canadian Arctic. In *Global Land Ice Measurements From Space*, pages 205–228. Springer, 2014. doi: 10.1007/978-3-540-79818-7_9.

Slangen, A., Adloff, F., Jevrejeva, S., Leclercq, P., Marzeion, B., Wada, Y., and Winkelmann, R. A review of recent updates of sea-level projections at global and regional scales. *Surveys in Geophysics*, 38(1):385–406, 2017. doi: 10.1007/s10712-016-9374-2.

Slangen, A. B., Church, J. A., Agosta, C., Fettweis, X., Marzeion, B., and Richter, K. Anthropogenic forcing dominates global mean sea-level rise since 1970. *Nature Climate Change*, 6(7):701–705, 2016. doi: 10.1038/nclimate2991.

Slawinska, J. and Robock, A. Impact of volcanic eruptions on decadal to centennial fluctuations of arctic sea ice extent during the last millennium and on initiation of the Little Ice Age. *Journal of Climate*, 31(6):2145–2167, 2018. doi: 10.1175/JCLI-D-16-0498.1.

Solomina, O. N., Bradley, R. S., Hodgson, D. A., Ivy-Ochs, S., Jomelli, V., Mackintosh, A. N., Nesje, A., Owen, L. A., Wanner, H., Wiles, G. C., et al. Holocene glacier fluctuations. *Quaternary Science Reviews*, 111:9–34, 2015. doi: 10.1016/j.quascirev.2014.11.018.

Solomina, O. N., Bradley, R. S., Jomelli, V., Geirsdottir, A., Kaufman, D. S., Koch, J., McKay, N. P., Masiokas, M., Miller, G., Nesje, A., et al. Glacier fluctuations during the past 2000 years. *Quaternary Science Reviews*, 149:61–90, 2016. doi: 10.1016/j.quascirev.2016.04.008.

Stoffel, M., Khodri, M., Corona, C., Guillet, S., Poulain, V., Bekki, S., Guiot, J., Luckman, B. H., Oppenheimer, C., Lebas, N., et al. Estimates of volcanic-induced cooling in the Northern Hemisphere over the past 1,500 years. *Nature Geoscience*, 8(10): 784–788, 2015. doi: 10.1038/ngeo2526.

Svizzero, S. Persistent controversies about the Neolithic Revolution. *Journal of Historical Archaeology & Anthropological Sciences*, 1(2):00013, 2017. doi: 10.15406/jhaas.2017.01.00013.

Taylor, K. E., Stouffer, R. J., and Meehl, G. A. An overview of CMIP5 and the experiment design. *Bulletin of the American Meteorological Society*, 93(4):485–498, 2012. doi: 10.1175/BAMS-D-11-00094.1.

Thomas, E. K., Szymanski, J., and Briner, J. P. Holocene alpine glaciation inferred from lacustrine sediments on northeastern Baffin Island, Arctic Canada. *Journal of Quaternary Science*, 25(2):146–161, 2010. doi: 10.1002/jqs.1286.

Thomson, L. I., Zemp, M., Copland, L., Cogley, J. G., and Ecclestone, M. A. Comparison of geodetic and glaciological mass budgets for White Glacier, Axel Heiberg Island, Canada. *Journal of Glaciology*, 63(237):55–66, 2017. doi: 10.1017/jog.2016.112.

Tsai, C.-Y., Forest, C. E., and Pollard, D. Assessing the contribution of internal climate variability to anthropogenic changes in ice sheet volume. *Geophysical Research Letters*, 44(12):6261–6268, 2017. doi: 10.1002/2017GL073443.

Uppala, S. M., Kållberg, P., Simmons, A., Andrae, U., Bechtold, V. D. C., Fiorino, M., Gibson, J., Haseler, J., Hernandez, A., Kelly, G., et al. The ERA-40 re-analysis. *Quarterly Journal of the Royal Meteorological Society*, 131(612):2961–3012, 2005. doi: 10.1256/qj.04.176.

van der Bilt, W. G., Born, A., and Haaga, K. A. Was common era glacier expansion in the Arctic Atlantic region triggered by unforced atmospheric cooling? *Quaternary Science Reviews*, 222:105860, 2019. doi: 10.1016/j.quascirev.2019.07.042.

Varma, V., Prange, M., Spangehl, T., Lamy, F., Cubasch, U., and Schulz, M. Impact of solar-induced stratospheric ozone decline on Southern Hemisphere westerlies during the Late Maunder Minimum. *Geophysical Research Letters*, 39(20), 2012. doi: 10.

1029/2012GL053403.

Vaughan, D., Comiso, J., Allison, I., Carrasco, J., Kaser, G., Kwok, R., Mote, P., Murray, T., Paul, F., Ren, J., Rignot, E., Solomina, O., Steffen, K., and Zhang, T. *Observations: Cryosphere*, book chapter 4, pages 317–382. Cambridge University Press, Cambridge, United Kingdom and New York, NY, USA, 2013. ISBN 978-1-107-66182-0. doi: 10.1017/CBO9781107415324.012.

Vieira, L. E. A., Solanki, S. K., Krivova, N. A., and Usoskin, I. Evolution of the solar irradiance during the Holocene. *Astronomy & Astrophysics*, 531:A6, 2011. doi: 10.1051/0004-6361/201015843.

WGMS. Fluctuations of glaciers database. World Glacier Monitoring Service, Zurich, Switzerland. 2017. doi: 10.5904/wgms-fog-2017-10v.

WGMS. Fluctuations of glaciers database. World Glacier Monitoring Service, Zurich, Switzerland. 2020. doi: 10.5904/wgms-fog-2020-08.

Wolken, G. J., England, J. H., and Dyke, A. S. Changes in late-Neoglacial perennial snow/ice extent and equilibrium-line altitudes in the Queen Elizabeth Islands, Arctic Canada. *The Holocene*, 18(4):615–627, 2008. doi: 10.1177/0959683608089215.

Wouters, B., Gardner, A. S., and Moholdt, G. Global glacier mass loss during the GRACE satellite mission (2002-2016). *Frontiers in Earth Science*, 7:96, 2019. doi: 10.3389/feart.2019.00096.

Young, N. E., Schweinsberg, A. D., Briner, J. P., and Schaefer, J. M. Glacier maxima in Baffin Bay during the Medieval Warm Period coeval with Norse settlement. *Science Advances*, 1(11):e1500806, 2015. doi: 10.1126/sciadv.1500806.

Yue, S. and Wang, C. The Mann-Kendall test modified by effective sample size to detect trend in serially correlated hydrological series. *Water Resources Management*, 18(3): 201–218, 2004. doi: 10.1023/B:WARM.0000043140.61082.60.

Zekollari, H., Huss, M., and Farinotti, D. Modelling the future evolution of glaciers in the European Alps under the EURO-CORDEX RCM ensemble. *The Cryosphere*, 13 (4):1125–1146, 2019. doi: 10.5194/tc-13-1125-2019.

Zemp, M., Huss, M., Thibert, E., Eckert, N., McNabb, R., Huber, J., Barandun, M., Machguth, H., Nussbaumer, S. U., Gärtner-Roer, I., et al. Global glacier mass changes and their contributions to sea-level rise from 1961 to 2016. *Nature*, 568(7752):382, 2019. doi: 10.1038/s41586-019-1071-0.

List of Abbreviations

CAA	Canadian Arctic Archipelago
CCSM	Community Climate System Model
CERA-20C	Coupled ReAnalyses of the 20^{th} Century
CESM-LE	Community Earth System Model Large Ensemble
CESM-LME	Community Earth System Model Last Millennium Ensemble
CMIP	Coupled Model Intercomparison Project
CRU TS	Climatic Research Unit Time Series
CRU CL	Climatic Research Unit Climatology
DEM	Digital Elevation Model
ECMWF	European Centre for Medium-Range Weather Forecasts
ELA	Equilibrium Line Altitude
ERA5	ECMWF ReAnalysis 5th Generation
ERA-40	ECMWF 40-year ReAnalysis
ERA-interim	ECMWF ReAnalysis covering 1 January 1979 to 31 August 2019
GCM	Global Circulation Model
GHG	Greenhouse Gas
GIC	Glaciers and Ice Caps
GlacierMIP	Glacier Model Intercomparison Project
GMSL	Global Mean Sea Level
GRACE	Gravity Recovery and Climate Experiment
ITMIX	Ice Thickness Models Intercomparison eXperiment
LIA	Little Ice Age
LULCC	Land Use and Land Cover Change
MWP	Medieval Warm Period
OGGM	Open Global Glacier Model
PMIP	Paleo Model Intercomparison Project
SMB	Surface Mass Balance

RACMO	Regional Atmospheric Climate Model
RGI	Randolph Glacier Inventory
RCP	Representative Concentration Pathway
TraCE-21k	Simulation of Transient Climate Evolution over the Last 21,000 Years
WGMS	World Glacier Monitoring Service

Declaration in lieu of an oath

I,

Anouk Vlug
Faculty of Geosciences
Klagenfurter Strasse 2
28359 Bremen

declare in lieu of an oath by my signature that I have completed the thesis above myself and without any third-party assistance, and have identified as such all parts I have cited in letter or spirit from publications, and that I have not used any literature or any other aids other than those stated.

I declare in lieu of an oath that I have provided the information above to the best of my knowledge and belief and that the information provided is the truth and that I have not with-held anything.

I am aware that making a false declaration in lieu of an oath is a punishable offence, namely the punitive sanction pursuant to §156 StGB (German Penal Code) of up to three years' imprisonment or a fine, when the commission was intentional, or up to one year's imprisonment or a fine pursuant to §161 Para. 1 StGB when it was negligent.

Innsbruck, 19-14-2021

Place, Date

Signature

Acknowledgements

With this thesis coming to an end I would like to thank quite some people. First of all I would like to thank my supervisors Matthias Prange, Michael Schulz, Ben Marzeion and Fabien Maussion for their trust in me and supervising me in a way that let me free to find my path on this PhD journey. Matthias, thank you a lot for always having your door open to discuss results and your ability to reduce my concerns from mountains to hills. Going to your office came with a guarantee of laughing and your laughter made me smile countless times in my office. Ben, I'm very thankful for both the scientific input you gave as well as the caring way of your supervision. Michael, I have very much appreciated your genuine interest in my research, detailed feedback and rapid responses to everything I sent you over the course of my PhD. Fabien, I'm fortunate that I got to know you early on in my PhD. I'm grateful for all your support and very happy to be working with you. Thanks to Gerard Roe for the enthusiastic and positive reply to my thesis review request.

My PhD project was funded by the Deutsche Forschungsgemeinschaft (DFG) through the International Research Training Group Processes and impacts of climate change in the North Atlantic Ocean and the Canadian Arctic (IRTG 1904 ArcTrain). In the final phase of my PhD, I was supported by the Fonds zur Förderung der wissenschaftlichen Forschung through funding from the project "Scaling regional sea level changes with climate forcings" (FWF project P30256). I'm very grateful for that, so thanks to all the tax payers. In addition to doing this PhD, ArcTrain gave me the opportunity to join meetings, conferences, workshops, retreats and the Floating University (special thanks to Rüdiger Stein). However, to me ArcTrain has been much more than these somewhat official lines. It is a great community that offered me an opportunity to learn and grow. Thanks to all involved, both on the German and the Canadian side, for creating this amazing environment. Thanks Michal Kucera, Siccha and Gabriella for all the work and love you put into this over the years. Valentin it was great to be PhD representative together with you, thanks for your support and jokes in times of avalanches. Remi, thanks for all the coffee breaks, boulder sessions and your wise advise! To Beatriz, Lina, Mattia, Charles, Jade and the people of the pizza group, I'm very happy that I got to know you, that you were part of my PhD journey, that you were there both through the ups and downs of the experience, that you made me laugh till I had to cry on countless occasions and your generosity with hugs!

I'm grateful to the welcome centre of the university for giving me a smooth start in Bremen. I would like to thank the GEOMOD group and specifically Andreas for technical support and bringing the group together by making coffee, Jeroen (I think you know why), Charlotte for introducing me to bouldering, Diana for daily hugs, Sri for yoga sessions and nice diners, Kerstin for being a super hero and my office mates: Marilena and Brian. To the last two, I wish the time of sharing the office wouldn't have ended so abruptly. I really enjoyed our office dynamics and I think it's sad that it just stayed with one sharing-pizza-and-beer-while-working-late-at-the-office session. I would like to thank the DAAD RISE program for granting me an intern. Special thanks to Eliza for being both a great intern and the first student that I supervised. I learned a lot from you. Acknowledging GLOMAR doesn't go without mentioning Tina and Chelsea. I would like to thank the IMAU, and in particular Brice Noël and Michiel van den Broeke, for hosting me during what turned out to be a fruitful research stay. I would like to thank the OGGM community, for being awesome, open and supportive. In this context a special thanks to Fabien and Timo, just the thought of you being there was of great comfort when I was trying to solve an error in my code. Thanks to NCAR and many others for making their data and packages freely available, without that this thesis wouldn't have been possible. Thanks to Bord & Stift for making my time in home office way more comfortable by letting me borrow office equipment during times of social distancing. Thanks to ACINN and in specific the Ice and Climate group in Innsbruck for your warm welcome. I'm looking forward to get to know you better in real life. Special thanks to Valentin for translating the summary; to Charlotte and Melanie for proofreading chapters; and Brian for proofreading this whole thesis!

Because it didn't seem fair to me to only acknowledge those who played a role during my PhD and not those who got me to the start: I would hereby like to acknowledge some of my primary school teachers: Betty, Hadewich, Els and Maaike. A selection of the teachers of the Montesorri Lyceum Amsterdam: Pieter, Carline, Mareike, Carrie, Willem, Rolf (I never thought that knowing a bit of German might be very useful to me one day, so in hindsight thanks for giving great classes and getting me motivated either way for one of my least favorite subjects), Herman, Cor, Ron and Marjane. Thanks to Sara Boonman & Janni Goslinga from Theater Group Amsterdam, for giving me a great and forming experience during the junior production. I'm indebted to everyone from the EGEA Amsterdam-Krakow exchange in 2009, for planting the seed that made me switch my studies to Earth Sciences. Thanks to those involved in my education at the University of Amsterdam, Wageningen University (including Studium Generale Wageningen), the University Centre in Svalbard and Climate KIC. From my time at UNIS, I would like to send a special thanks to: Anne Hormes, Riko Noormets, Doug Benn and Andy Hodson for introducing me to the Arctic with courses that were both

amazing and inspiring. Kenneth Rijsdijk, Nicolas Jourdain and Ryan Teuling, thanks for the experience I gained under your supervision.

On a more personal level, I would like to thank my friends and family and especially my parents and bonus parents: Pim, Renee, Hans, Mary and Kristel. I'm grateful for my diverse upbringing, lots of love, always being there for me and all the support for finding, choosing and walking my own path. I would like to thank those who inspired me to go on adventures. Jip, thank you for being a lovely sister and all your late night bicycle ride calls, which made at least one of us secretly looking forward to your series of night shifts. Rover and Pippa, I'm grateful for the special connection we continue to have, despite the great distance and me being gone most of the time. Mara you're awesome, thanks for keeping in touch over the years. Charlotte, I cannot find the words for what I would like to say. As you can read my mind most of the times I will leave it with: thank you for being a special person in my live and for the last year, and I hope you understand it anyway. Almer, I would like to thank you for being supportive throughout my academic journey, giving me that little push to go out of my comfort zone to follow my dreams and for visiting me every where I moved a long the way. I know it wasn't easy. Therefore even more, I am grateful that you were there.